VARIABLE PERTURBATION SIZE MAXIMUM POWER POINT TRACKING ALGORITHMS FOR PHOTOVOLTAIC SYSTEMS

Neil Savio D'Souza

A Thesis

In

The Department

Of

Electrical and Computer Engineering

Presented in Partial Fulfillment of the Requirements
For the Degree of Master of Applied Science at
Concordia University
Montréal, Québec, Canada

June 2006

Your file Votre référence
ISBN: 978-0-494-20741-3
Our file Notre référence
ISBN: 978-0-494-20741-3

ABSTRACT

VARIABLE PERTURBATION SIZE MAXIMUM POWER POINT TRACKING ALGORITHMS FOR PHOTOVOLTAIC SYSTEMS

Neil Savio D'Souza

The perturbation and observation (P&O) or hill-climbing maximum power point tracking (MPPT) algorithms are commonly used in PV systems due to their easy implementation. A P&O algorithm based on peak current control (PCC) and on the use of instantaneous sampled values to calculate the next perturbation can provide faster transient responses and small oscillations around the maximum power point (MPP) than when pulse width modulation (PWM) and averaged control values are used. However, the use of a fixed size perturbation (variation of the reference current for the PCC) results in a compromise solution between transient and steady-state responses.

This thesis focuses on alternatives for implementing variable size perturbations in peak current controlled P&O MPPTs. First a Fuzzy logic based implementation is proposed and designed. Then hybrid region-based methods, where the MPPT algorithms operate differently depending on where in the PV panel Volt-current characteristics the system operates, are considered. The concept of non-switching zones is proposed as a means for moving the operating point of the PV system towards the vicinity of the MPP in the shortest possible interval. The potential performance of four different P&O algorithms is investigated by means of simulations. Experimental results are then used to verify how the computational burden of each algorithm and the processing speed of a common digital signal processor (DSP) affect the performance of each method in a practical prototype.

ACKNOWLEDGMENTS

The author would like to express his sincere gratitude to his supervisor, Dr. Luiz A. C. Lopes for his invaluable guidance, advice, friendship and financial support throughout the course of this study.

The author would also like to thank his colleagues in the P. D. Ziogas Power Electronics Laboratory. A special word of thanks to Mr. Joseph Woods for his outstanding technical support. Smart suggestions from and helpful discussions with Xuejun Liu, Avishek Mukherjee, Zhixiang Luo, Huili Sun, Su Chen, Yongzheng Zhang, Maged and Ninad are unforgettable.

Last but not least, the author is very grateful towards his family whose constant support made it possible to finish the project.

To my Parents

TABLE OF CONTENTS

LIST OF FIGURES

LIST OF TABLES

LIST OF ACRONYMS

A/D	Analog to Digital
CCS	Controlled Current Source
CRI	Compositional Rule of Inference
CS	Current Sensor
CVS	Controlled Voltage Source
D/A	Digital to Analog
DSP	Digital Signal Processing
FPGA	Field Programmable Gate Array
GMP	Generalized Modus Ponens
GUI	Graphical User Interface
FIS	Fuzzy Inference System
IncCond	Incremental Conductance
IC	Integrated Circuit
I/O	Input Output
MOM	Middle Of Maxima
MPP	Maximum Power Point
MPPT	Maximum Power Point Tracking
N	Negative
NB	Negative Big
NM	Negative Medium
NS	Negative Small

P	Positive
PB	Positive Big
PC	Power Circuit
PM	Positive Medium
PS	Positive Small
PCC	Peak Current Control
PI	Proportional and Integrated
P&O	Perturbation and Observation
PPC	PowerPC processor
PV	Photovoltaic
PWM	Pulse Width Modulation
RC	Resistor and Capacitor
SAS	Solar Array Simulator
SC	Short Circuit
ZZ	Zero
Z	Zero

LIST OF PRINCIPAL SYMBOLS

$\Delta E(k)$	Change in error;
ΔI_{PV}	The difference in PV panel output current between two sampling instants;
ΔI_{REF}	The variation in peak reference current;
ΔP_{PV}	The difference in PV panel output power between two sampling instants;
ΔV_{PV}	The difference in PV panel output voltage between two sampling instants;
τ	The time constant of system;
ω_n	The natural angle frequency;
ζ	The damping ratio;
A	The p-n junction ideality factor;
di/dv	The incremental panels conductance;
D	The duty ratio of the MPPT converter;
D_{max}	The maximum duty ratio;
D_{min}	The minimum duty ratio;
f_{SW}	The switching frequency;
G	The Fuzzy input scaling gain;
h	The Fuzzy output scaling gain;
I/V	The instantaneous panels conductance;
I_j	The current though the nonlinear impedance of p-n junction;
I_{MPP}	The PV output current at the MPP;
I_{ph}	PV cell photocurrent;
I_{PV}	The PV panels output instantaneous current;

I_{PV} The PV panels output DC current;

$\tilde{i}_{PV}$ The ac component in the PV panel output current;

I(k) The present current sampling and holding block;

I_{REF} The peak current reference;

I_{rs} The PV cell reverse saturation current;

I_{SC} The short-circuit current of PV panels;

k Boltzmann's constant, which is 1.38×10^{-23}(eV/K);

L The inductor of the MPPT converter;

n_p The number of PV modules connected in parallel;

n_s The number of PV cells connected in series;

P_{MPP} The PV output power at the MPP;

P_{PV} PV panels output instantaneous power;

P_{PV} PV panels output DC power;

$\tilde{p}_{PV}$ The ac component in the PV panel output power;

P(K) The present power sampling and holding block;

q The charge of an electron, which is 1.9×10^{-19}(C);

R_j The nonlinear impedance of p-n junction;

R_o The resistance load of the PV cell;

R_s The intrinsic series resistance of PV cell;

R_{sh} The intrinsic shunt resistance of PV cell;

S The irradiance in mW/cm^2;

T The cell temperature (K);

T_{settle} The settling time of the MPPT system;

V_b The battery voltage;

V_{MPP} The PV output voltage at MPP (Maximum Power Point);

V_{OC} The open circuit voltage of PV panels;

V_{PV} The PV panels output instantaneous voltage;

V_{PV} The PV panels output DC voltage;

$\tilde{v}_{PV}$ The ac component in the PV panel output voltage;

V_{REF} The voltage reference to the 3842 PWM IC;

CHAPTER 1

INTRODUCTION

1.1 BACKGROUND [1]

"The use of solar energy has never been more important now that it is evident that exploitation of fossil fuel energy sources maybe affecting the planet's ambient. Other renewable means of power generation e.g. hydroelectric, wind and wave power also depend on the sun as the primary source. The use of photovoltaics as an energy source is imperative to help reduce the levels of green house gases in the atmosphere and reduce global warming. At present the direct conversion of light into electricity through the use of photovoltaics, is becoming an important form of power generation. The production rate has been increasing at almost 20% annually over the last decade and is likely to reach the scale of gigawatts in the early decades of this millennium. Photovoltaic power generation is reliable, involves no moving parts, and presents low operation and maintenance costs. The operation of a photovoltaic system is silent, and creates no atmospheric pollution. Photovoltaic systems are modular, and can be quickly installed. Power can be generated where required without the use of transmission lines. Several photovoltaic installations operate in locations where other means of electricity supply would be out of the question, providing benefits to rural communities throughout the world. The cost of solar electricity already compares favorably with other small power sources such as diesel generators. The one major drawback is a high capital cost. However financing mechanisms put in place to spread the payments over a lifetime can

help solve the problem. The economic comparison with conventional energy sources is certain to receive a further boost as the environmental and social costs of power generation are considered." UNESCO (2000)

1.2 PHOTOVOLTAIC BASICS [1]

"Solar cells represent the fundamental power conversion unit of a photovoltaic system. Solar cells are usually assembled into modules for practical operation. Devices with efficiency exceeding 30% have been demonstrated in the laboratory. The efficiency of commercial devices however is half this value. The solar cell operation is based on the ability of semiconductors to convert sunlight directly into electricity by exploiting the photovoltaic effect. The electric current generated in the semiconductor is extracted by contacts to the front and rear of the cell." UNESCO (2000)

1.2.1 The equivalent circuit of a PV cell [2]

The voltage versus current [$V_{PV} \times I_{PV}$] characteristic of a solar cell can be obtained from an equivalent circuit of the device as shown in Fig.1.1. The generation of current I_{ph} by light is represented by a current source in parallel with a nonlinear resistance which represents the p-n junction. The intrinsic shunt and series resistance of the cell are represented by R_{sh} and R_s respectively. The value of R_{sh} is very large and the value of R_s is very small and can be neglected to simplify the analysis.

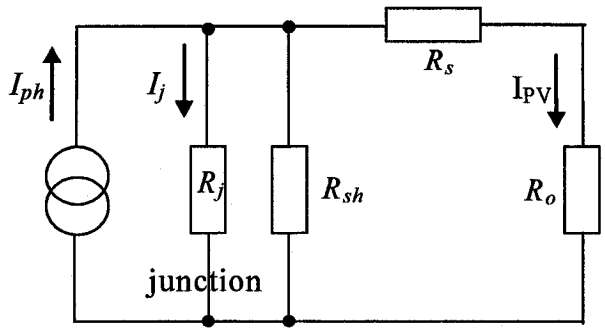

Fig.1.1 The equivalent circuit of a solar cell [2]

1.2.2 Mathematical model of PV panels [2]

The output PV panel current I_{PV} is then equal to the difference between the light generated current I_{ph} and the current I_j through the non-linear resistance. Hence we have,

$$I_{PV} = n_p I_{ph} - n_p I_{rs}[\exp(\frac{q}{kTA}\frac{V_{PV}}{n_s}) - 1] \quad (1.1)$$

where

I_{PV} : PV panels output current (A);

V_{PV} : PV panels output voltage (V);

n_s : number of cells connected in series;

n_p : the number of modules connected in parallel;

q :charge of an electron, which is $1.9\text{x}10^{-19}$(C);

k : Boltzmann's constant, which is $1.38\text{x}10^{-23}$(eV/K);

A : *p-n* junction ideality factor;

T : cell temperature (K);

I_{rs} is the cell reverse saturation current.

The factor A in Eq. (1.1) determines the cell deviation from the ideal *p-n* junction characteristics; it varies between 1 and 5, 1 being the ideal value.

1.2.3 Output characteristic curves of PV panels [2]

Fig.1.2 shows the characteristic curves of a PV panel under varying conditions of temperature and irradiance. In order to obtain the current versus voltage curves V_{PV} is varied and the corresponding value of I_{PV} is obtained from equation 1.1. In order to obtain the power versus voltage and the power versus current curves, V_{PV} is multiplied with I_{PV} to obtain photovoltaic panel power P_{PV} and the same is then plotted versus V_{PV} and I_{PV}. Fig.1.2(a) shows the curves of PV panel output current versus panel voltage. Fig.1.2(b) shows the curves of PV panel output power versus PV panel voltage. Fig.1.2(c) shows the curves of PV panel output power versus PV panel current.

It is evident that the output characteristics of the PV panel are non-linear in nature and vary with atmospheric conditions namely temperature, irradiance etc. From Fig.1.2(a) it can be seen that short-circuit current is approximately a linear function of irradiance i.e. variation of irradiance mainly affects the short-circuit current. Cell temperature is usually higher than the ambient air temperature and depends on factors such as the ambient air temperature, intensity of sunlight falling on the module, wind velocity etc. Manufacturers in their datasheets normally specify a temperature cycling range of -40 to 80 °C as qualification test parameters as per the IEC 1215 test requirements. Datasheets generally provide curves for cell temperatures in the range of 0-75 °C. Hence, the curves shown in Fig.1.2 are for typical values of cell temperature. Also from Fig.1.2(a) it can be seen that open circuit voltage has a negative temperature coefficient i.e. variation of cell temperature mainly affects the open circuit voltage. It is also noticeable that the power

versus current and power versus voltage curves present a unique maximum power point (MPP) under given atmospheric conditions. The MPP varies under different atmospheric conditions, thus I_{PV} or V_{PV} should be adjusted in an adequate way to track the MPP under these varying conditions, which is the fundamental principle of a Maximum Power Point Tracker (MPPT).

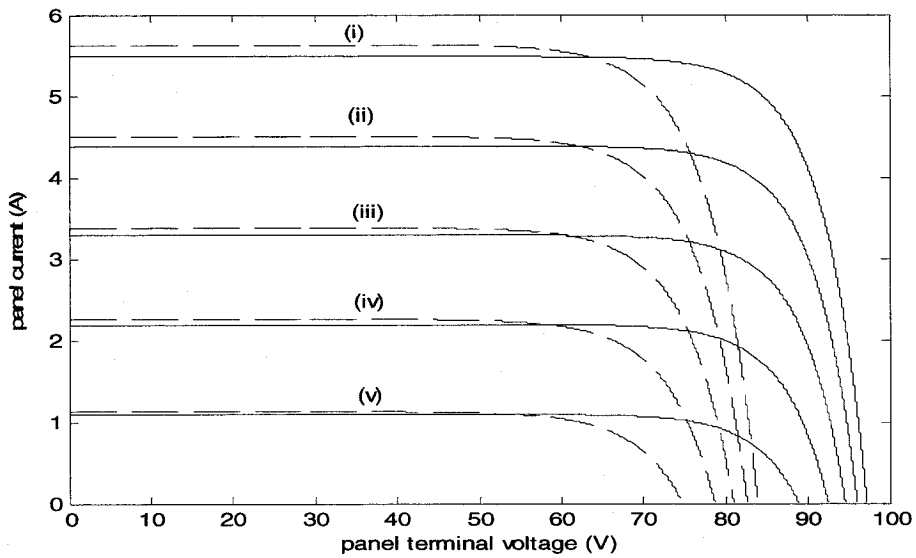

(a)

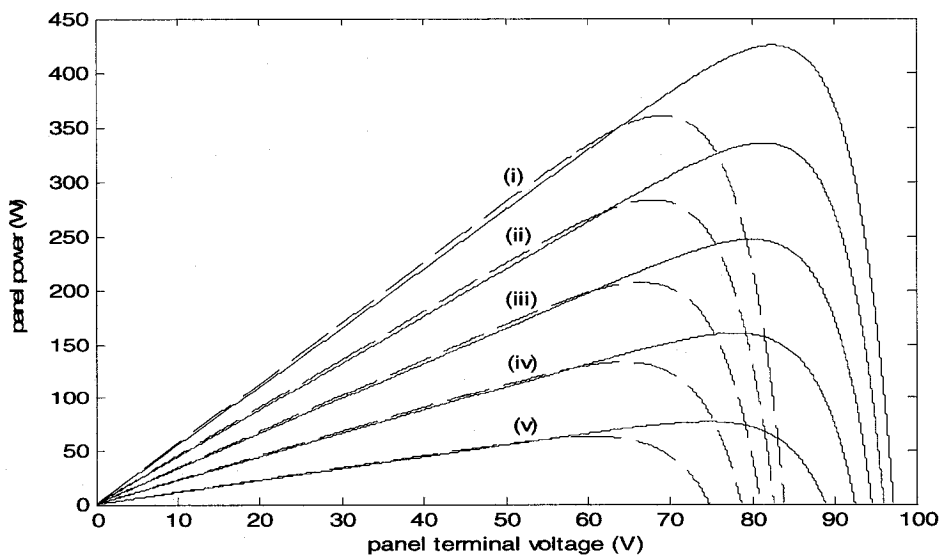

(b)

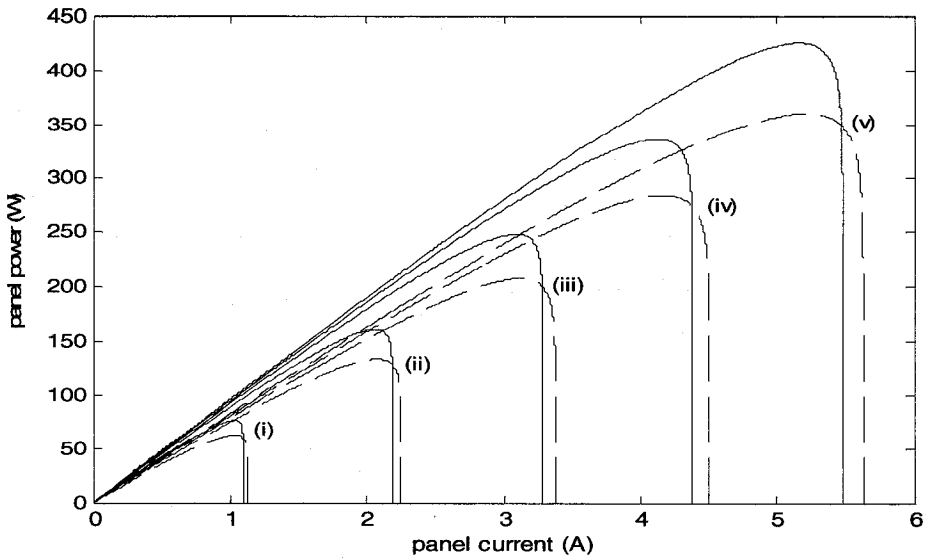

(c)

Fig.1.2 Output characteristic curves of PV panels [2]

(a) PV output current *vs.* output voltage;

(b) PV output power *vs.* output voltage;

(c) PV output power *vs.* PV output current;

___ 28°C ---- 56°C

(i) irradiance = 100mW/cm^2; (ii) irradiance = 80mW/cm^2;

(iii) irradiance = 60mW/cm^2; (iv) irradiance = 40mW/cm^2;

(v) irradiance = 20mW/cm^2;

The PV panel power-current or power-voltage characteristics may present two or more local maxima due to partial-shading or other conditions, however the analysis of these characteristics is beyond the scope of this thesis.

1.3 Maximum Power Point Trackers (MPPT)

"An MPPT is a control algorithm that can be included in the PV panel connections in order to track the maximum power point, which is going to be different from the STC (Standard Test Conditions) rating under almost all situations. Under very cold conditions a PV panel can output more power because the output goes up as temperature goes down – but in the absence of an MPPT, this power could be lost, whereas under very hot conditions, the power drops - you lose power as the temperature goes up." [3]

When a PV module is connected directly to a battery bank, it's output voltage is imposed by the battery and cannot be varied to track the MPP. In order to be able to track the MPP, one has to use a power converter between the PV module and battery so that the PV panel voltage can be selected independently of the battery voltage.

Traditional charge controllers only protect the battery from overcharging, which can reduce the life-cycle of the battery. A power electronics based charge controller with MPPT varies the ratio between voltage and current delivered to the battery, in order to deliver maximum power. If there is excess power available from the PV panel, then it converts that to additional current in the battery. As the MPP of the PV array varies with temperature and other conditions. It tracks this "variance" and adjusts the ratio accordingly. Hence it is called the maximum power point tracker. [4]

1.4 MPPT ALGORITHMS [2]

Several MPPT algorithms have been mentioned in the literature. MPPT Algorithms can be basically classified into two categories

On-line methods [5-16]: These methods measure operating voltage and/or current and compare the present value of power with the previously obtained values and appropriate changes in the reference value are made so as to cause a further increase in power ultimately tracking the operating point that operates at maximum power. Online methods track the maximum power point based on actual values of PV array voltage and current and hence can provide the optimum operating point for the system. Online methods are usually more expensive due to extra circuitry employed and are usually only used in large PV systems. However with the availability of low-cost based microcontrollers and field programmable gate arrays (FPGAs) these methods can also be applicable to module-based power electronic interfaces.

Off-line methods [17-22]: These methods rely on the measurement of parameters like irradiance, panel temperature, short circuit current, open circuit voltage of the PV array etc. and the use of prior training data to set the reference signal corresponding to operation at the maximum power point. Several methods based on neural networks [20], genetic algorithms [21] and fuzzy logic objective modeling [22] are available to implement these methods. These methods present reduced implementation costs, but sub-optimum performance.

Online Methods include:

1. **Perturbation And Observation (P&O) Algorithm [5-12]**

This class of MPPT algorithms operates as the name suggests by perturbing or varying continuously the operating point of the photovoltaic system and observing the variation in PV output power. The next perturbation or variation of the reference signal is carried out so as to cause an increase in PV output power ultimately leading to operation about the maximum power point. The perturbation variable can be the reference value for the PV panel terminal voltage, PV panel output current, or duty cycle of the MPPT converter. The P&O algorithm displays desirable response under slowly varying atmospheric conditions like irradiance, temperature and variation of the PV panel's own characteristics. This algorithm is also easy to implement with digital circuits. However, continuously perturbing the reference signal to track the MPP means that the operating point does not settle at the actual operating point but oscillates around it, leading to power loss in the steady-state conditions. Besides the P&O algorithm may also lead to temporary deviation of the operating point from the MPP under rapidly fluctuating atmospheric conditions.

Fuzzy logic is being increasingly used in present times as a convenient tool to model and control systems, which are nonlinear in nature, the solar PV array being no exception. Besides, the use of Fuzzy logic for control purposes does not require a detailed or accurate mathematical model of the system. It has been used in the past along with commonly used MPPT algorithms such as P&O [10-12]. Its main goal is usually to determine the incremental duty ratio or PWM modulating signal based on one or more parameters of the PV array. The *Error* E(k) and *Change in Error* $\Delta E(k)$, where E(k)=

$\Delta P_{PV}/\Delta I_{PV}$, have been used in [11] to vary the reference voltage for the PWM control. In [12], the change in PV power (ΔP_{PV}) and the ratio of change in PV power and duty cycle ($\Delta P_{PV}/\Delta d$) outputs the incremental duty ratio in order to track the MPP. It is worth mentioning that the parameters used in the previous calculations are usually average values.

2. Incremental Conduction (IncCond) Algorithm [13-14]

This algorithm works on the principle that the derivative of power versus current or voltage becomes zero at the MPP as it is the maxima of the power curve. Hence when $dp/dv = 0$, the operating point is at the MPP. When $dp/dv > 0$ the system operates to the left of the MPP and the reference current or voltage should be increased and when $dp/dv < 0$ the operating point of the system is to the right of the MPP and the reference current or voltage should be decreased.

We have, $dp/dv = d(iv)/dv = I + V di/dv$

$$(1/V)dp/dv = (I/V) + di/dv$$

Hence the PV panel voltage or current can be adjusted to reach the MPP by measuring the incremental and instantaneous panel conductance (di/dv and I/V) and using the above equations. IncCond algorithms in principle can mitigate oscillations about the MPP and allow the operating point to settle at the MPP when the $dp/dv = 0$ condition is reached. These algorithms can track the MPP under rapidly varying atmospheric conditions. The disadvantage of the IncCond Method is control circuit complexity results in a higher system cost. If the speed of computation of the incremental conductance is slow, the IncCond method cannot guarantee operation at the MPP under rapidly varying environmental conditions and a problem similar to the P&O algorithm causing deviation

of the operating point from the MPP under rapidly changing atmospheric conditions also occurs.

3. Ripple Correlation Control (RCC) Algorithm [15-16]

Algorithms of this type dynamically extrapolate the characteristic of PV arrays, often through the employment of the input ripple of the DC-DC converter, and generate a continuous signal that drives the duty cycle of the converter. In this algorithm the switching ripple information is used to track the MPP instead of the external perturbation. The ripple is considered as a dynamic perturbation. The ripple will cause the operating point to move back and forth on the PV panel characteristic. The MPP is tracked by following the correlation between PV panel output power and either the voltage or current ripple waveform. The products $P_{PV}'.V_{PV}'$ *or* $P_{PV}'.I_{PV}'$ give the necessary phase information on the average, where " ' " denotes the time derivative. $P_{PV}'.V_{PV}'$ *or* $P_{PV}'.I_{PV}'$ will be negative if $I_{PV} < I_{MPP}$, positive if $I_{PV} > I_{MPP}$ and zero when the maximum power point is being tracked. The actual implementation does not require a measurement of power. By the chain rule

$$P_{PV}'.V_{PV}' = (I_{PV}.V_{PV}' + V_{PV}.I_{PV}')\, V_{PV}' \qquad (1.2)$$

For control flexibility a parameter α is added

$$P_{PV}'.V_{PV}' = (\alpha I_{PV}.V_{PV}' + V_{PV}.I_{PV}')\, V_{PV}' \qquad (1.3)$$

The time integral of equation (1.3) represents a correlation function $c_p(t)$. This function can be directly fed to the duty ratio input of the converter.

If ac-coupled measurements of I_{PV} and V_{PV} are made, written as $\tilde{i}_{PV}$ and $\tilde{v}_{PV}$. Then the phase information is contained in $\tilde{p}_{PV}\tilde{v}_{PV}$. The ac portion of the power is the product $(V_{PV} + \tilde{v}_{PV})(I_{PV} + \tilde{i}_{PV})$ less the dc portion $V_{PV}I_{PV}$. This product can be written as

$$\tilde{p}_{PV}\tilde{v}_{PV} = (V_{PV}\tilde{i}_{PV} + I_{PV}\tilde{v}_{PV})\tilde{v}_{PV} \quad (1.4)$$

This is just like (1.3), except that ac coupled signals have been substituted for time derivatives. The time integral of equation (1.4) can serve as a control signal. This simple method tracks the maximum power point continuously, just as c_p does.

The advantages of this system are that no external perturbation is required. Also power efficiency is a function of converter design rather than the algorithm, since only a few low-power analog ICs are needed in the implementation. The disadvantage of this system is that algorithm performance depends on signal-to-noise ratio i.e. the system will not work well if aggressive filtering is used to eliminate the ripple. Thus high switching frequency would mean low ripple and possible problems with the algorithm. Besides, the solar cells exhibit a voltage dependent capacitance. At high speeds a dynamic V-I characteristic is observed. In these situations the algorithm fails.

1.5 Peak Current Control Based MPPT [2,23]

A novel implementation of the P&O algorithm was suggested based on comparing instantaneous values instead of average values of I_{PV} and V_{PV} and peak current control that present one-cycle speed of response for small variations in the reference current. The proposed algorithm used a Boost DC/DC converter with an inductor designed to meet the current ripple requirements. The MPPT algorithm supplies a reference signal for peak current control of the Boost Converter. No capacitor is employed across the PV panel of the system, as the capacitor reduces the speed of the response of the MPPT system to varying atmospheric conditions. This may cause an increase in the voltage ripple but the locus of the operating point lies on the P-I characteristic of the PV panel. Most of the

MPPT techniques in the literature use PWM methods to regulate V_{PV} or I_{PV}, where a PI controller processes the error between the reference and the actual average value of the PV current/voltage and provides a modulation signal for the PWM. The typical response of a DC/DC converter with a linear controller is of an under-damped second order system with a damping ratio (ζ) between 0.4~0.6 for 25%~10% overshoot. The settling time for a 2% band is given by $T_{settle} = 4\tau = 4\zeta\omega_n$. In practical systems the bandwidth of the system is selected as 10% of the switching frequency of the power converter, resulting in a settling time of roughly 12 switching cycles. Hence, for the actual current or voltage of the PV panel to follow accurately a reference signal, the refresh or update rate of this reference signal, that is calculated by the MPPT should be smaller than the inverse of the settling time of the control loop. This may be the main factor in the relatively slow speed of response of traditional MPPT algorithms. The use of instantaneous samples instead of average values and peak current control seemed to have considerably improved the response speed of the MPPT system. By comparing instantaneous samples of P_{PV} and I_{PV} in two consecutive switching cycles, the peak current algorithm provides a reference signal that would result in an increase of PV power. For example, let us assume that the PV system operates on the left side of the MPP and the average PV current increasing due to an increasing peak reference current. When the switch of the Boost Converter is switched ON the current in the inductor of the Boost Converter, which is also the PV panel output current, increases and when the switch is turned OFF the PV panel output current decreases. Let A and B be two sampling instants corresponding to two consecutive switching cycles T(k-1) and T(k). Suppose the instantaneously sampled value of current at point A, (i_A) is less than that at point B (i_B). Also the instantaneous

power at point A (p_A) is less that that at point B (p_B). Hence a positive variation of reference current caused a positive variation of instantaneous PV output power. Thus, the reference for the peak current should be increased. We can also infer that the operating point of the PV system is to the left of the MPP. Similarly if a positive variation of reference current causes a negative variation of instantaneous PV output power the reference for the peak current should be decreased.

1.6 Scope And Contributions Of This Thesis

It has been shown in [2,23] for a P&O method that the speed of response of the MPPT can be increased by using a one-cycle control type scheme. It employs peak current control with a reference current that changes in every switching cycle. The choice of increasing or decreasing the reference current is based on the comparison of two instantaneous, not average samples of P_{PV} and I_{PV}. These are obtained in two consecutive switching cycles, one sample per switching cycle, for two different values of reference current. However it used a fixed variation of reference current, which was chosen as a compromise between transient and steady state performance.

The main contributions of this thesis are the following:

1. The proposed use of a Fuzzy logic based controller along with instantaneous values of PV voltage and current and peak current control for determining not only the direction of the next perturbation (variation of reference current) but also its magnitude, by which one can enhance both transient and steady-state operation simultaneously.[24]
2. The use of a complex fuzzy controller leads to the requirement of a higher computation burden while implementing the system in real-time. To overcome

this difficulty this thesis proposes hybrid schemes based on the division of the PV panel $V_{PV} \times I_{PV}$ characteristic into three regions: two non-MPP containing regions or non-switching zones and one MPP containing region or switching zone. While operating in the non-MPP zones, the switch is operated with a duty cycle of 0 or 1 to accelerate the operating point towards the MPP region, where an MPPT technique with the peak current control scheme can operate with a low incremental reference current resulting in better steady-state performance without compromising on the transient performance. The use of a reduced Fuzzy controller in the MPP region is also proposed, which has lesser membership functions and rules thus easing the computation burden. [25]

3. In [2] it was seen that if the peak current control logic was implemented in the DSP, in the case of the standard scheme with a fixed ΔI_{REF}, the switching frequency was restricted to 10 kHz in order to have a good enough resolution of duty cycle. In addition the computation time required by the DSP to process the Fuzzy controller block in the schemes involving Fuzzy logic, places a further restriction on the switching frequency of the boost converter, if the peak current control logic was implemented in the DSP. This thesis proposes the analog implementation of the peak current controller in order to improve the converter switching frequency and duty cycle resolution. An external sample & hold circuit is also suggested to synchronize the obtention of sampled values with the switching cycle of the DC/DC Converter. With the analog implementation of peak current control and the external sample and hold circuit we can achieve a higher

boost converter switching frequency along with a lower sampling frequency to meet the requirements of the slower processing time of the DSP microcontroller.

1.7 Thesis Outline

The outline of the thesis is as follows:

In Chapter 2, the Fuzzy logic based scheme with variable incremental reference current is proposed and a brief description of the Fuzzy logic controller is provided. The design of the controller with the choice of input and output variables, choice of membership functions, rule base etc. is also provided.

In Chapter 3, two non-switching zones based schemes are proposed and the algorithm for the same is discussed. The design of the reduced Fuzzy controller is also provided.

In Chapter 4, simulation results carried out in the MATLAB/Simulink environment are presented. A comparison is drawn between the four peak current control based MPPT schemes to assess the theoretical potential of these methods.

In Chapter 5, experimental results of the prototype are presented and the design of the proposed control schemes is presented. A DSP based microcontroller (dSPACE) has been used to implement the control system. The limitations of the dSPACE system has been identified and suitable measures to overcome these have been described which include the analog implementation of peak current control as well as the use of an external clock and interrupt generator circuit. A second comparison of the performance of the four MPPT methods is carried out now considering the practical implementation limitations imposed by a current DSP system.

CHAPTER 2

FUZZY LOGIC CONTROLLER

2.1 INTRODUCTION

As was mentioned before in Chapter 1, the conventional peak current control based algorithm used a fixed magnitude variation of reference current, which was chosen as a compromise between transient and steady state performance. In this thesis we use a Fuzzy logic based controller along with instantaneous values of PV voltage and current and peak current control for determining not only the direction of the next perturbation (variation of reference current) but also its magnitude, by which one can enhance both transient and steady-state operation simultaneously.

A subjective Fuzzy model of the system is designed based on prior expert knowledge of the system. The Fuzzy logic controller (Fig.2.1) is divided into four sections: Fuzzification, rule-base, inference and defuzzification. The inputs to the Fuzzy logic controller are change in PV array power (ΔP_{PV}) and change in PV array current (ΔI_{PV}) and the output is the step change in converter reference current (ΔI_{REF}).

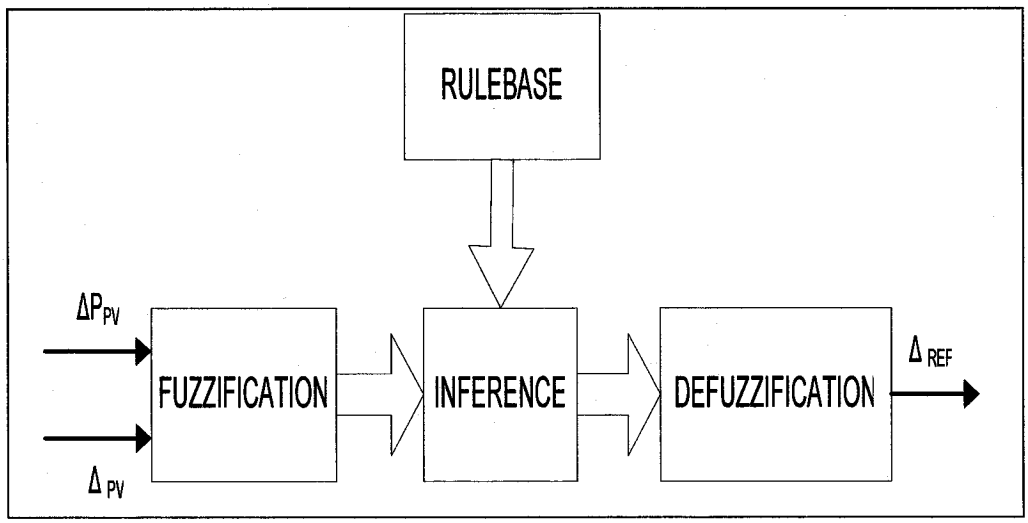

Fig.2.1 Block Diagram of the Fuzzy controller

2.2 FUZZIFICATION

The Fuzzy model for this thesis is based on the model presented in [10]. However a few modifications were carried out to improve the performance of our system. As is the norm with Fuzzy systems, model development has no systematic approach. Thus modifications were carried out by way of testing the Fuzzy model with the whole PV system through computer simulations and checking if the desired performance was attained.

The universe of discourse for input variable 1 (ΔP_{PV}) is divided into seven Fuzzy sets: PB (Positive Big), PM (Positive Medium), PS (Positive Small), ZZ (Zero), NS (Negative Small), NM (Negative Medium) and NB (Negative Big). As opposed to [10] where the Fuzzy set PS assumes a membership value greater than zero beginning at the origin, in the present model the Fuzzy set PS is offset from the origin in order to speed up the start-up process and at the same time prevent variation of the reference current at the MPP. Additional Fuzzy sets PM and NM have also been added to improve the control surface and allow a smooth transition from the transient to the steady-state.

The universe of discourse for input variable 2 (ΔI_{PV}) is divided into 3 Fuzzy sets: N (Negative), Z (Zero) and P (Positive).

The universe of discourse for the output variable (ΔI_{REF}) is divided into 7 Fuzzy sets: PB (Positive Big), PM (Positive Medium), PS (Positive Small), ZZ (Zero), NB (Negative Big), NM (Negative Medium) and NS (Negative Small). The Fuzzy sets PM, PB and NM, NB of the output variable associated with the transient response are constructed separate from the rest of the membership functions which are associated with the steady-state response. This enhances both the transient and the steady state performance providing a larger step variation of current during the transient phase and an almost zero step variation of current in the steady-state.

The membership functions for the input and output variables are displayed in the Fig.2.2-2.4. The membership functions for the input and output variables were designed to model the unsymmetrical nature of the PV panel $P_{PV} \times I_{PV}$ curve. The Membership functions are denser at the center to provide greater sensitivity in the region near the MPP. Input membership functions are normalized and suitable tuning gains are used to match the inputs to the respective universes of discourse. The selection of these tuning gains is discussed later in this Chapter and in Chapter 4.

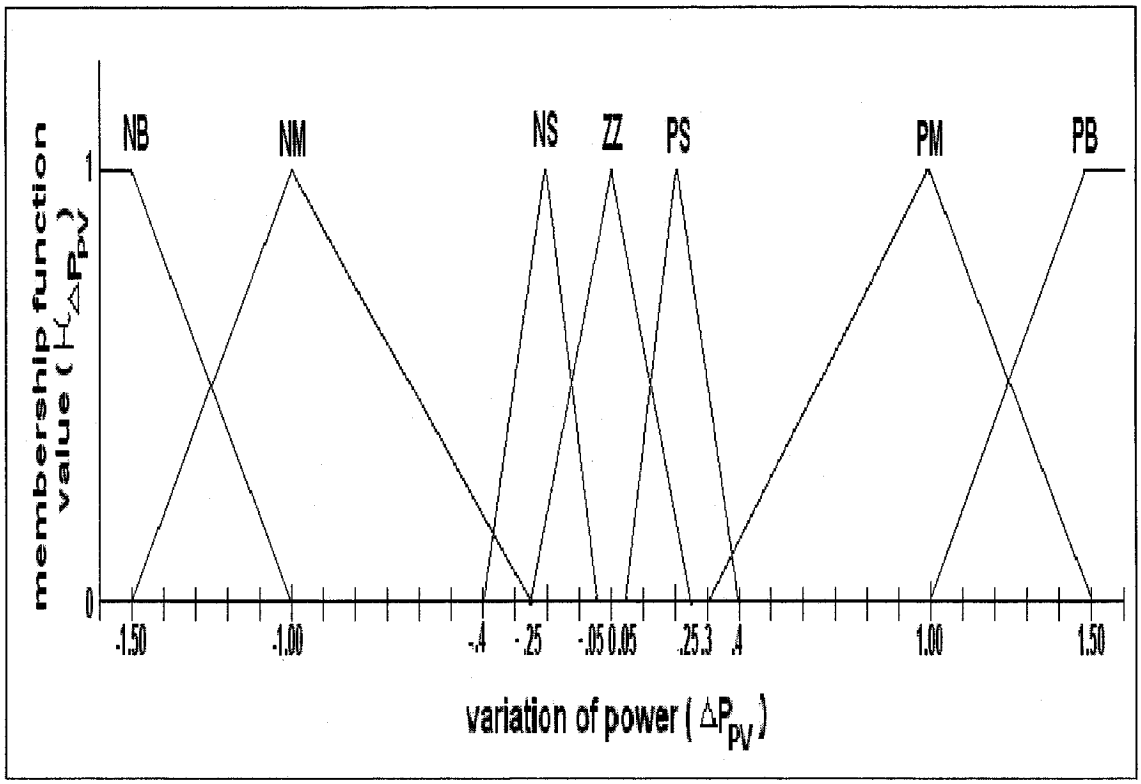

Fig.2.2 Membership functions for the Input ΔP_{PV}

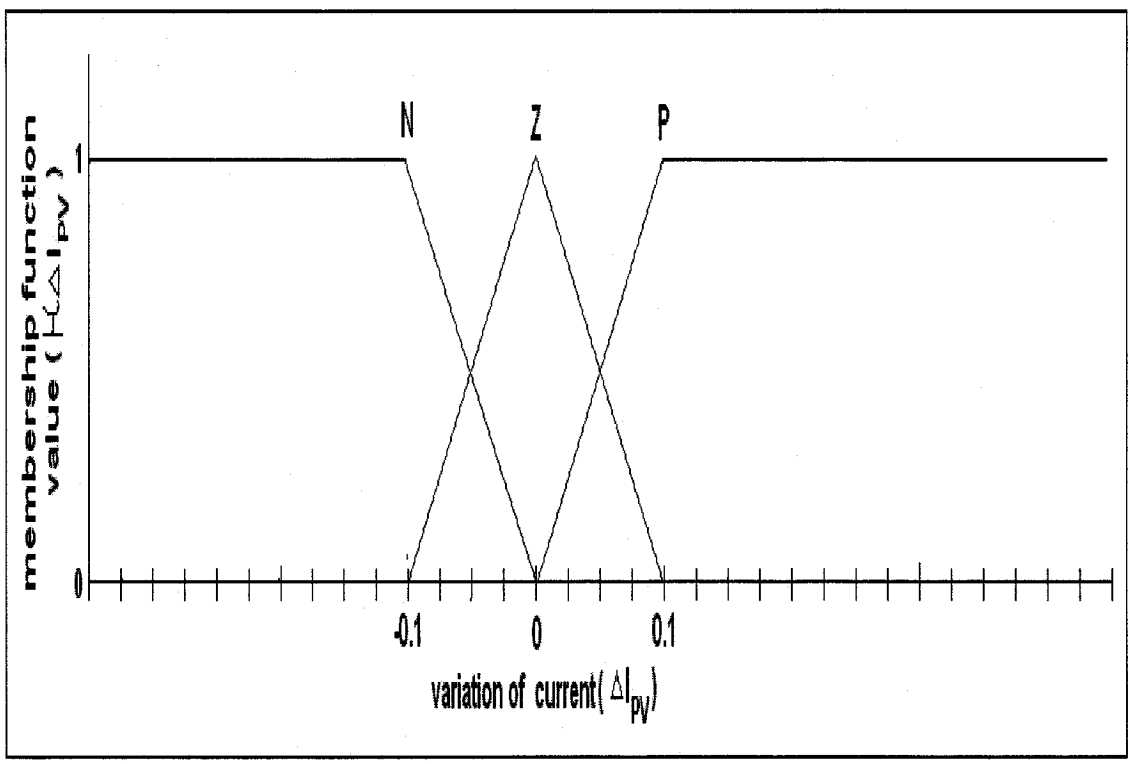

Fig.2.3 Membership functions for the input ΔI_{PV}

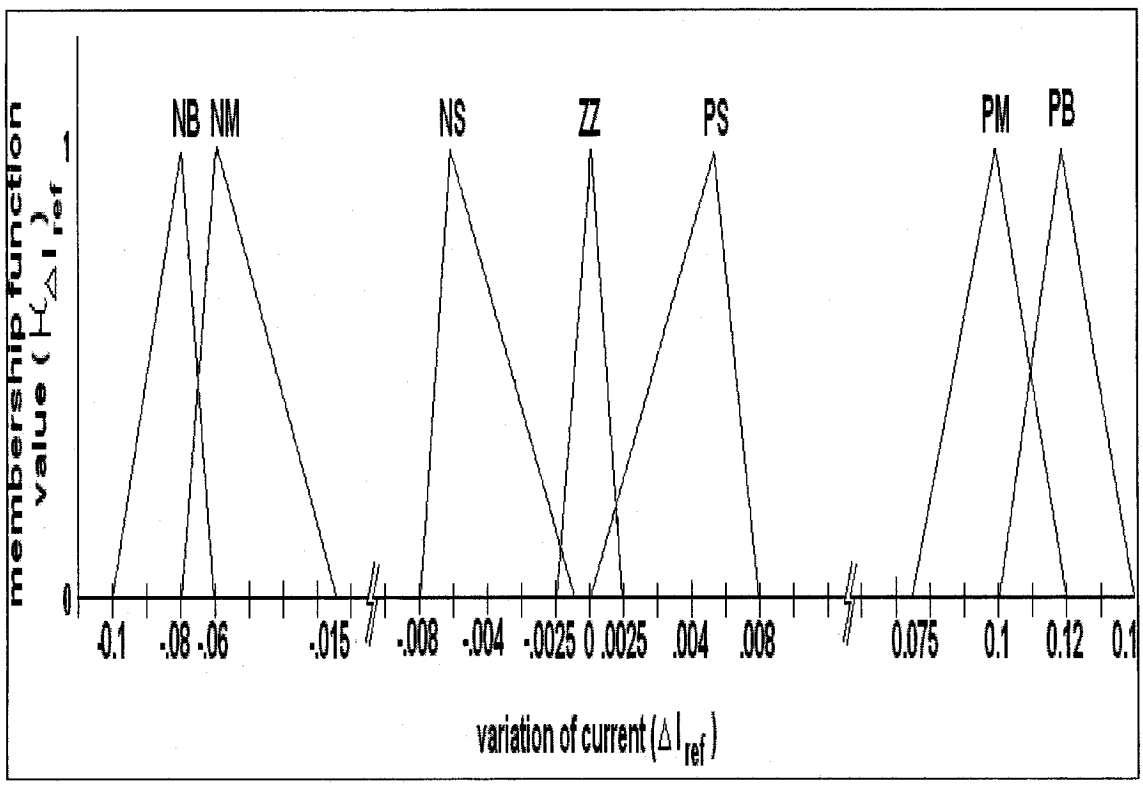

Fig. 2.4 Membership functions for the output ΔI_{REF}.

2.3 Rule Base [10]

The rule base for the Fuzzy logic controller is designed based on the rule base provided in [10] as it matches the requirements of our application. The Fuzzy algorithm tracks the maximum power based on the master-rule: "If the last change in the reference current (I_{REF}) has caused the power to increase keep changing the reference current in the same direction; else if it has caused the power to drop, move it in the opposite direction" which is the basic principle of the P&O Method. A rule base consisting of 19 rules is designed. The master rule is converted into the first 12 rules displayed in Table 2.1. Additional rules are required to compensate for the change of the PV array characteristic curves with atmospheric conditions, leading to an overall drift of the optimum point. Rules 13-16 are designed for this purpose. It is shown in [10] that an artificial inertia is required in order

to keep the system from stopping whenever a zero-crossing of the power is detected, resulting in a tendency for ongoing motion for a few cycles. Rules 17-18 are also designed to prevent the stabilizing effect in a region other than that of true peak power. Finally a single rule 19 is provided to stabilize the operation of the system at the MPP.

Weights are generally added to rules to improve the reasoning accuracy and to reduce undesirable consequent [26]. Different rule weights have been used in [10] to cover varying conditions. The highest weights are given to the first set of 12 rules as they represent the normal system operation. Rules 13-18 are used to account for special conditions and hence are given a lower weight. Rule 19 is activated only when the system operates at the MPP and hence needs only a light weight.

The control surface for the Fuzzy model (with normalized membership functions) is shown in Fig.2.5, which represents the nonlinearity that is implemented by the Fuzzy controller [27]. It displays the response of the system to different combinations of ΔP_{PV} and ΔI_{PV}. The edges of the cube depict the behavior of the system in the transient state while the center of the cube represents the system response in the steady state. Variation of the tuning gains will modify the slope of the surface however the general behavior will remain the same.

Rule No.	If ΔP_{PV} is....	And ΔI_{PV} is....	Then ΔI_{REF} is....	Rule weights
1	PB	P	PB	1.0
2	PM	P	PM	1.0
3	PS	P	PS	1.0
4	PB	N	NB	1.0
5	PM	N	NM	1.0
6	PS	N	NS	1.0
7	NB	P	NB	1.0
8	NM	P	NM	1.0
9	NS	P	NS	1.0
10	NB	N	PB	1.0
11	NM	N	PM	1.0
12	NS	N	PS	1.0
13	PB	Z	PM	0.5
14	PM	Z	PS	0.5
15	NB	Z	NM	0.5
16	NM	Z	NS	0.5
17	ZZ	P	PS	0.5
18	ZZ	N	NS	0.5
19	ZZ	Z	ZZ	0.25

Table 2.1 Rule base for the Fuzzy model

2.4 INFERENCE METHOD

The inference method determines the output of the Fuzzy controller. Mamdani's inference method has been used in our system along with the max-min composition method. This is because this method is computationally more efficient and has better interpolative properties than other inference methods such as those based on the Compositional Rule of Inference (CRI) and Generalized Modus Ponens (GMP) and

Sugeno inference methods. Hence, Mamdani's inference method is usually popular for most control engineering applications.

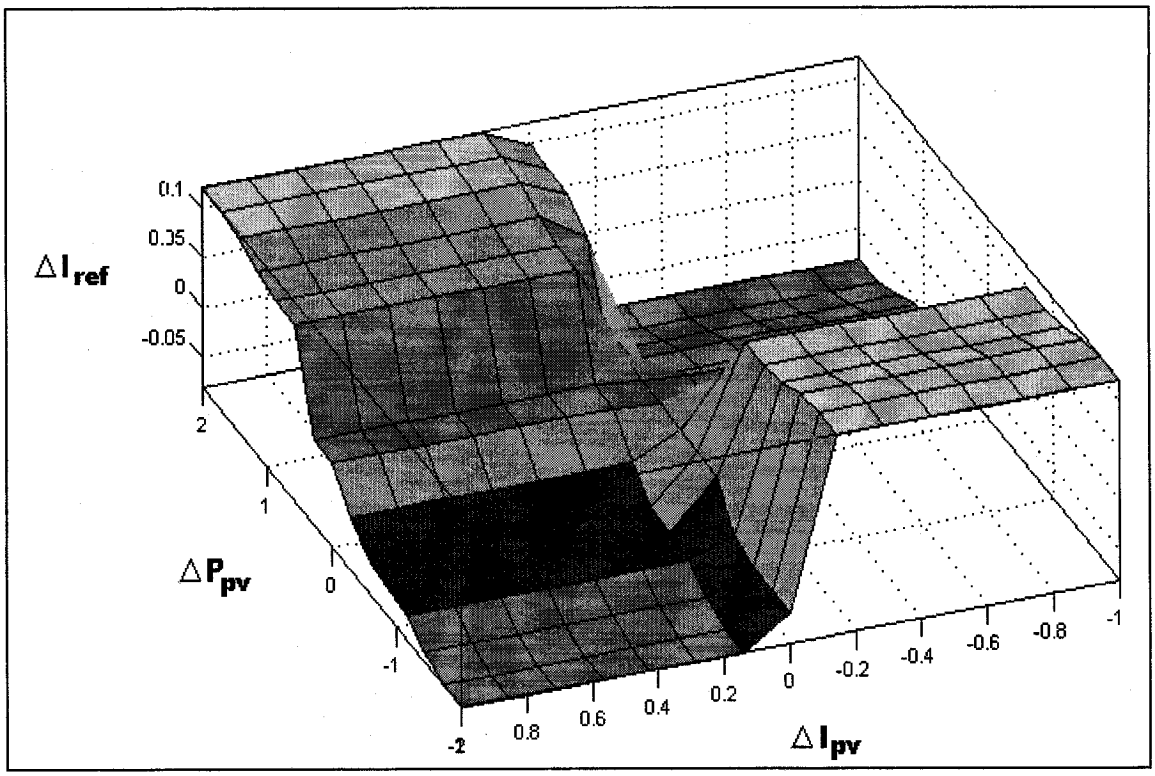

Fig. 2.5 Control surface for the Fuzzy model.

2.5 DEFUZZIFICATION METHOD

The output of the Fuzzy controller is a Fuzzy set. However a crisp output value is required. Hence the output of the Fuzzy controller should be defuzzified. The centroid method is one of the commonly used defuzzification methods and is the one we will employ for the proposed system. This method has good averaging properties and simulation results showed that it provided the best results as compared to other defuzzification methods such as bisector, Middle of Maxima (MOM) etc.

2.6 TUNING VIA SCALING UNIVERSES OF DISCOURSE [27]

Scaling gains can be used at the input and output of the system to influence the performance of the resulting Fuzzy control system and hence are a convenient parameter for tuning.

2.6.1 Input Scaling Gains

Let us observe the effects of using input scaling gains. The same effect as that of the use of scaling gains can be obtained by changing the labeling of the horizontal axis of the membership functions. When the scaling gain is 1 it corresponds to the originally designed membership functions of the corresponding input. The use of a scaling gain say G results in scaling the horizontal functions of the membership functions by $\frac{1}{G}$.

The effects of the scaling gains can be observed as follows

- If G = 1 there is no effect on the membership functions.
- If G < 1 each number on the horizontal axis of the membership function is multiplied by $\frac{1}{G}$ i.e. the membership functions are uniformly "spread out" by a factor of $\frac{1}{G}$.
- If G > 1 membership functions are uniformly "contracted" by a factor of $\frac{1}{G}$.

The scaling gains affect the meaning of the linguistics that forms the basis for the design of the Fuzzy controller.

- If G = 1, there is no effect on the meaning of the linguistic values.

- If G < 1, the membership functions are uniformly "spread out" and the meaning of the linguistics is altered, i.e. for example Fuzzy set Positive Big 'PB' of input (ΔP_{PV}) is characterized by a membership function that represents larger numbers.
- If G > 1, the membership functions are uniformly "contracted" and the meaning of the linguistics is altered, again, Fuzzy set Positive Big 'PB' of input (ΔP_{PV}) is characterized by a membership function that represents smaller numbers.

Similar comments can be made about the linguistics associated with the other Fuzzy sets. Thus the input scaling factors have an inverse relationship in terms of their effect on scaling.

2.6.2 Output Scaling gains

Scaling gains can also be used to tune output membership functions. The effect of scaling gain 'h' on the output membership functions can be defined as follows.

- If h = 1 , there is no effect on the membership functions.
- If h < 1 , the output membership functions are contracted and their linguistics quantify smaller numbers.
- If h > 1 , the output membership functions are spread out and their linguistics quantify larger numbers.

Thus there exists a proportional effect between the scaling gain 'h' and the output membership functions.

The tuning of scaling gains for a Fuzzy system is also termed as "scaling a Fuzzy system".

2.6.3 Initial Guess for Tuning Gains of Proposed Fuzzy Model

We desire the step-size of reference current to be approximately 0.14 A during start up. Hence a change in current of 0.14 A should correspond to the Fuzzy set P of the input ΔI_{PV}. Hence the tuning gain for ΔI_{PV} could be 1 to begin with. From the simulated PV power versus current characteristic corresponding to a short circuit current $I_{SC} = 3.45$ the change in power ΔP_{PV} corresponding to ΔI_{PV} of 0.14 A is about 3W. This should correspond to Fuzzy set PB of input ΔP_{PV}. Hence the initial tuning gain for input ΔP_{PV} could be 0.5.

The output tuning gain is taken to be unity as the membership functions for the output variable are designed based on the desired values of step-changes of reference current. However, further simulations are run with the model of the PV system to determine the ideal tuning gains which are illustrated in Chapter 4.

2.7 TESTING

Results of computer simulations and experimental work undertaken to analyze the transient and steady state behavior results for the scheme described in this chapter will be presented in Chapters 4 and 5 and compared with the other peak current control based MPPT schemes.

2.8 CONCLUSIONS

The use of a Fuzzy Logic based controller has been suggested to output an incremental reference current that varies with both magnitude and direction depending on the operating point of the system on the PV panel $V_{PV} \times I_{PV}$ characteristic.

The design of the membership functions for the input and the output variables of the Fuzzy controller are presented. Even though no systematic procedure exists with regards

to the development of the Fuzzy controller, an attempt has been made to incorporate prior knowledge of the PV system in the design of the Fuzzy controller. The rule base is specified and the criteria for the selection of specific rules are discussed. The choice of the inference and defuzzification method is mentioned.

Finally a brief discussion of Fuzzy scaling gains is provided and an initial guess for the tuning gains to be used with the Fuzzy controller is provided.

CHAPTER 3

HYBRID MPPT SYSTEM

3.1 INTRODUCTION

As was mentioned before in Chapter 1, the use of fixed variation of reference current in a peak current control based MPPT algorithm to track the MPP results in a sub-optimum solution based on a compromise between the transient and steady-state performance. In recent times new hybrid MPPT systems have been introduced which use different strategies for the transient and the steady state operation periods in order to speed up the transient response of the system. These methods [28,29] use a particular strategy to move the operating point towards the vicinity of the MPP faster than with any of the conventional MPPT algorithms and then control is shifted back to the conventional MPPT algorithm which may be of the types such as P&O, IncCond etc. In [28] a novel MPPT method was used along with the Incremental conduction MPPT method. In this method the PV panel $V_{PV} \times I_{PV}$ characteristic is divided into two regions by a linear or polynomial function: one which contained the MPP and the other which did not. If the operating point was found to be in the latter, it was rapidly accelerated towards the MPP through larger step changes in reference voltage. Once in the vicinity of the MPP the algorithm was shifted to the Incremental Conduction MPPT method. [29] involves the calculation of a certain factor 'β' which is dependent on PV panel current and voltage and atmospheric conditions like irradiance level and temperature. Once this factor is within a

certain range corresponding to operation in the vicinity of the MPP, control is shifted back to the conventional MPPT algorithm.

3.2 Fixed ΔI_{REF} and Non-Switching Zones

The strategy mentioned in [28] has been modified and implemented in this thesis to accelerate the transient response of the system. The implementation in this thesis is based on the division of the V_{PV} x I_{PV} characteristics of a PV panel into three regions or zones as shown in Fig.3.1. Two of these regions do not contain any MPP and are non-switching zones while the third contains the MPP and is a switching zone.

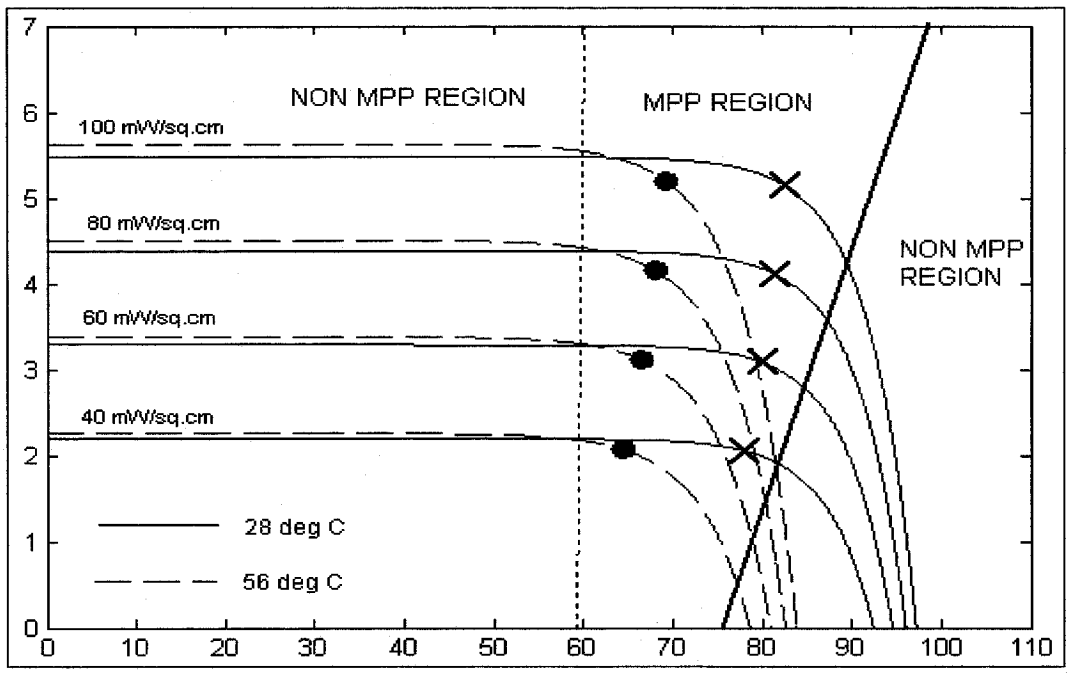

Fig.3.1 PV Panel V_{PV} x I_{PV} characteristics with MPP and Non-MPP Regions

The algorithm mentioned in [28] had to be modified to suit the peak current control based algorithm. In our case when the operating point is to the right of the linear function 'CHAR 1' represented by the solid line in Fig.3.1, the switch of the power converter is always turned 'ON' with duty cycle (D) equal to 1 to increase I_{PV} at maximum rate for minimum possible operation at this non-MPP region. Thus the current in the inductor of

the boost converter continuously increases, which means the PV panel output current also continuously increases and hence the PV power increases. The energy is initially stored in the boost inductor and then supplied to the output. Once the operating point crosses into the MPP containing region, the algorithm is switched to the conventional fixed-step size based MPPT algorithm. A second curve 'CHAR 2' can be used to define a second non-MPP region for large values of I_{PV}, represented by a dashed line in Fig.3.1. Operation in this region can occur for sudden reductions in irradiance levels. When the operating point is to the left of the linear function 'CHAR 2' the switch of the power converter is always turned 'OFF' with D equal to 0, resulting in the maximum rate of fall for I_{PV} . Thus the current in the inductor of the boost converter continuously decreases and the operating point accelerates towards the MPP containing region. Once the operating point crosses into the MPP containing region, the algorithm is switched to the conventional fixed-step size based MPPT algorithm. However it must be noted that a small value can be used for the incremental reference current for improved steady-state performance. Since this value is very small no compromise is required as regards the selection of the incremental reference current and a suitable value can be chosen corresponding to operation in the steady-state.

It is mentioned in Chapter 1 that with the increase in irradiance, the short circuit current I_{SC} increases proportionally and the open circuit voltage, V_{OC} increases logarithmically. V_{OC} decreases linearly with increase in PV panel ambient temperature. The maximum power point (MPP) of the PV panel also moves around with varying temperature and irradiance but the region where the MPP occurs is still limited. The values of open circuit

voltage V_{OC}, short circuit current I_{SC} , current at MPP I_{MPP} and Voltage at MPP V_{MPP} can be calculated or measured at standard conditions of temperature and irradiance.

3.2.1 Description of proposed algorithm

Fig.3.2 shows the flowchart for the proposed MPPT scheme based on non-switching zones. Fig.3.3 and Fig.3.4 show the V_{PV} x I_{PV} characteristic for a particular condition of operating temperature and irradiance. The two linear characteristics 'CHAR 1' and 'CHAR 2' as described before divides the V_{PV} x I_{PV} characteristic of the PV panel into three regions. The right-side of the characteristic 'CHAR 1' does not contain the MPPT. Similarly the left-side of characteristic 'CHAR 2' does not contain the MPPT. The algorithm operates as follows: Fig.3.3 describes the operation of the system when the operating point is to the right of 'CHAR 1'. The sampled values of I_{PV} and V_{PV} are obtained as is required by the conventional peak current control based MPPT algorithm. Let us consider operation at time instant 'n' in Fig.3.3 when the operating point is to the right of 'CHAR 1'. From the sampled value of I_{PV}, i.e. $I_{PV}(n)$, the corresponding value of Voltage, $V_{TO}(n)$ on the linear characteristic is obtained, which is compared with the sampled value of V_{PV}, i.e. $V_{PV}(n)$. As seen in Fig.3.3, if $V_{PV}(n)$ is greater than $V_{TO}(n)$ then the operating point of the PV system is in the region that does not contain the MPP. Hence the switch of the boost converter remains 'ON' so that current ramps up and consequently the output power of the PV panel also increases. At time instant 'm' $V_{TO}(m)$ is greater than or equal to $V_{PV}(m)$, which means the operating point of the PV system is close to or operating in the region that contains the MPP. Hence the control is shifted back to the original conventional algorithm based on the fixed-step size increment

of reference current. Thus the transfer to the conventional algorithm takes place in the vicinity of the MPP.

Fig.3.4 describes the operation of the system when the operating point is to the left of 'CHAR 2'. At time instant 'n' the operating point is to the left of 'CHAR 2'. From the sampled value of I_{PV}, i.e. $I_{PV}(n)$ the corresponding value of Voltage, $V_{TS}(n)$ on the linear characteristic 'CHAR 2' is obtained, which is compared with the sampled value of V_{PV}, i.e. $V_{PV}(n)$. As seen in Fig.3.4, if $V_{PV}(n)$ is less than $V_{TS}(n)$ then the operating point of the PV system is in the region that does not contain the MPP. Hence the switch of the boost converter remains 'OFF' so that current decreases and consequently the output power of the PV panel increases. At time instant 'm' $V_{TS}(m)$ is less than or equal to $V_{PV}(m)$, which means the operating point of the PV system is close to or operating in the region that contains the MPP. Hence the control is shifted back to the original conventional algorithm based on the fixed-step size increment of reference current. Thus the transfer to the conventional algorithm takes place in the vicinity of the MPP. The equation of the linear characteristic is selected so that it intersects the V_{PV} x I_{PV} curve of the PV panel close to the MPP but does not interfere with the working of the conventional peak current control-based algorithm during steady state operation.

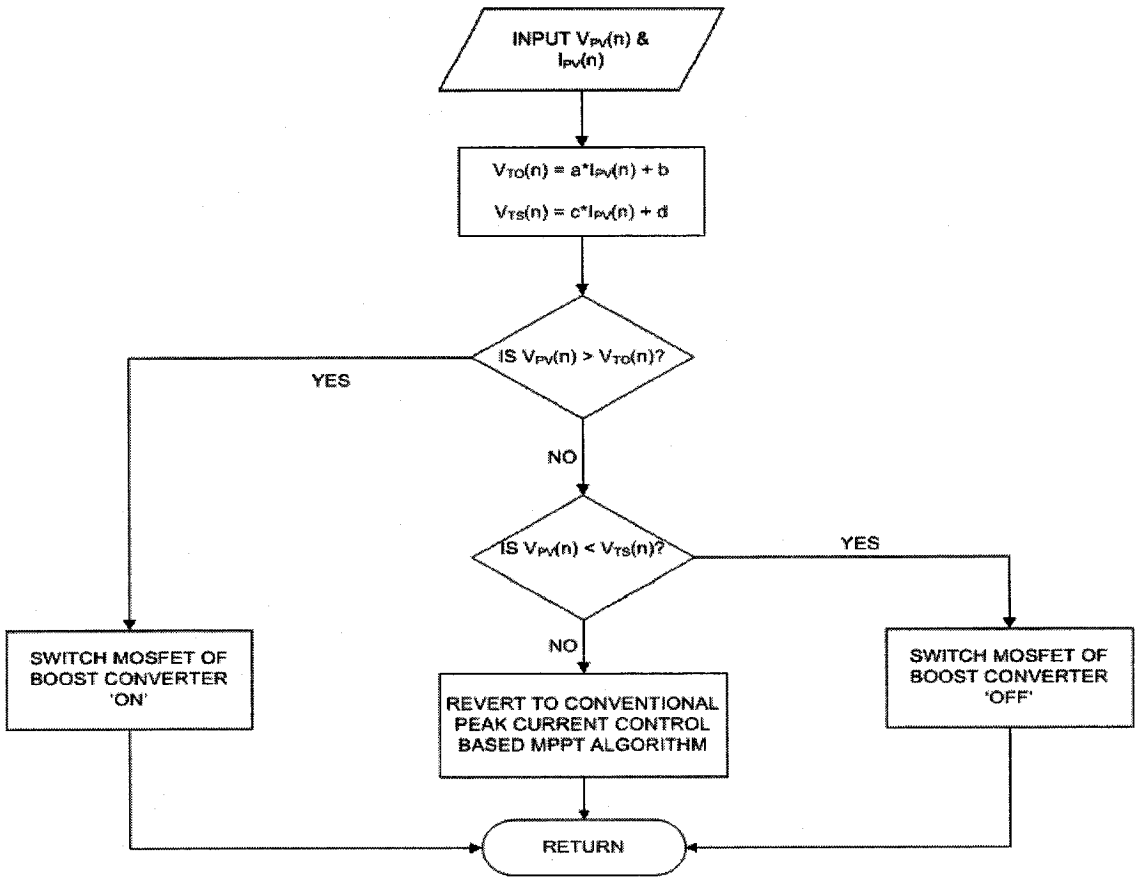

Fig. 3.2 Algorithm for operation with non-switching zones

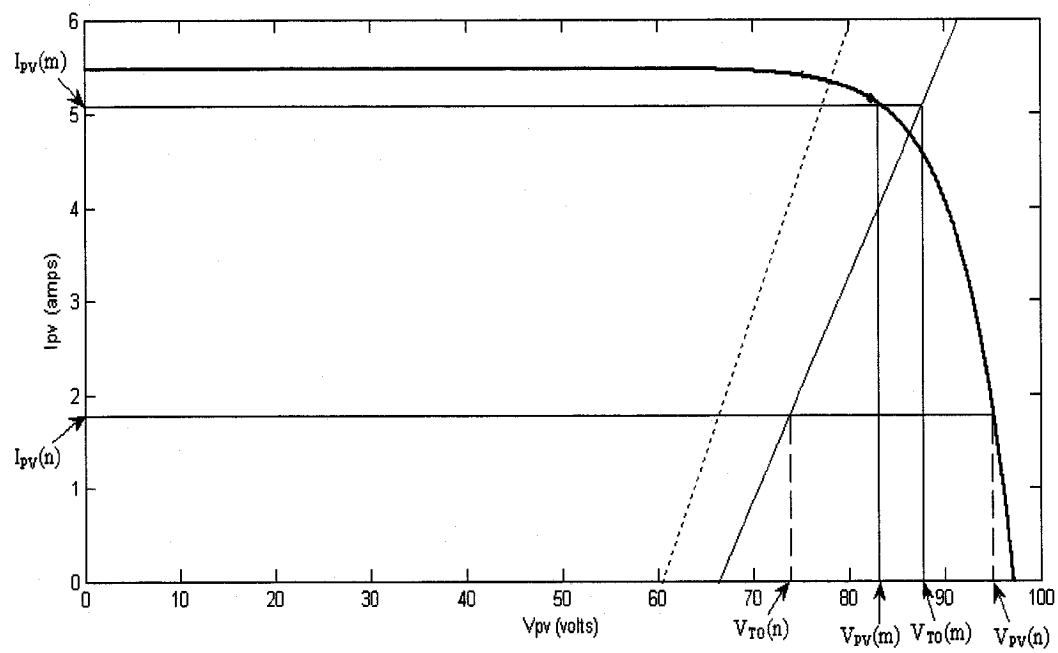

Fig.3.3 Operation in non-switching zone to the right of 'CHAR 1'

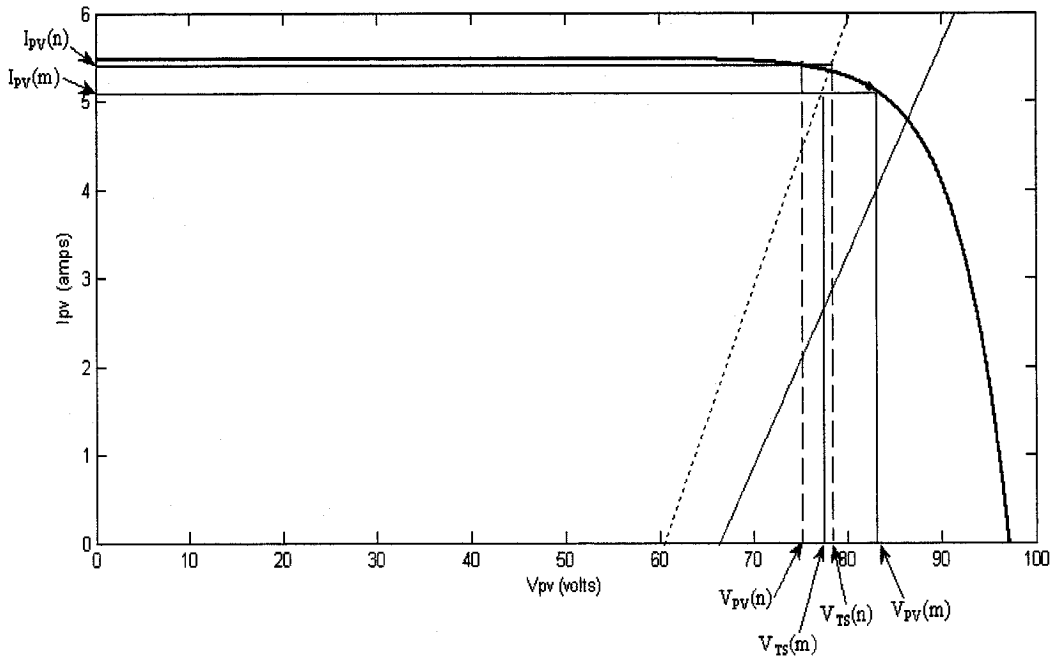

Fig.3.4 Operation in non-switching zone to the left of 'CHAR 2'

3.3 Reduced Fuzzy and Non Switching Zones

The Hybrid MPPT system described before can be used along with the Fuzzy-based MPPT system described in Chapter 2. As described before once the operating point crosses into the MPP containing region the control can be shifted to the Fuzzy logic based peak current control MPPT algorithm. However the use of the original fuzzy controller described in Chapter 2 presents an increased computational burden due to the increased number of fuzzy sets of both the input and output variables and increased number of rules to model both the transient and steady-state behavior of the system. In this case the Fuzzy controller can be scaled down so as to take into account operation only in the vicinity of the MPP i.e. in the MPP containing region. The modified membership functions are presented in Figs.3.5-3.7. It is seen that the input variable ΔP_{PV} has three fuzzy sets NS, ZZ and PS as compared to the Fuzzy logic controller described

in Chapter 2 where it had seven Fuzzy sets. Similarly the output variable ΔI_{REF} has three Fuzzy sets as compared to seven in the Fuzzy logic controller described in Chapter 2.

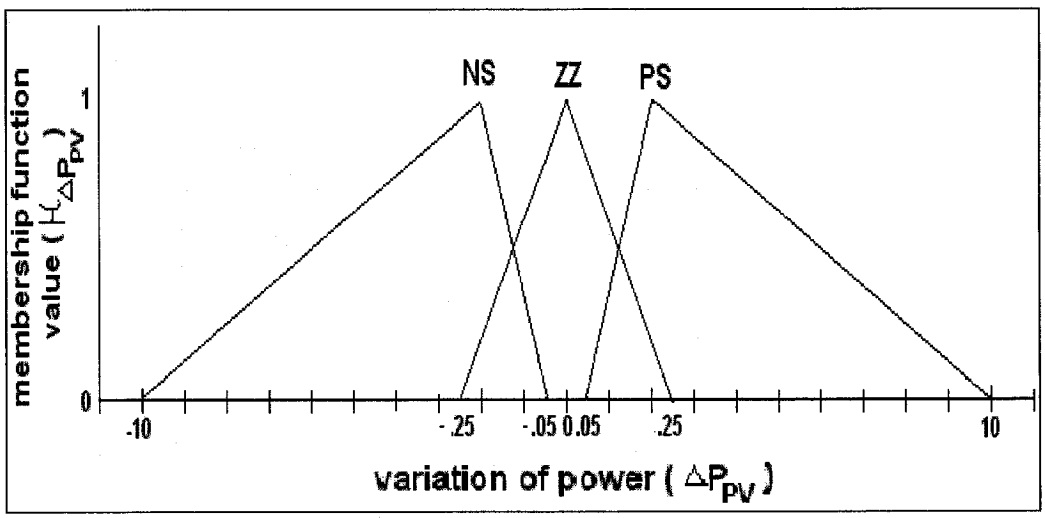

Fig.3.5 Membership functions for the Input ΔP_{PV}

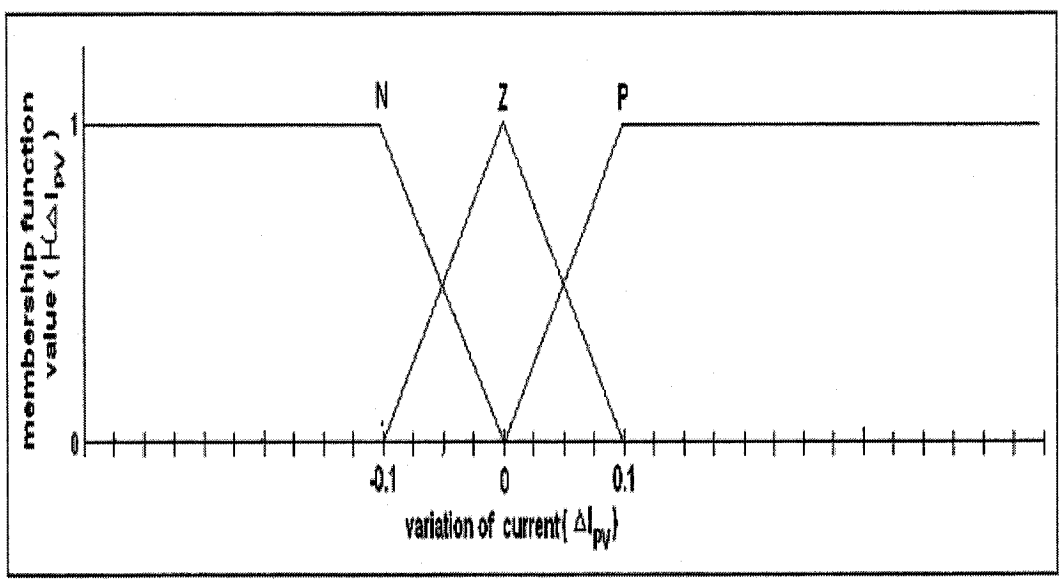

Fig.3.6 Membership functions for the input ΔI_{PV}

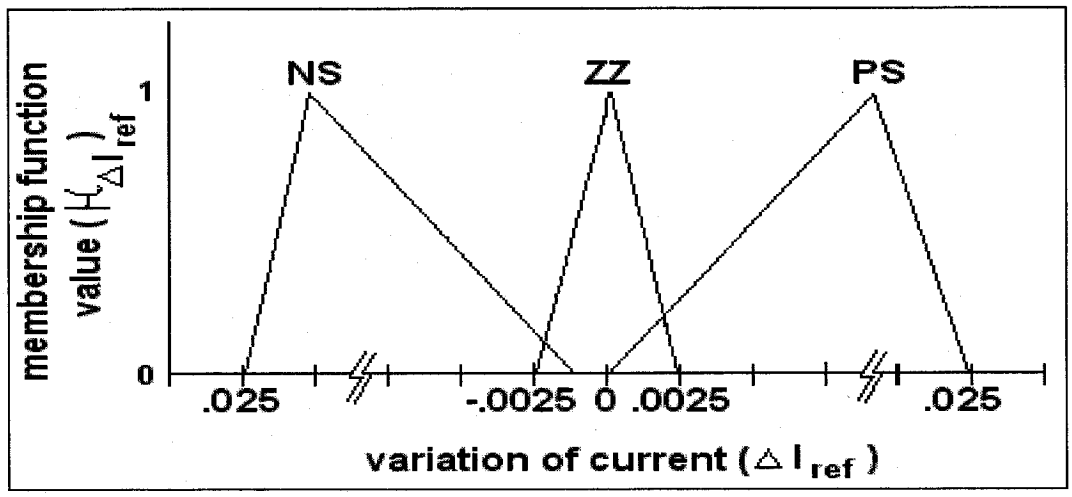

Fig. 3.7 Membership functions for the output ΔI_{REF}.

The modified Rule base has been displayed in Table 3.1. It can be seen as compared to Table 2.1 that the number of rules has been reduced to 5 from 19. This could provide an advantage in terms of computational time.

Rule No.	**If** ΔP_{PV} is....	**And** ΔI_{PV} is....	**Then** ΔI_{REF} is....	Rule weights
1	PS	P	PS	0.5
2	PS	N	NS	0.5
3	NS	P	NS	0.5
4	NS	N	PS	0.5
5	ZZ	Z	ZZ	1.0

Table 3.1 Rule base for the reduced Fuzzy model

3.4 TESTING

Results of computer simulations and experimental work undertaken to analyze the transient and steady state behavior results for the schemes described in this Chapter will be presented in Chapters 4 and 5 and compared with the previously described peak current control based MPPT schemes.

3.5 CONCLUSION

This Chapter introduced the concept of non-switching zones in the V_{PV} x I_{PV} plane for implementing hybrid MPPT algorithms. By operating the power electronics converter with *D* equal to 0 or *D* equal to 1, depending on which non-MPP region the system operates, one pushes the operating point the fastest way possible towards the MPP region, where the conventional peak current control based P&O MPPT is used. The hybrid scheme allows the use of smaller perturbations, reducing the power oscillation around the MPP and increasing the power yield in the steady-state without compromising the transient response. The use of variable size perturbations based on a reduced Fuzzy logic controller should further reduce the power oscillations around the MPP.

CHAPTER 4

SIMULATION RESULTS

4.1 INTRODUCTION

The Fuzzy logic based Peak Current Control MPPT algorithm described in Chapter 2 and the non-switching zones based schemes with fixed ΔI_{REF} and the reduced Fuzzy controller described in Chapter 3 were simulated in the MATLAB/Simulink environment and compared with the standard scheme using fixed ΔI_{REF}. Simulations were also used to tune the gains of the Fuzzy controller.

4.2 SIMULATION SCHEMATICS OF THE STANDARD SCHEME WITH FIXED ΔI_{REF} [2]

The main circuit schematic for the simulation of the standard scheme with fixed ΔI_{REF} is shown in Fig.4.1. The various blocks used are similar to those in [2]. A brief description of the blocks is given below.

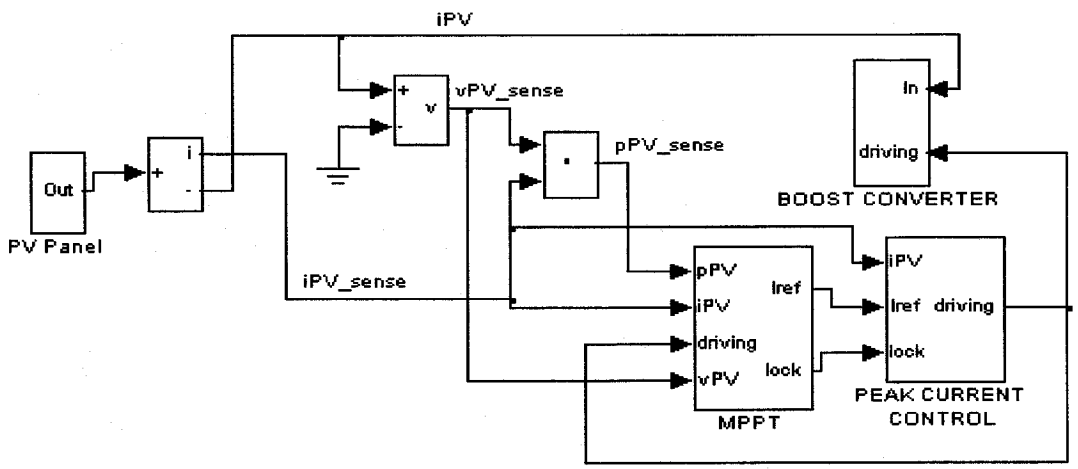

Fig. 4.1 Main simulation schematic for standard scheme with fixed ΔI_{REF} [2]

4.2.1 PV Panels [2]

The simulation model of the PV panel, as shown in Fig.4.2 consists of a current source in parallel with a voltage source. The effect of varying irradiance on the short circuit current I_{SC} of the PV panel can be emulated by varying the value of current in the current source CS1. The blocks to the right of CS represent the shunt branch of the PV panel model. The output of the PV panel is represented by the connector 'out'. The PV output voltage is obtained from the look-up table in [2].

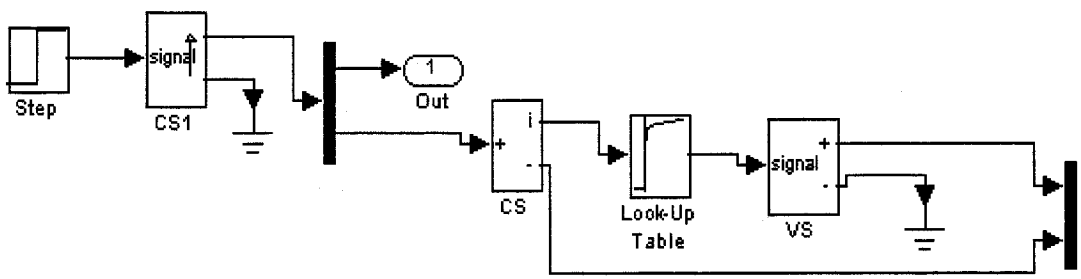

Fig.4.2 The Simulation Model of PV Panel

4.2.2 Boost Converter Simulation Model

A Boost DC/DC converter is used as the MPPT power converter in the PV system. The simulation model of the Boost DC/DC converter is shown in Fig.4.3. The Boost converter is modeled as a diode in series with a controlled voltage source, CVS1. If the driving signal is 'low' which corresponds to OFF state of the MOSFET a voltage of 24 V corresponding to the output battery voltage appears at the inductor terminal, and if the driving signal is 'high' corresponding to the ON state of the MOSFET a voltage of 0V would appear at the inductor terminal.

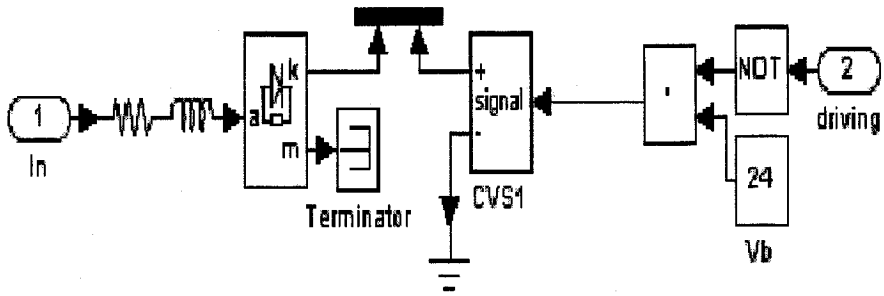

Fig. 4.3 Simulation Model of the Boost Converter

4.2.3 MPPT Block

The MPPT Algorithm is implemented in the MPPT block shown in Fig.4.4. Samples of PV power P_{PV} and PV current I_{PV} are taken every switching cycle and the direction of perturbation of I_{REF} is updated depending on the operating point of the system on the PV $V_{PV} \times I_{PV}$ characteristic as determined by ΔP_{PV} and ΔI_{PV}.

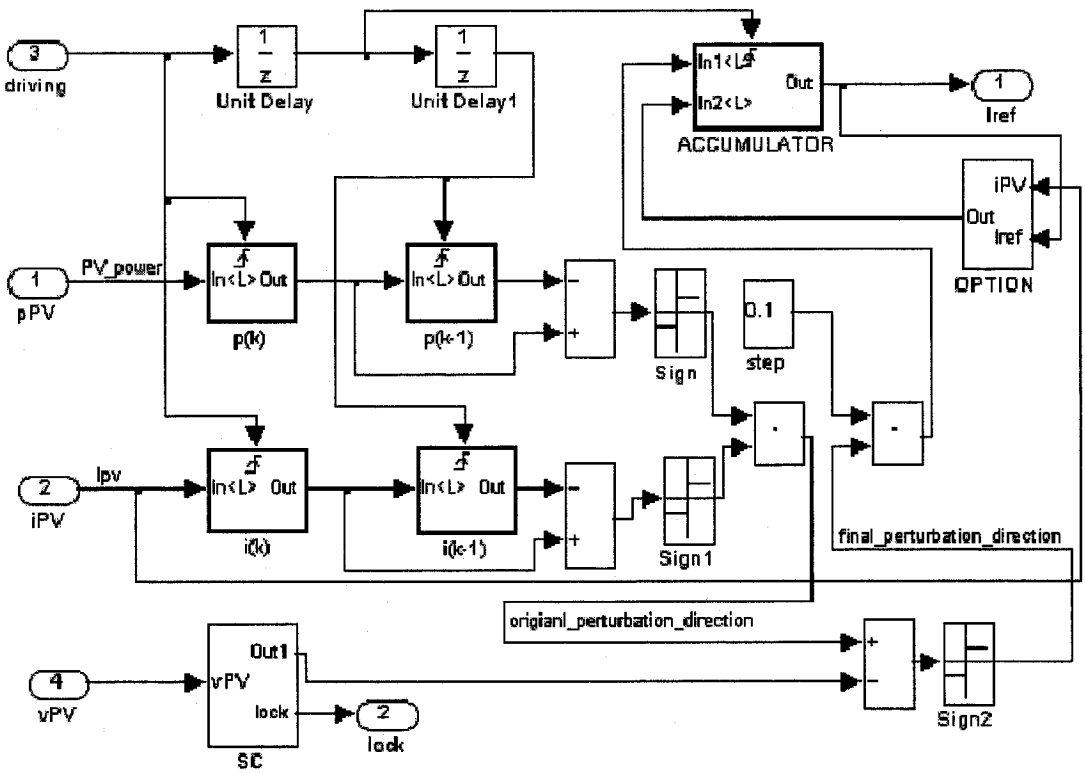

Fig. 4.4 Simulation Model of the MPPT block

Additional blocks such as the Short Circuit (SC) block and OPTION block described in [2] had been used to improve the operation of the system under rapidly changing atmospheric conditions. The SC block upon detection of a low value for V_{PV}, sends a signal to the MPPT algorithm to reduce I_{REF} continuously and a signal to the PCC block to keep it operating with minimum duty cycle. Otherwise, the PCC block would always operate with maximum duty cycle, since I_{PV} cannot reach I_{REF} with $V_{PV} = 0$ V, leading to a long transient with $P_{PV} = 0$ W. The OPTION block resets the value of I_{REF} to the instantaneous value of I_{PV}, when the difference between them exceeds a certain value. This block would usually come into effect during start-up and transient conditions such as large irradiance variations.

4.2.4 Peak Current Control Block

The schematic for the peak current control block is shown in Fig.4.5. At the start of the switching cycle, when *Dmin* becomes '1', the output of the OR gate is '1' and the switch turns 'ON'. This in turn also enables the 'AND' gate. The output of the comparator block is usually determined by the relationship between the I_{PV} and I_{REF}. At the start of the switching cycle I_{PV} is usually less than I_{REF} and hence the output of the comparator block is '1'. Thus even though *Dmin* returns to '0' after a short duty cycle the switch remains on till I_{PV} is greater than or equal to I_{REF} after which the AND gate is disabled and the switch turns off as the Gating signal returns to '0'. In case I_{PV} cannot reach I_{PV}, The switch will turn off when *Dmax* returns to '0'. Thus the duty cycle of the switch is restricted between *Dmin* and *Dmax*. The unit delay is added to avoid any algebraic loop in the simulation.

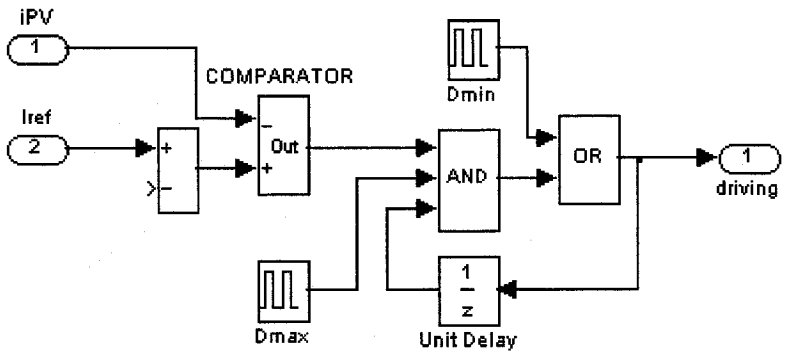

Fig. 4.5 Simulation Schematic of the Peak Current Control Block

4.3 Simulation Schematics Of The Fuzzy Logic Based Scheme With Variable ΔI_{REF}

Figure 4.6 shows the schematic of the Fuzzy logic based scheme with variable ΔI_{REF} system for simulation with MATLAB/Simulink. The PV output current I_{PV} and V_{PV} are measured and multiplied to obtain instantaneous PV power P_{PV}. The Sample and Hold block outputs variation of PV output current and PV output power at two consecutive sampling instants, which were taken for two different values of I_{REF}. These serve as inputs to the Fuzzy Logic block. The Fuzzy Logic block processes the inputs and outputs the incremental reference current ΔI_{REF}. The Accumulator block outputs the current reference I_{REF}. I_{REF} is given as an input to the Peak Current Control Block which outputs the driving signal to the Boost Converter so that I_{PV} follows I_{REF}. Similar simulation schematics have been used for the PV Panel, Peak Current Control and Boost Converter for the standard scheme with fixed ΔI_{REF} and the Fuzzy logic based scheme with variable ΔI_{REF}.

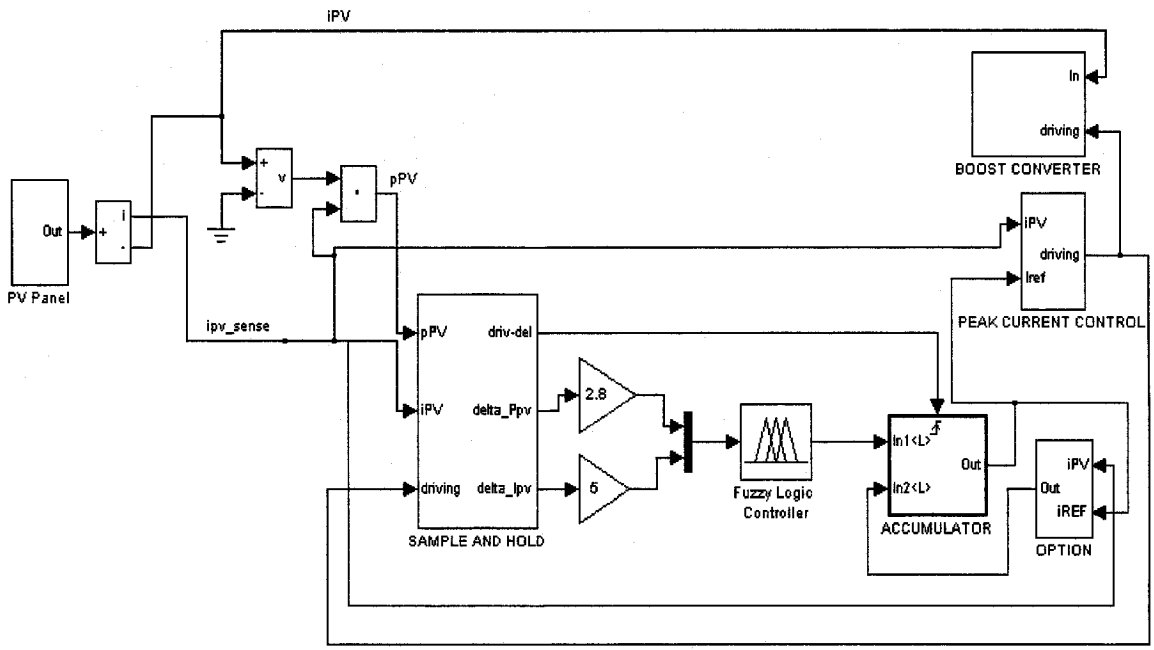

Fig.4.6 Main simulation schematic for the Fuzzy logic based scheme with variable ΔI_{REF}

4.3.1. Fuzzy Logic Controller

The Fuzzy Logic Controller is implemented using the Fuzzy Logic ToolBox available in MATLAB/Simulink. The designed Fuzzy Controller along with the input and output membership functions is input using the Fuzzy Inference system (FIS) editor available with MATLAB/Simulink. The suitable composition and aggregation method and the defuzzification method can be selected using the FIS editor. The Fuzzy Logic block outputs the incremental reference current (ΔI_{REF}) of suitable magnitude and direction depending on the location of the operating point of the system on the $P_{PV} \times I_{PV}$ curve of the PV panel model.

4.3.2 Fuzzy Inference System (FIS) Editor

The FIS editor is an effective Graphical User Interface (GUI) tool provided with the fuzzy logic toolbox in MATLAB/Simulink to facilitate the design of the Fuzzy logic controller. The FIS Editor pops up upon typing 'fuzzy' at the MATLAB prompt. The

Fuzzy logic controller can then be designed using the FIS editor and saved in the disk as a .fis file. Before the simulation has to be run the .fis file is exported to workspace and the name of the file is entered in the Fuzzy logic controller block in simulink.

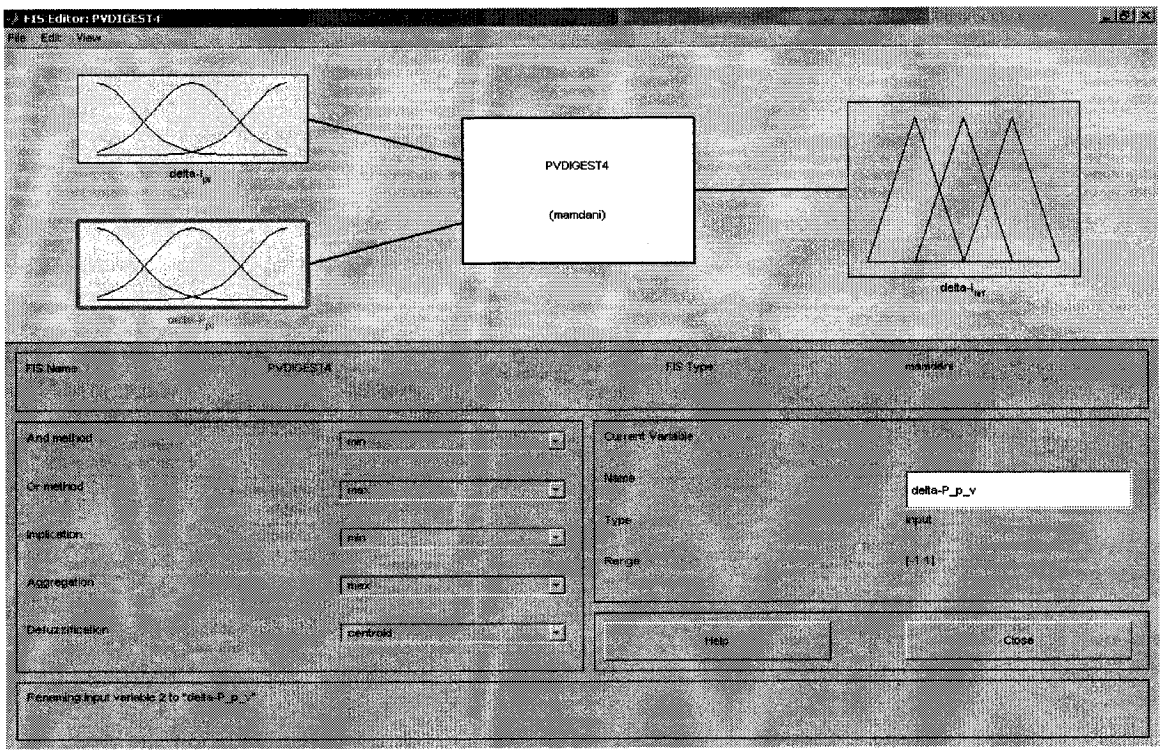

Fig.4.7 Fuzzy Inference System (FIS)

As shown in Fig. 4.7 the number of input variables can be selected along with various parameters of the Fuzzy Controller such as the implication method, aggregation method and the defuzzification method. As shown in Fig.4.8, Fig.4.9 and Fig.4.10, the membership functions for the input variables can be designed using the FIS editor. The shape of the membership function can be altered by selecting the desired shape from the drop-down menu corresponding to type. By adjusting the parameters corresponding to the 'Params' field one can adjust the location of the membership functions on the universe of discourse.

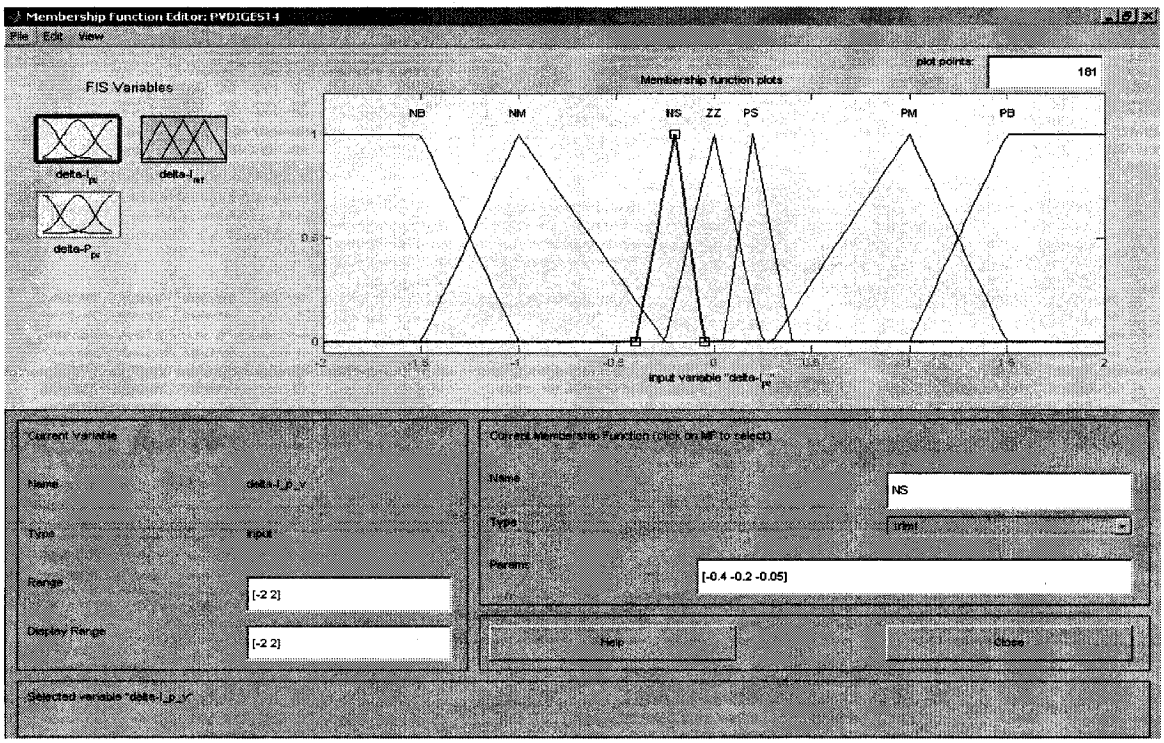

Fig.4.8 Membership function editor for ΔP_{PV}

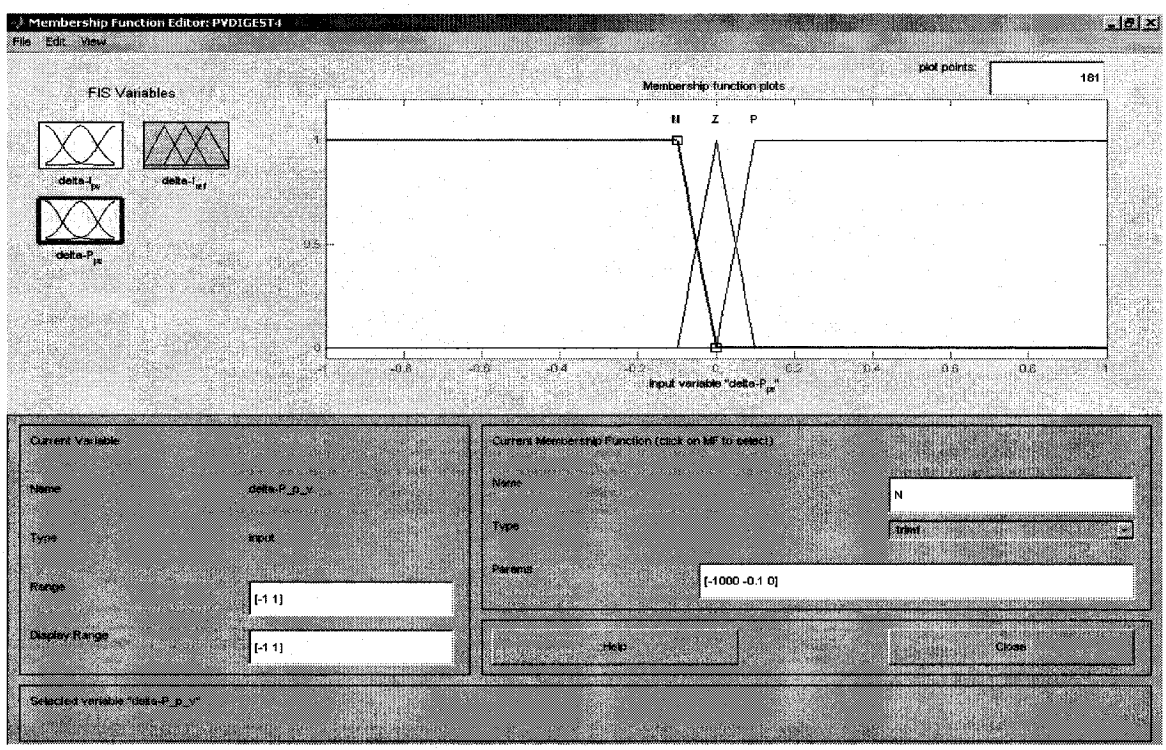

Fig. 4.9 Membership function editor for ΔI_{PV}

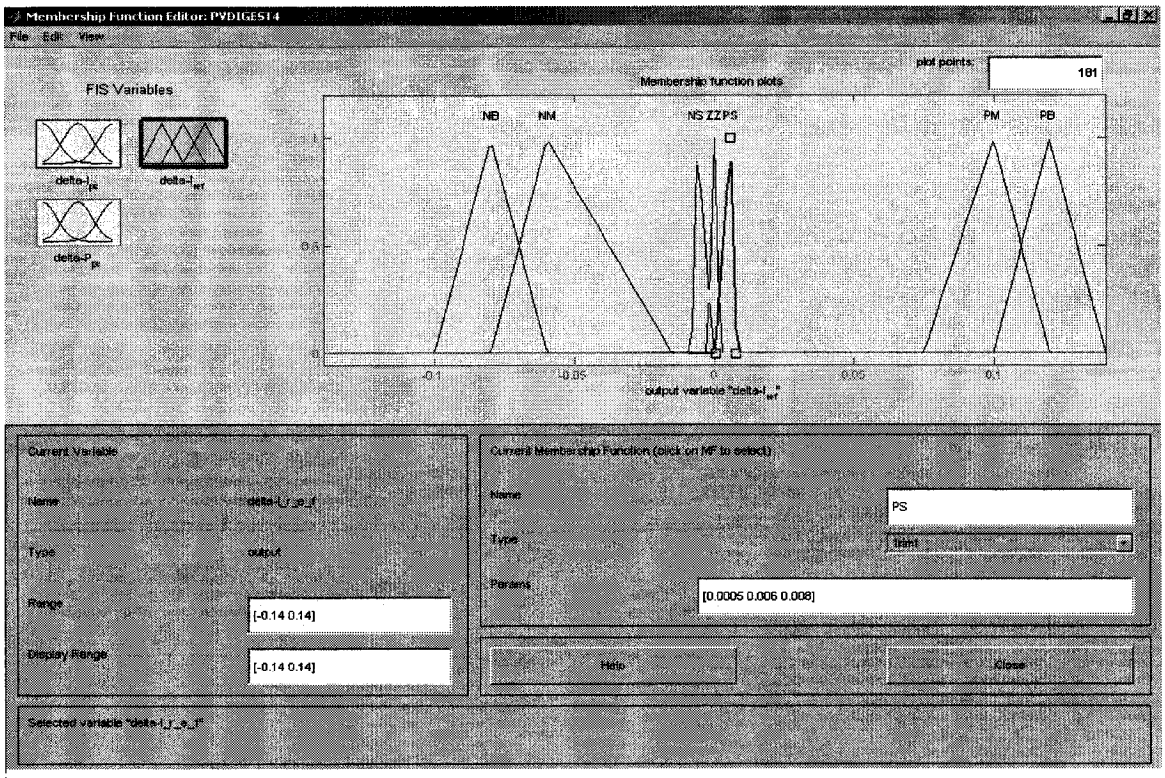

Fig.4.10 Membership function editor for ΔI_{REF}

The rules of the fuzzy controller can be designed as shown in Fig.4.11. Rules can be added, deleted and modified using the appropriate buttons. Suitable Rule weights can be assigned as well. The effect of the rules can be viewed as shown in Fig.4.12 using the view rules option. The rules that come into play for different values of inputs and the corresponding outputs can be viewed using the rule-viewer function.

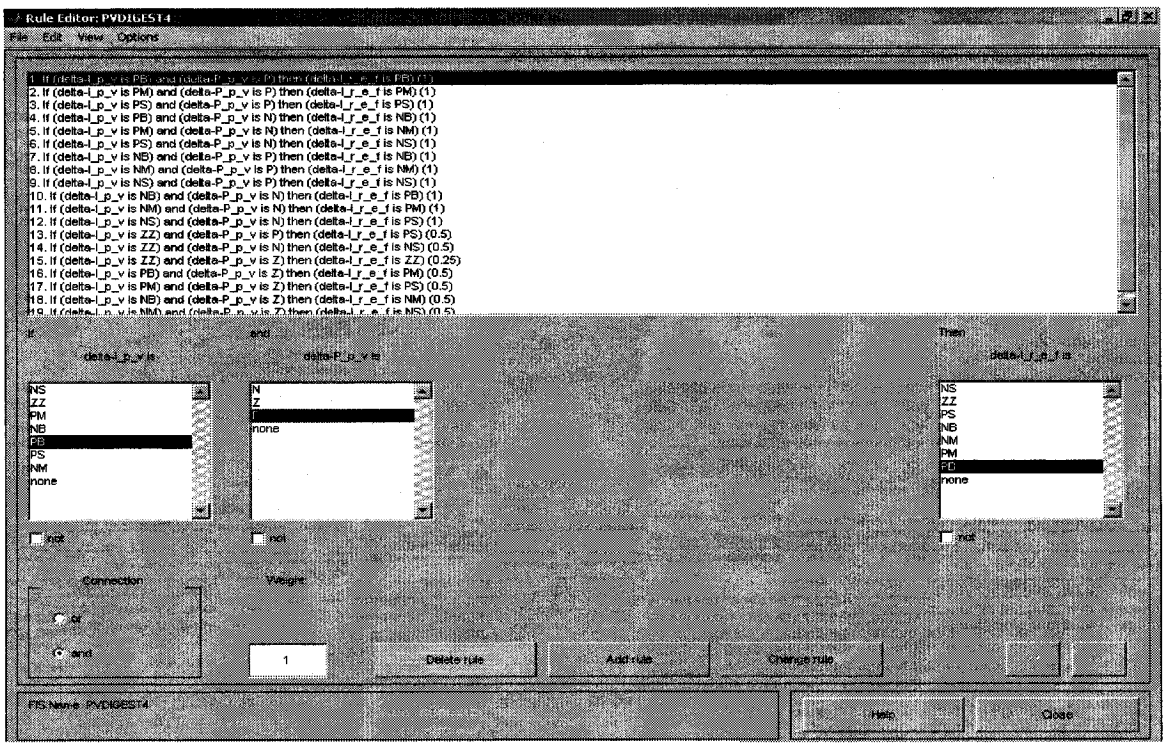

Fig.4.11 Rule-base editor

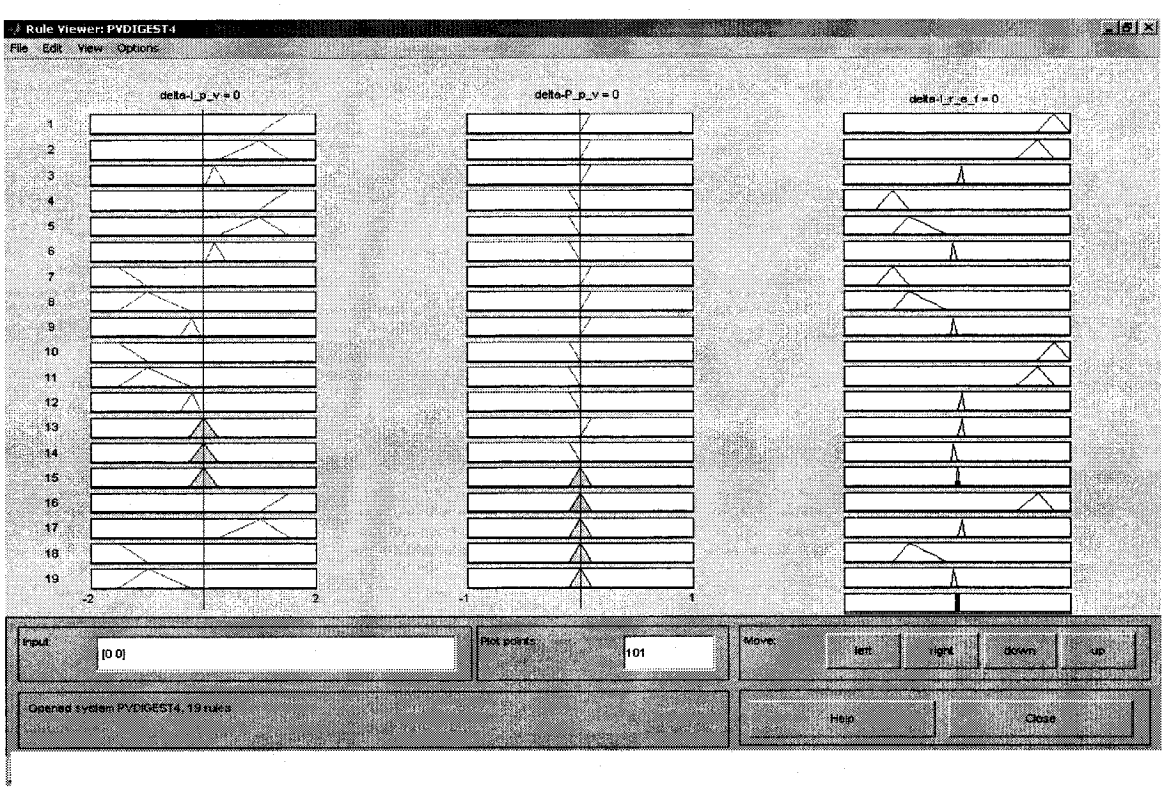

Fig.4.12 Rule viewer

4.3.3 Sample and Hold block

In the simulation schematic for the Sample and Hold block as shown in Fig.4.13, P(k), P(k-1), I(k) and I(k-1) are triggered Sample and Hold blocks. The rising edge of the driving signal determines the sampling instant in each switching signal. The difference block calculates the difference between values of PV power and PV output current at the two sampling instants giving incremental PV power (ΔP_{PV}) and incremental PV output current (ΔI_{PV}) which are supplied as inputs to the Fuzzy block after multiplication by suitable Fuzzy tuning gains.

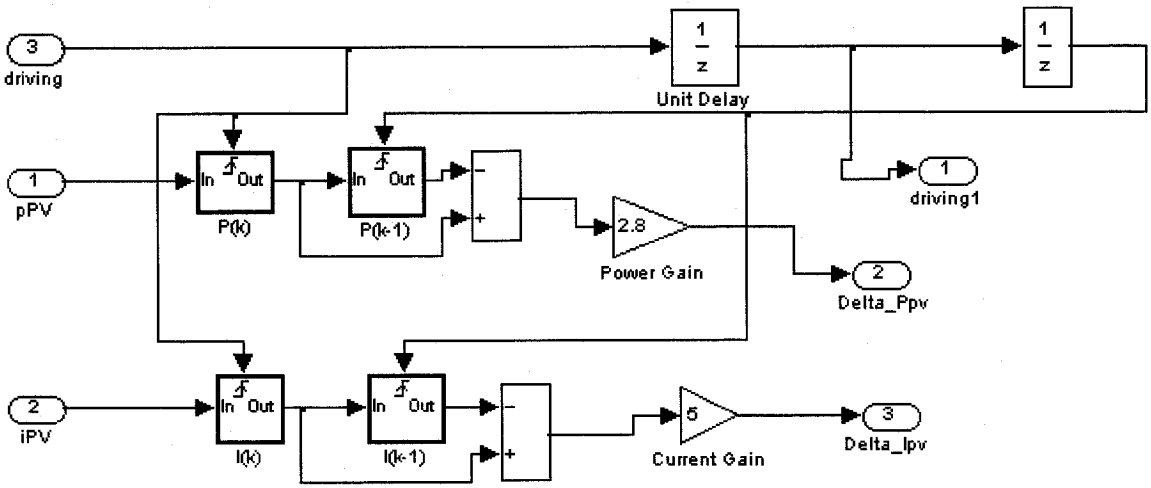

Fig.4.13 Simulation schematic of the Sample & Hold block

4.3.4 Accumulator Block

The Accumulator block as shown in Fig.4.14 is a triggered block, triggered by the rising edge of the driving signal. The first input to the accumulator block is the incremental reference current (ΔI_{REF}) and the second input is its output itself (I_{REF}). Hence at every triggered instant the reference current is updated.

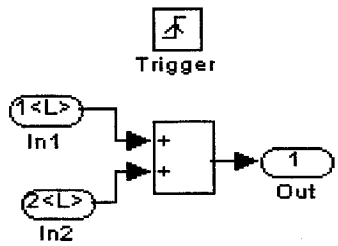

Fig.4.14 Simulation schematic of the accumulator block

4.4 SCHEMATIC DIAGRAM FOR NON-SWITCHING ZONES AND FIXED ΔI_{REF}

The schematic diagram for the scheme with non-switching zones and fixed ΔI_{REF} is shown in the Fig.4.15. Most of the blocks are the same as those used in the conventional system with fixed ΔI_{REF} however a fixed ΔI_{REF} = 0.025 A was used in this case. In the schematic for this scheme two extra blocks CHAR1_OC and CHAR2_SC are used in addition to those used in the conventional system to model the two curves as described in Chapter 3 and demarcate the switching and non-switching zones. The SC block was not used in the MPPT block as was the case with the conventional system with the fixed ΔI_{REF} as in this case the second characteristic corresponding to operation in the short-circuit region was used which would perform a similar function to that of the SC block.

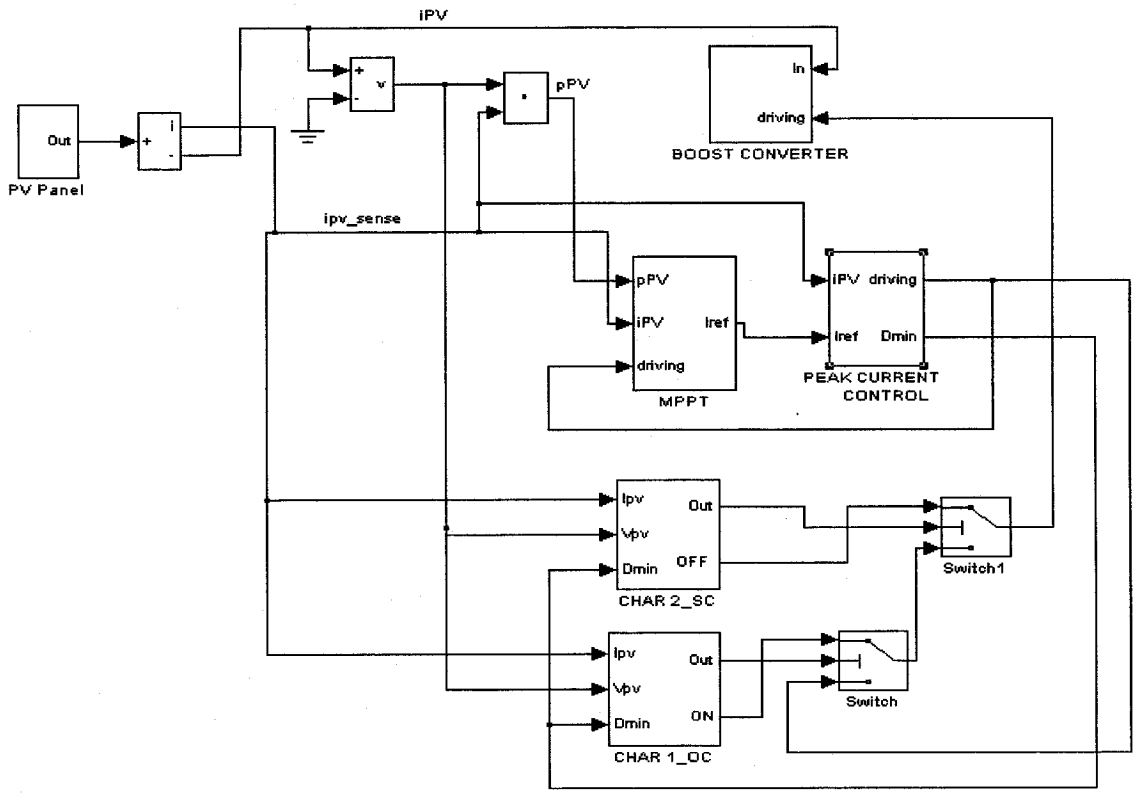

Fig.4.15 Main circuit diagram for simulation of Non-switching zones and reduced ΔI_{REF}

4.4.1 CHAR 1_OC Block

The CHAR1_OC block is shown in the Fig. 4.16. The equation of the line that separates the MPP containing region and the non-MPP containing non-switching zone corresponding to lower values of I_{PV} is implemented. The algebraic constraint block is used to prevent an algebraic loop. As described in Chapter 3 the value of voltage V_{TO} is obtained from the characteristic corresponding to the value I_{PV}. V_{TO} is compared with V_{PV} and if the former is lesser than the latter then the logic block outputs a high signal. Based on the comparison between V_{TO} and V_{PV} the switch will pass through the ON signal to keep the switch for $D = 1$ or the output of the conventional peak current algorithm.

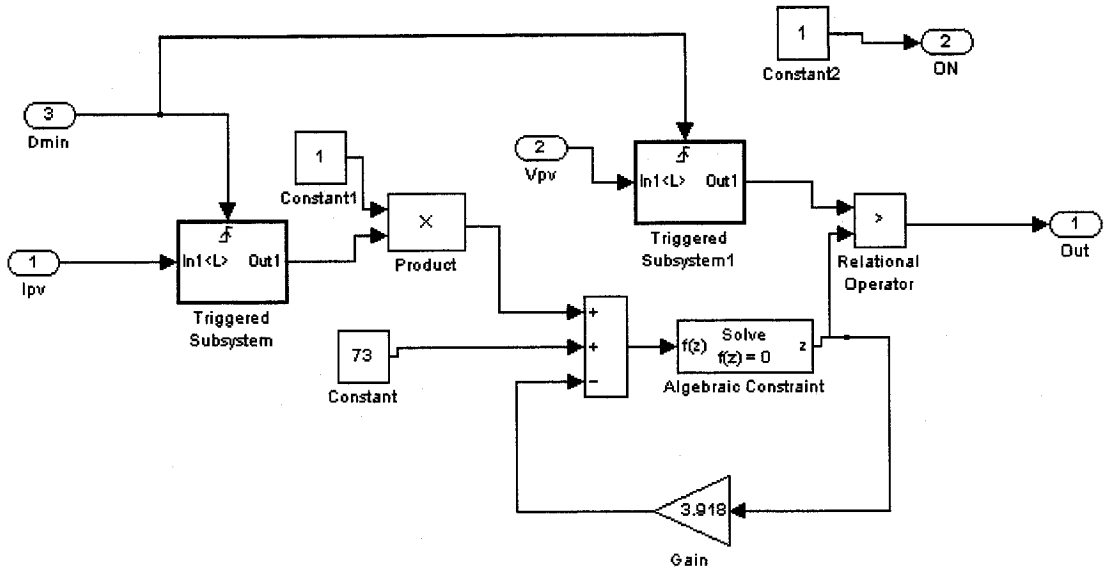

Fig.4.16 Simulation model of the CHAR1_OC block

4.4.2 CHAR 2_SC Block

The CHAR2_SC block is shown in the Fig.4.17. The equation of the line that separates the MPP containing region and the non-MPP containing non-switching zone corresponding to higher values of I_{PV} is implemented. The algebraic constraint block is used to prevent an algebraic loop. As described in Chapter 3 the value of voltage V_{TS} is obtained from the characteristic corresponding to the value I_{PV}. V_{TS} is compared with V_{PV} and if the former is lesser than the latter then the logic block outputs a high signal. Based on the comparison between V_{TS} and V_{PV} the switch will pass through the OFF signal to keep the switch for $D = 0$ or the output of the switch corresponding to the CHAR1_OC block.

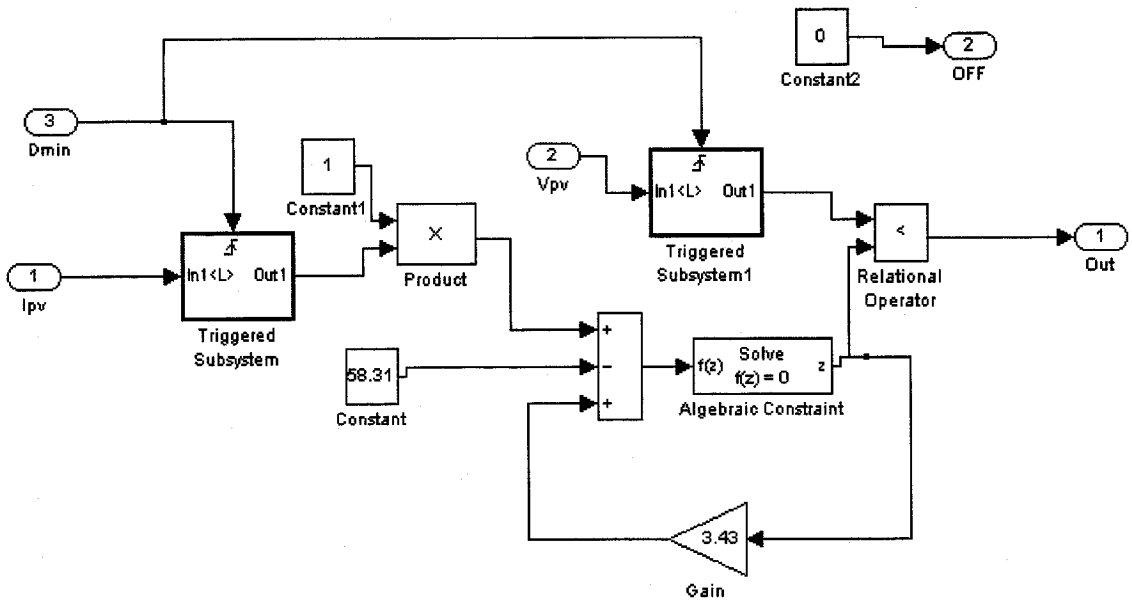

Fig.4.17 Simulation model of the CHAR2_SC block

4.5 SCHEMATIC DIAGRAM FOR NON-SWITCHING ZONES AND REDUCED FUZZY CONTROLLER

The simulation schematic for the scheme with non-switching zones and the reduced Fuzzy logic controller is shown in Fig. 4.18. The simulation schematic is the same as that used in Section 4.3 for the Fuzzy logic based system. However as in Section 4.4 two extra blocks CHAR1_OC and CHAR2_SC are used in addition to those used in Section 4.3 to model the two curves, as described in Chapter 3, and demarcate the switching and non-switching zones. In addition the name of the .fis file entered in the fuzzy logic controller block should be the one that corresponds to the reduced Fuzzy logic controller described in Section 3.3 of Chapter 3

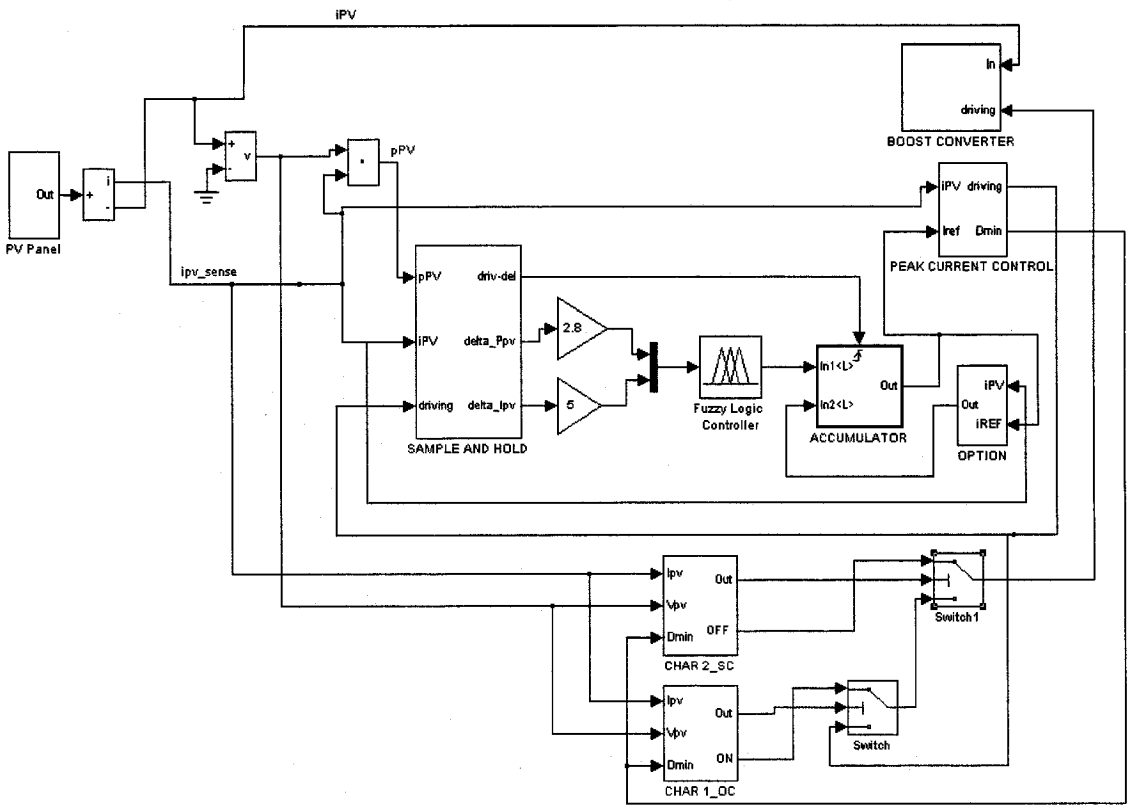

Fig .4.18 Main circuit diagram for simulation of non-switching zones and reduced Fuzzy

4.6 SIMULATION PARAMETERS

The simulation parameters are the same as those used in [2] for comparison purposes.

PV panel (at rated irradiance levels)

Short-circuit current (I_{SC}) = 3.452 A

Current at the MPP (I_{MPP}) = 3.29 A

Voltage at the MPP (V_{MPP}) = 18.62 V

Open-circuit voltage (V_{OC}) = 21.8 V

Boost converter

Inductor (L) = 1 mH

Switching frequency (f_{SW}) = 100 kHz

Battery bank

Output voltage (V_b) = 24 V

4.7 Simulations Results And Analysis

Figures 4.19, 4.21, 4.23 and 4.25 shows the start-up process under rated ambient conditions and the response to a step variation of irradiance to 50% of the initial value for the standard scheme with fixed ΔI_{REF}, the Fuzzy logic based scheme with variable ΔI_{REF}, the scheme with fixed ΔI_{REF} and non-switching zones and the scheme with reduced Fuzzy and non-switching zones respectively. Figures 4.20, 4.22, 4.24 and 4.26 show the detailed steady-state waveforms for the above-mentioned peak current control based algorithms. It must be stated that optimum tuning gains have been used for the fuzzy controllers which is 2.8 for the ΔP_{PV} input and 5 for the ΔI_{PV}. For the switching zone based schemes, the equations used for defining the regions in the V_{PV} x I_{PV} plane are:

CHAR 1 : $V_{TO} = 0.255\ I_{PV} + 18.63$

CHAR 2 : $V_{TS} = -0.29\ I_{PV} + 17$

It can be seen from Fig.4.23 and Fig.4.25 that the non-switching zones based schemes present the fastest rise time of 0.17ms with both the fixed and the variable ΔI_{REF} because the converter operates with D = 1. As seen from Fig.4.21 the all Fuzzy logic based scheme presents a faster rise time of 0.27 ms as compared to 0.32 ms for the standard scheme with fixed ΔI_{REF} because the use of the Fuzzy logic controller allows the use of a larger variation of reference current during the transient state.

The standard scheme with fixed ΔI_{REF} responds well to the sudden step-down of irradiance due to the use of the SC and the OPTION blocks described in [2]. The fuzzy logic based variable ΔI_{REF} scheme also presents a reasonable response. In this case only

the OPTION block was used. The non-switching zones based methods also present good recovery due to the presence of the second characteristic CHAR2, as described in Chapter 3, which comes into play when the operating point of the system moves into the short-circuit region. The OPTION block was used in both the non-switching zones based methods. The non-switching zones based method with the reduced Fuzzy system however presented the best recovery of all.

In the steady state as seen in Fig.4.20 the standard scheme with fixed ΔI_{REF} presents maximum power drops as well as a large peak-to-peak ripple in I_{PV} (0.17A). This is primarily due to the use of a relatively large value of fixed ΔI_{REF}. As seen in Figs.4.22 and 4.26 the Fuzzy based schemes present lowest power drops and peak-to-peak ripple in I_{PV} (0.045A) in the steady-state because $\Delta I_{REF} = 0$ A in the steady-state. The current ripple for these cases is only due to the intrinsic switching of the converter and does not include the variations of I_{REF} that appear in the case of the fixed variation of reference current. As seen in Fig.4.24 the non-switching zones based scheme with fixed ΔI_{REF} presents a lower power drop and peak-to-peak ripple for I_{PV} (0.08A) than the standard scheme implemented with fixed ΔI_{REF} because it employs a smaller ΔI_{REF}.

For further increasing the power drawn from the PV array one should reduce the current ripple. This can be done by using a higher value of inductance for the Boost inductor, increasing the switching frequency or using interleaved boost converters. Besides, the DC/DC converter should be of the soft switching type for increased efficiency.

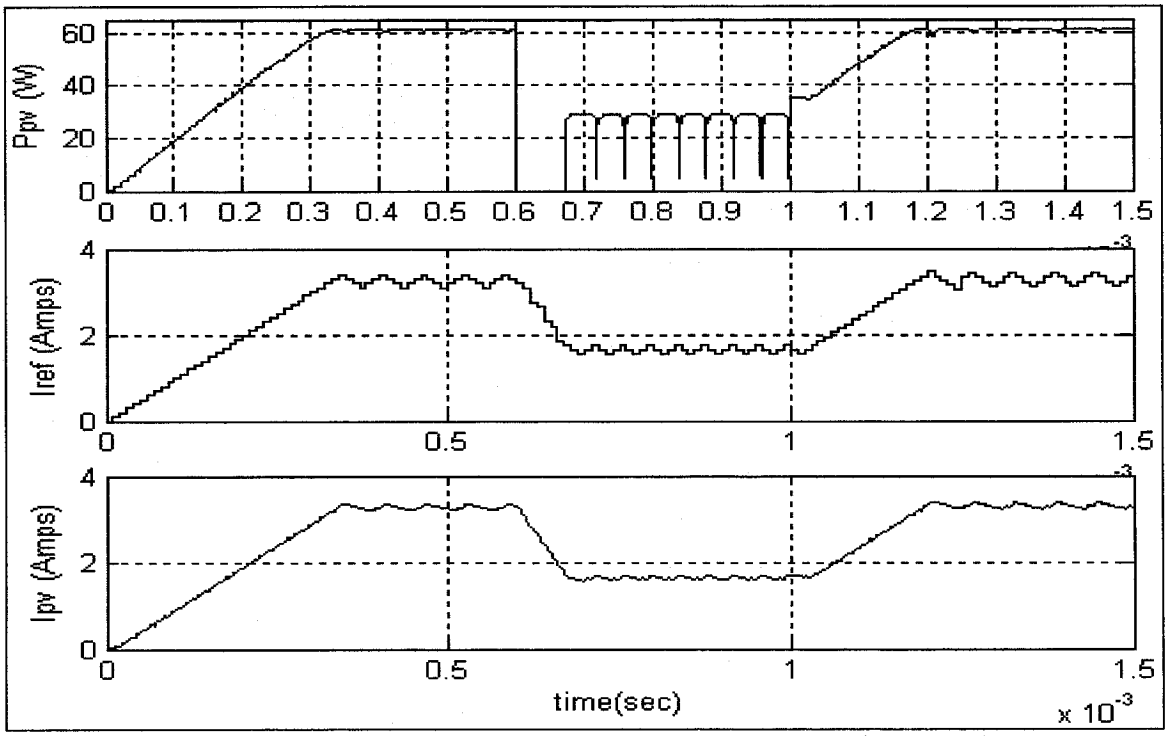

Fig. 4.19 Start-up of the MPPT system under rated ambient conditions and response to sudden step-down of irradiance for standard scheme with fixed ΔI_{REF}.

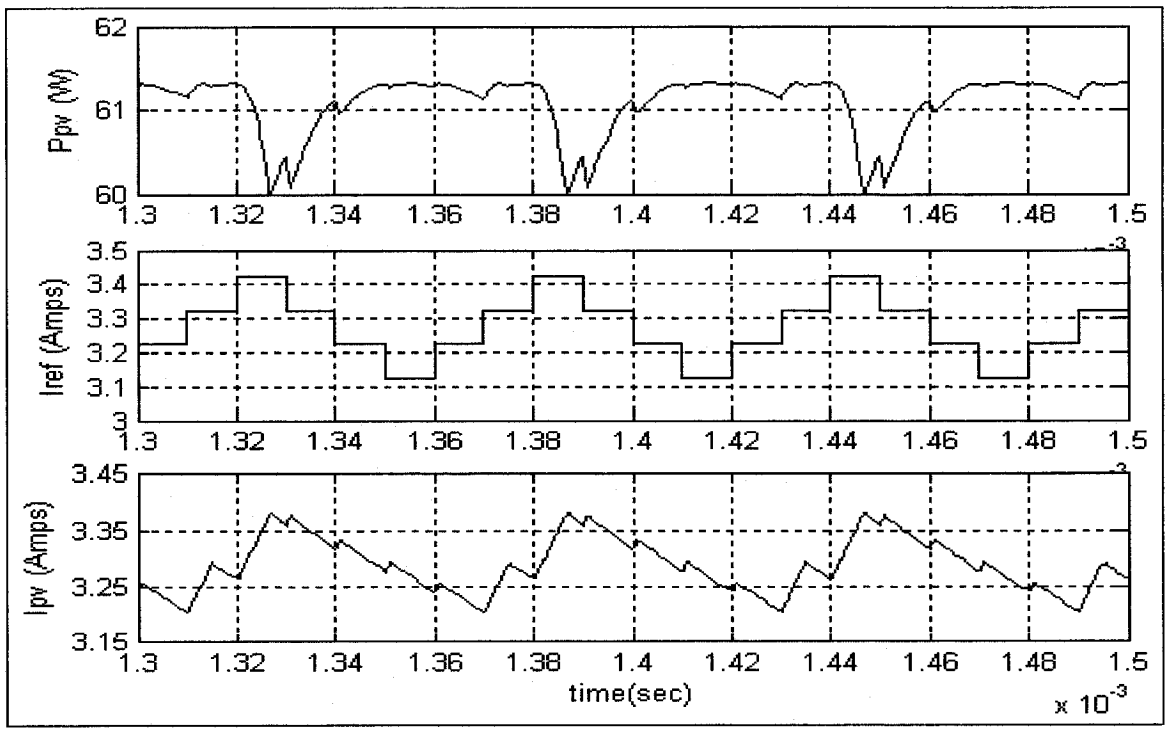

Fig.4.20 Detailed steady-state for standard scheme with fixed ΔI_{REF}

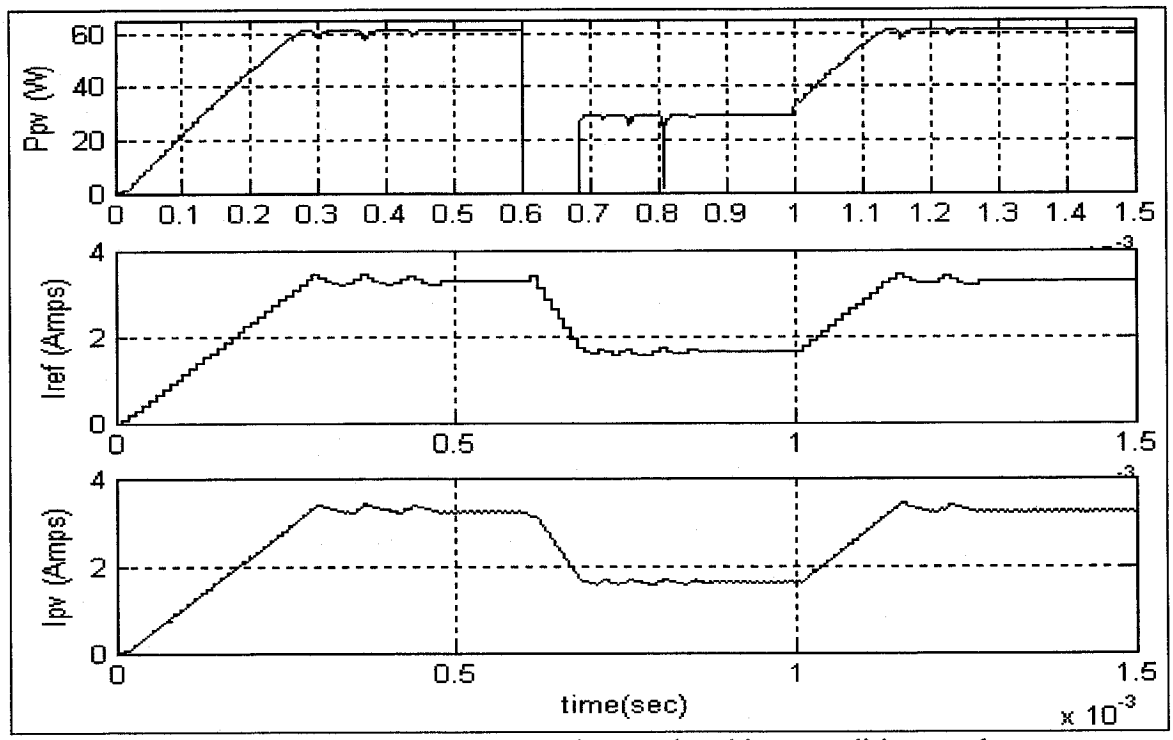

Fig.4.21 Start-up of the MPPT system under rated ambient conditions and response to sudden step-down of irradiance for Fuzzy logic based scheme with variable ΔI_{REF}

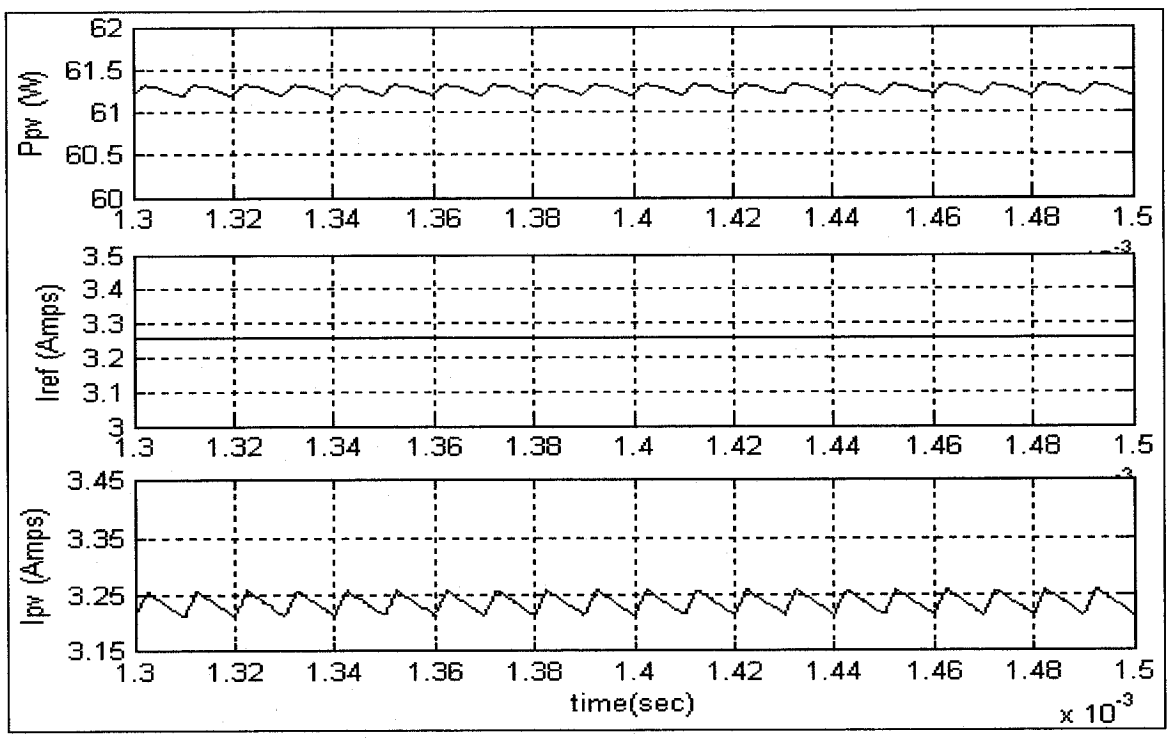

Fig.4.22 Detailed steady-state for Fuzzy logic based scheme with variable ΔI_{REF}

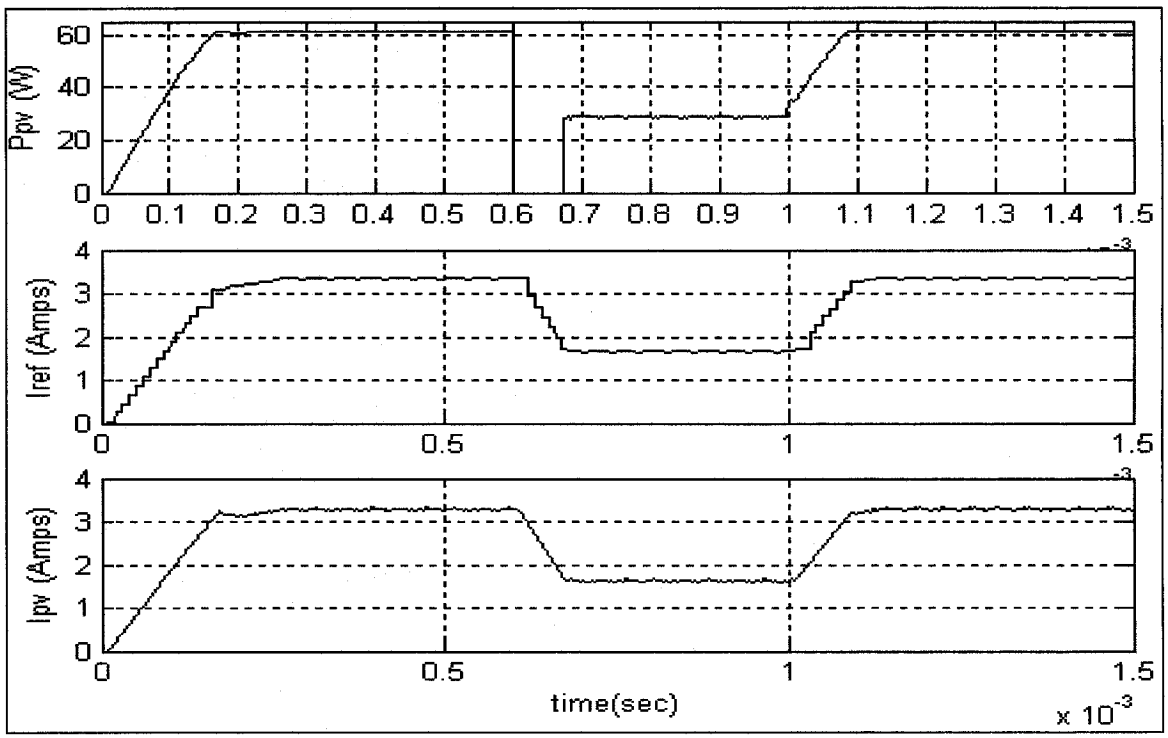

Fig.4.23 Start-up of the MPPT system under rated ambient conditions and response to sudden step-down of irradiance for scheme with fixed ΔI_{REF} and non-switching zones.

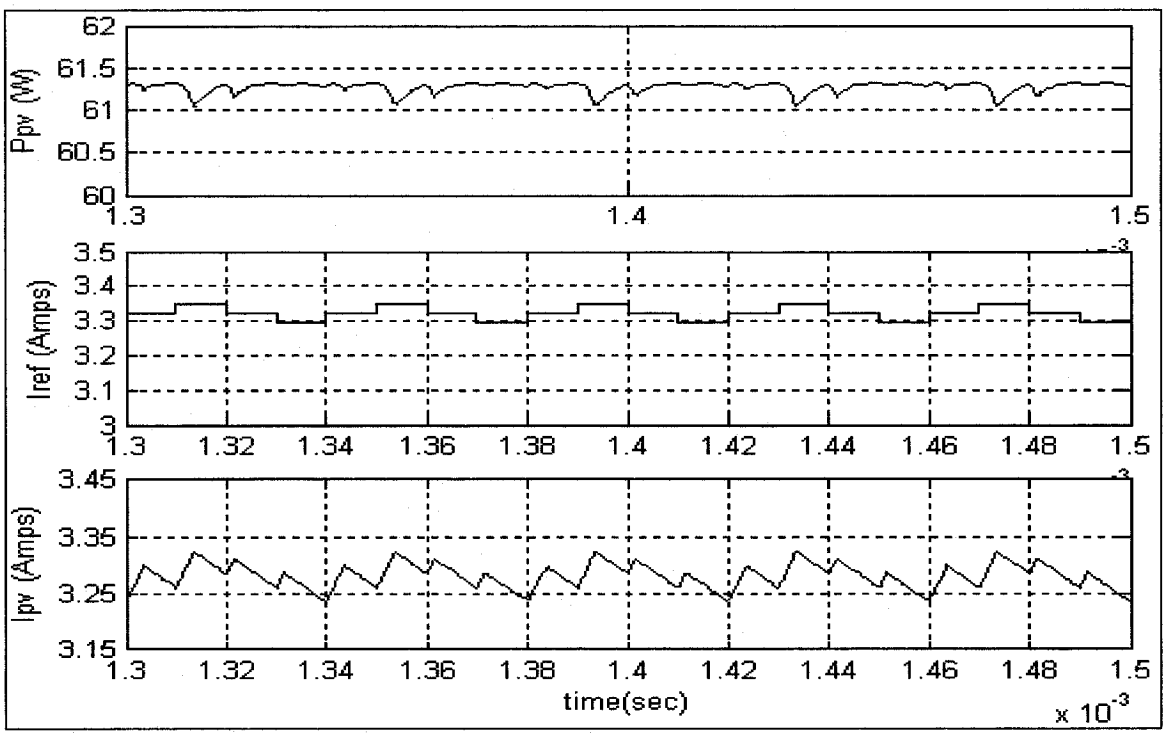

Fig.4.24 Detailed steady-state for scheme with scheme with fixed ΔI_{REF} and non-switching zones

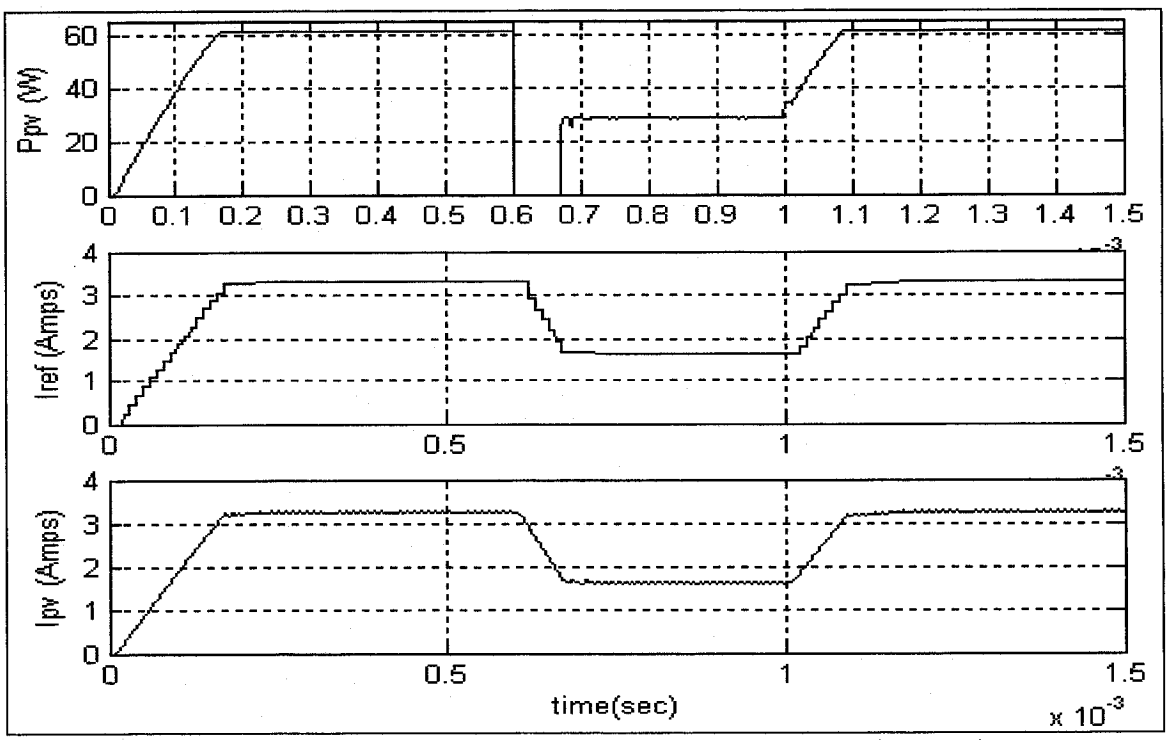

Fig.4.25 Start-up of the MPPT system under rated ambient conditions and response to sudden step-down of irradiance for Reduced Fuzzy and non-switching zones.

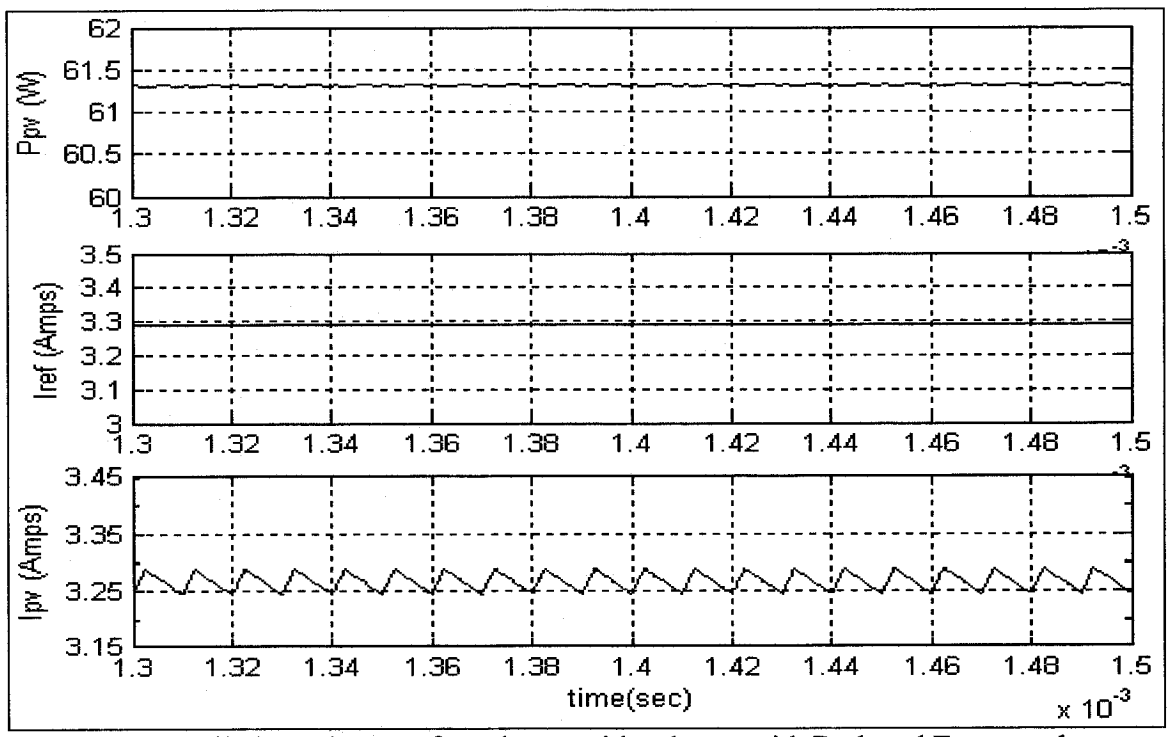

Fig.4.26 Detailed steady-state for scheme with scheme with Reduced Fuzzy and non-switching zones.

The importance of selection of appropriate Fuzzy tuning Gains is demonstrated in Figures 4.27-4.28. Simulations were first run with the estimated gains mentioned in Chapter 3. However, it can be seen from Figures 4.27-4.28 that the system does not start-up. After tuning the Fuzzy gains, suitable values i.e. 2.8 for ΔP_{PV} and 5 for ΔI_{PV} were obtained corresponding to optimum results demonstrated in Figures 4.21, 4.22, 4.25 and 4.26.

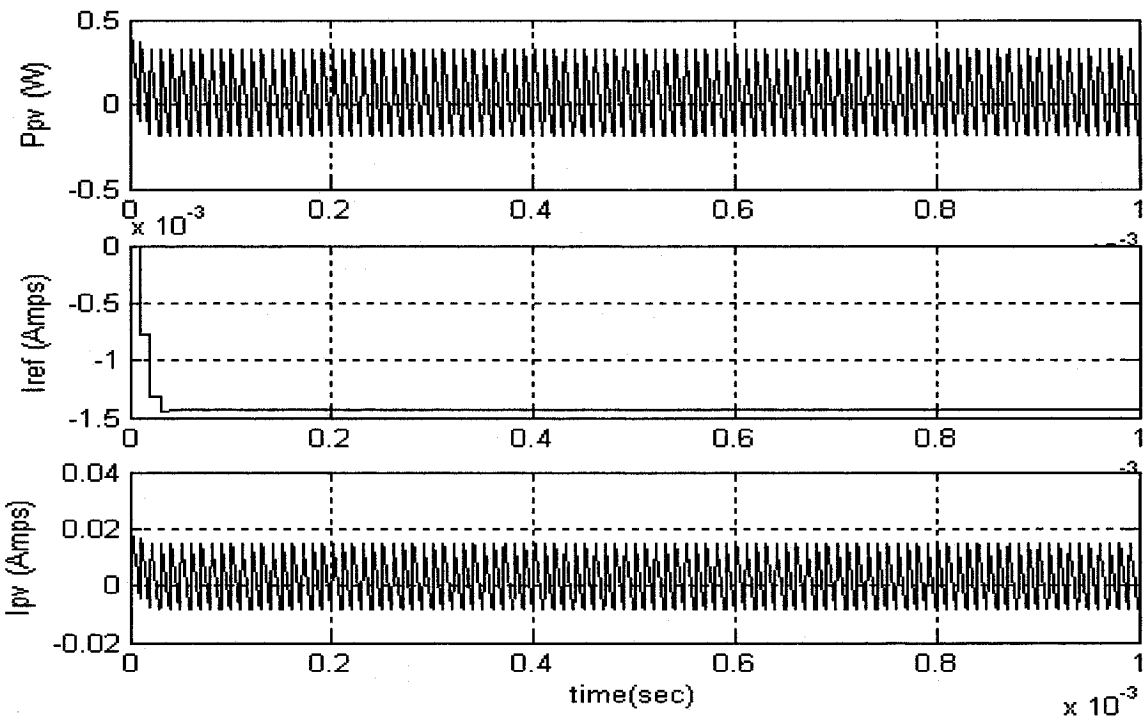

Fig. 4.27 Start-up of the Fuzzy logic based MPPT system under rated ambient conditions with Tuning gains of 0.5 and 1

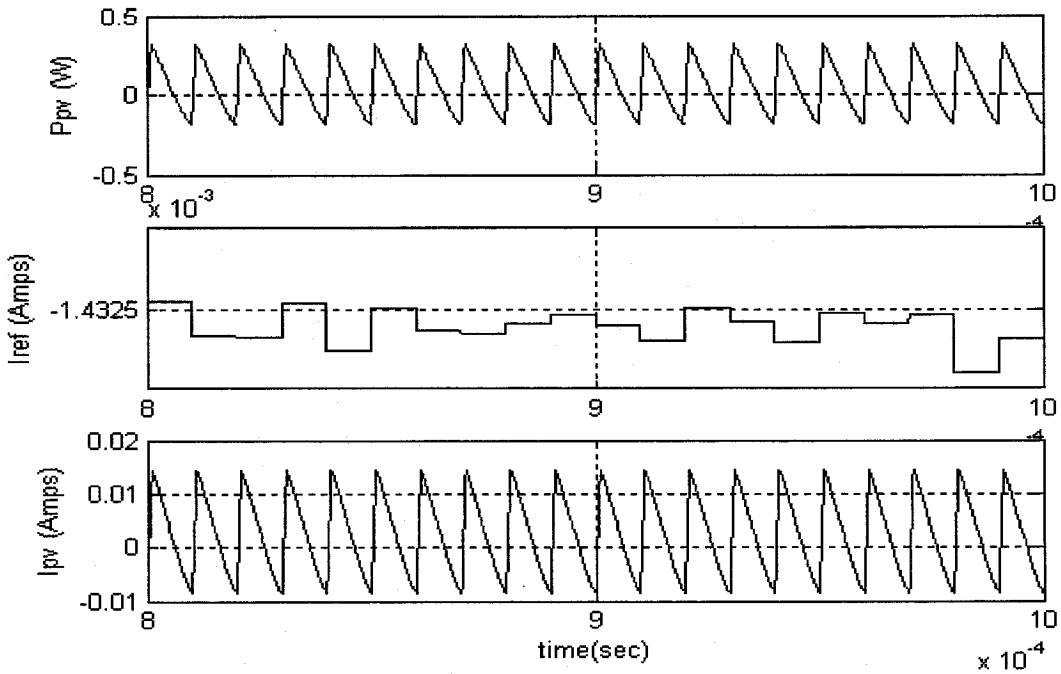

Fig.4.28 Detailed view of the steady state for the Fuzzy logic based MPPT for Tuning gains of 0.5 and 1

4.7.1 Comparison Table

	Standard Scheme with Fixed ΔI_{REF} (0.1 A)	Fuzzy Logic based Scheme with Variable ΔI_{REF}	Non-switching zones and Fixed ΔI_{REF} (0.025 A)	Non-switching zones and Reduced Fuzzy
Rise time	0.32 ms	0.27 ms	0.17 ms	0.17 ms
Power Drops	High	Lowest	Lower than standard scheme	lowest
Peak-peak current ripple	High	Lowest	Lower than standard scheme	lowest

Table 4.1 Comparison of the four peak current control based MPPT schemes based on simulation results

4.8 CONCLUSIONS

In this Chapter simulations were run in the MATLAB/Simulink environment to compare the performance of the four peak current control based MPPT algorithms. The simulation schematics for the different schemes are presented and the simulation parameters are specified. The non-switching zones based schemes with both fixed ΔI_{REF} and reduced fuzzy controller presented faster rise times under the given atmospheric conditions and design considerations. The non-switching zones based scheme with fixed ΔI_{REF} presented lower steady-state power drops as compared to the standard scheme with fixed ΔI_{REF} due to the choice of a lower value for the fixed ΔI_{REF}, while also presenting a better transient response. The non-switching zones based scheme with fixed ΔI_{REF} also presented a better transient response than the conventional Fuzzy logic based scheme with variable ΔI_{REF}. Both the conventional and the non-switching zones based Fuzzy logic schemes presented the ideal steady state response. Thus simulation results suggest that the ideal case would be the use of the non-switching zones based scheme along with the reduced fuzzy logic controller, for optimum transient and steady-state response.

CHAPTER 5

EXPERIMENTAL RESULTS

5.1 INTRODUCTION

The objectives in this chapter are two-fold: Firstly an attempt is made to identify the limitations with regards to the practical implementation of the peak current control based MPPT schemes. Secondly an attempt is made to compare the experimental performance of the four previously discussed peak current controlled based MPPT techniques and relate the performance to the simulation case. In the experiments, the MPPT algorithms are implemented with a DSP system from dSPACE.

5.1.1 Introduction to the dSPACE system [2]

The dSPACE system is a hardware architecture used for rapid prototyping of electrical control systems, which is comprised of DS1103 PPC controller board. It is equipped with a Motorola PowerPC 604e processor, whose computing power allows for the simulation of large-scale floating-point control algorithms in real-time. A full range of I/O devices including a TMS320F240 slave DSP is available on-board. Using the Real-Time Interface to Simulink, automatic code generation from block diagrams is possible. I/O functions are specified graphically as part of the simulation model.

5.1.2 Hardware Architecture [2]

The DS1103 PPC Controller Board is equipped with a Motorola PowerPC 604e processor for fast floating-point calculation at 333MHz. This high-performance superscalar microprocessor has three integer execution units, one floating-point arithmetic unit, and a separate load/store unit for fast memory access. The on-chip cache size is 32kByte for instruction and data. The processor's ability to execute instructions out-of-order leads to a performance improvement of about factor 2 for typical simulation models compared to strictly serial instruction flow.

A 2MByte local memory is used for program and data of the simulation model. The local memory is fully cached and cannot be accessed by the host PC in standard operation mode. For data buffering and exchange between PowerPC and the host, up to 128 MByte of non-cached global memory is available. The host interface of the board is used to perform board setups, program downloads, and runtime data transfer. It supports Plug&Play functionality for easy installation.

I/O Section

The board can be adapted to a wide range of closed-loop applications due to its large number of I/O devices. High-resolution A/D converters (16-bits and 12 bits) with a sampling time of 4us and 800 ns, respectively, are available, as well as D/A output channels with a resolution of 14-bit and a 5 us settling time. 32 digital I/O channels and a serial line interface complete the list of standard I/O units.

5.1.3Real-Time Interface to Simulink [2]

Using MATLAB and Simulink for modeling, analysis, design and offline simulation has become a de-facto standard for control system development. The Real-Time Interface enhances the Simulink block library with additional blocks, which provide the link between Simulink and the real-time hardware, as shown in Fig.5.1. To graphically specify an I/O channel the corresponding block icon has to be picked up from the I/O block library and attached to the Simulink controller model. I/O parameters, such as voltage ranges or resolutions, can be set in appropriate dialog boxes. The Simulink model then is transferred into real-time code, using the Real-Time Workshop, state flow control, and the Real-Time Interface. Code generation includes the I/O channel specification and the multitasking setup, which are translated into appropriate function calls of the Real-Time Library. The library is a C function library providing a high-level programming interface to the hardware. The Real-Time Library also includes access functions for the slave DSP. These blocks cover the I/O functionality of the prototyping hardware.

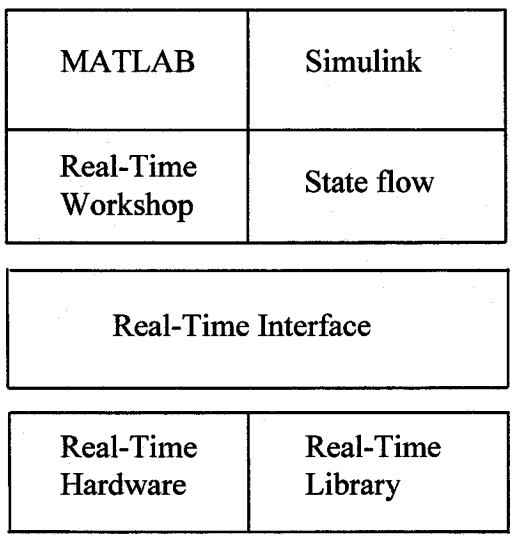

Fig.5.1 The Real-Time Interface in the MATLAB/Simulink environment [2]

5.1.4 Simulink Block Library for DS1103 [2]

The block library for the DS1103 PowerPC Controller Board is subdivided into two major parts according to the two microprocessor units on the board. The library shown in Fig.5.2 comprises all I/O units that are directly served by the PowerPC master processor. Block icons for the standard I/O channels such as A/D, D/A converters, and digital I/O are included as well as the more complex incremental encoder blocks.

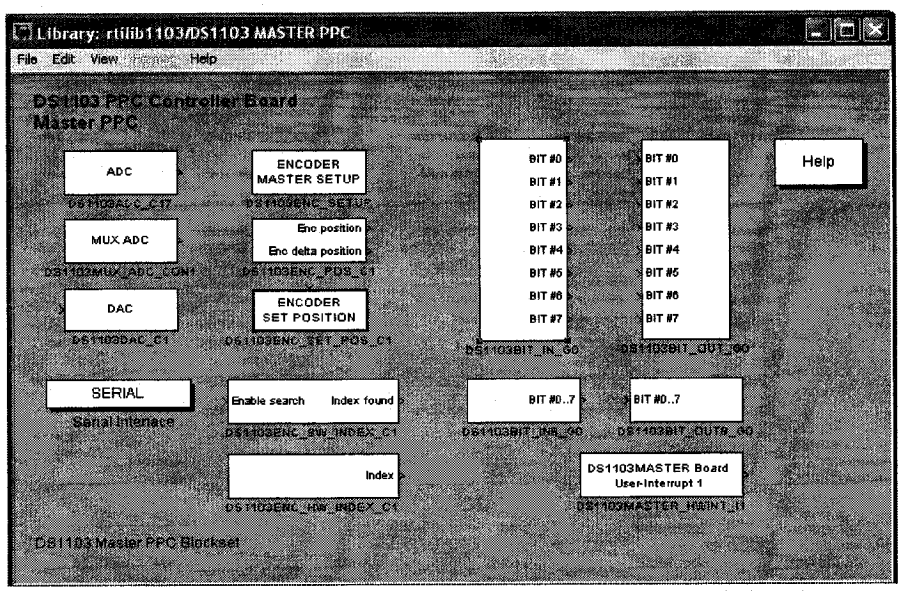

Fig.5.2 Master Processor block library for Simulink [2]

The slave DSP library, shown in Fig.5.3, offers frequently used functions of the TMS320F240, such as single-phase and three-phase PWM signal generation, frequency measurement, A/D conversion, and digital I/O. Because the real-time simulation is executed in the master PPC board, it is wished to employ the functions provided by the slave DSP as much as possible to save the computation time on the Master PPC board.

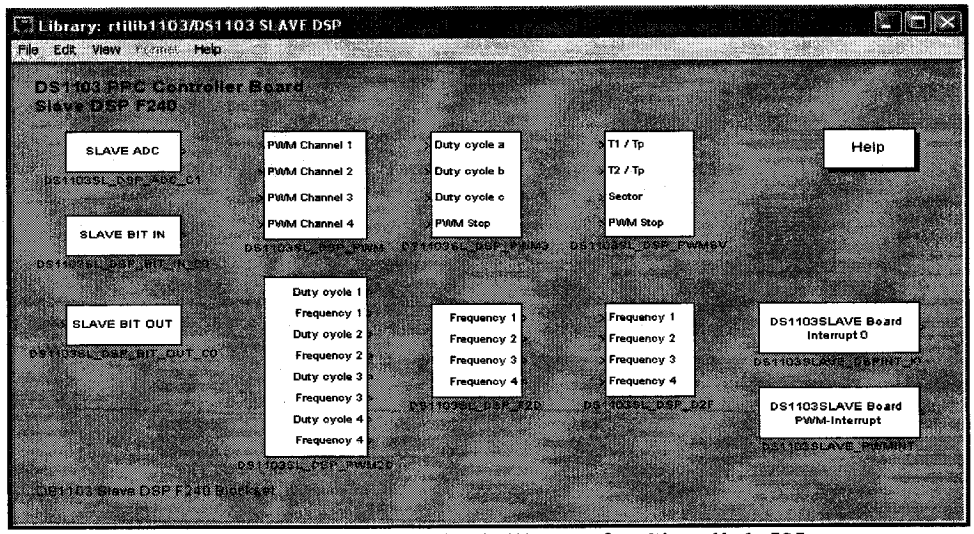

Fig. 5.3 Slave DSP block library for Simulink [2]

5.1.5 Practical Limitations of the dSPACE System

It is proposed to implement the previously discussed peak current control based MPPT systems in the DSP microcontroller from dSPACE and interface it with the prototype of a boost converter. In [2] it was seen that if the peak current control logic was implemented in the DSP, in the case of the standard scheme with a fixed ΔI_{REF}, the switching frequency was restricted to 10 kHz in order to have a good enough resolution of duty cycle. In addition, the computation time required by the DSP to process the Fuzzy controller block in the schemes involving Fuzzy logic, places a further restriction on the switching frequency of the boost converter, if the peak current control logic was implemented in the DSP. Hence, it was necessary to implement the peak current control strategy in hardware to keep the switching frequency independent of the sampling frequency. The PWM IC 3842 was used for the purpose. Although, it was desired to operate with a sampling frequency equal to the switching frequency of the MPPT converter, in this case the sampling frequency had to be reduced to suit the computational constraints of the dSPACE system. However, the switching frequency was independent

of the computational constraints of the dSPACE system. Thus the switching frequency is an integral multiple of the sampling frequency, which means the peak reference current is not updated every switching cycle but after an integral number of cycles.

5.2 EXPERIMENTAL SETUP

Fig.5.4 shows the basic experimental setup for the PCC based MPPT schemes. The setup is comprised of three parts, PV panels, boost converter and the MPPT controller.

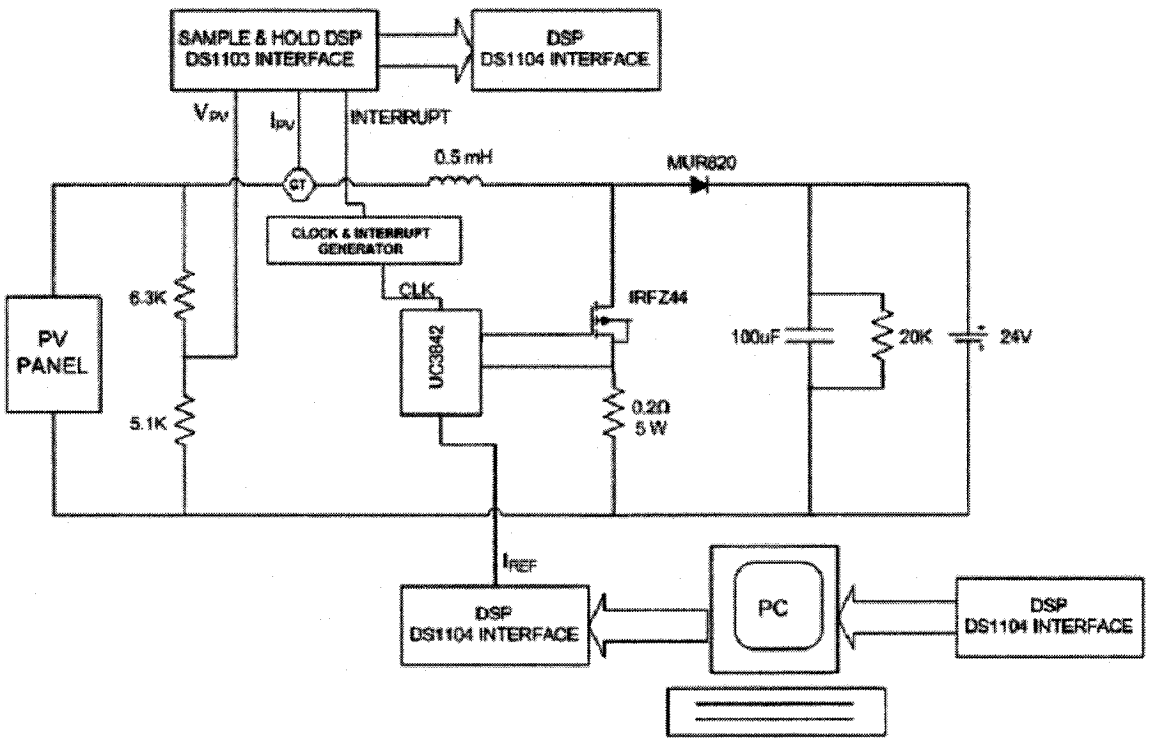

Fig.5.4 Experimental Set-up

5.2.1 PV Panel Simulator [2]

The Agilent E4350B Solar Array Simulator (SAS) is employed as the PV panel simulator. It is a dc power source that simulates the output characteristics of a solar array. The Agilent SAS is primarily a current source with very low output capacitance. It is capable of simulating the $V_{PV} \times I_{PV}$ curve of a solar array under different conditions such

as temperature and age. The $V_{PV} \times I_{PV}$ curve is programmable over the IEEE-488.2 bus and is automatically generated within the Agilent SAS. The Agilent SAS has three operating modes:

Fixed Mode: This is the default mode that occurs when the unit is first powered up. The $V_{PV} \times I_{PV}$ output has the rectangular characteristics of a standard power supply, but with excellent high speed constant current characteristics and low output capacitance.

Simulator Mode: An internal algorithm is used to simulate a $V_{PV} \times I_{PV}$ curve. One can easily approximate the curve through four input parameters: open circuit voltage (V_{OC}), short-circuit current (I_{SC}), current at the approximate maximum power point on the curve (I_{MPP}), and voltage at the approximate maximum power point on the curve (V_{MPP}).

Table Mode: The Agilent SAS provides a table mode for a more accurate $V_{PV} \times I_{PV}$ simulation of solar arrays. In this mode, a table of $V_{PV} \times I_{PV}$ points, often provided by the solar array manufacturer, specifies the curve.

In the experiment the Simulator Mode is used and the program to put the $V_{PV} \times I_{PV}$ curve in SAS is shown in Appendix A1.

5.2.2 The MPPT Converter

The PV Panel simulator is connected as an input to the MPPT boost converter which feeds a 24V battery load. An IRFZ44 MOSFET is used as the switch of the boost converter and a MUR820 is used as the diode of the boost converter. The MOSFET and the diode are selected so that the voltage rating is greater than 1.5 times the output voltage, which is $1.5 \times 24 = 36$ V, and the current rating exceeds 1.2 times the short-circuit current of the PV panels, i.e. $1.2 \times 3.45 = 4.14$ A. The input inductor was selected as 0.5 mH in order to limit the output ripple within acceptable limits. A 0.2 Ω, 5 W

current sense resistor is included to measure the current through the switch. The output capacitor is selected just large enough for a small output voltage ripple. A 20K discharge resistor is connected across the output capacitor.

5.2.3 MPPT Controller

The MPPT controller consists of four sections: the analog clock and interrupt generator circuit, the Sample and Hold DSP DS1103 microcontroller, the analog peak current control circuit and the MPPT DSP DS1104 microcontroller.

The PV voltage is sensed directly using the voltage-divider network and the PV current is sensed using a LA55P Hall-effect sensor. The PV voltage and current is sampled using the Sample and Hold DSP. The sampled values of PV voltage and current are fed to the MPPT DSP. These values are processed in the MPPT DSP and the updated value of reference current is supplied to the 3842 PWM IC by the D/A Converter. The 3842 PWM IC is used to implement peak current control in an analog fashion. The clock and interrupt generator circuit supplies the clock signal to the 3842 PWM IC and the interrupt signal to define the sampling instants of PV voltage and current values.

5.2.4 Analog clock and interrupt generator circuit

A detailed circuit layout for the analog clock and interrupt generator circuit for the standard scheme with fixed ΔI_{REF} is shown in Fig.5.5. Here an IC 555 timer is used to generate a 25 kHz 50% duty ratio clocking signal by suitable selection of resistor and capacitor components. The output of the 555 timer IC goes to the 3842 PWM IC to set the switching frequency of the boost converter. It must be noted however that the clock signal is inverted at the 3842 IC stage. Thus the falling edge of the clock pulse corresponds to the turn-ON of the boost converter MOSFET. The output of the 555 timer

also goes to the sampling circuit which comprises of 4017B decade counter and a dual monostable multivibrator 4528B IC. The 25 kHz clocking signal (shown in Fig.5.8(a)) is converted to a 2.5 kHz clock signal by the 4017B decade counter as shown in Fig.5.8(b) to meet the MPPT DSP requirements of a lower sampling frequency. The rising edge of the clock signal from the 4017B IC triggers a pulse in the first monostable multivibrator as shown in Fig.5.8(c). The falling edge of this pulse determines the sampling instant and triggers a second extremely short pulse in the second multivibrator as shown in Fig.5.8(d), which forms the interrupt signal. This interrupt signal from the second multivibrator is given to the interrupt input of the Sample and Hold DSP DS1103 interface which is used to sample and hold values of PV current and voltage. It can be seen from Fig.5.8 that the interrupt signal occurs a short delay after the rising edge of the clock signal. The rising edge corresponds to the turn-OFF of the MOSFET at maximum duty ratio operation. This means that the sampling of PV panel voltage and current values is guaranteed to always take place during the OFF period of the MOSFET switching cycle and hence, during a commutation noise-free instant.

The clock and interrupt generator circuit for the Fuzzy logic based scheme with variable ΔI_{REF} is shown in Fig.5.6. In this case a still lower sampling frequency had to be used, due to the larger computation time required to model the complex Fuzzy model. Hence a second decade counter is added to reduce the sampling frequency to 250 Hz

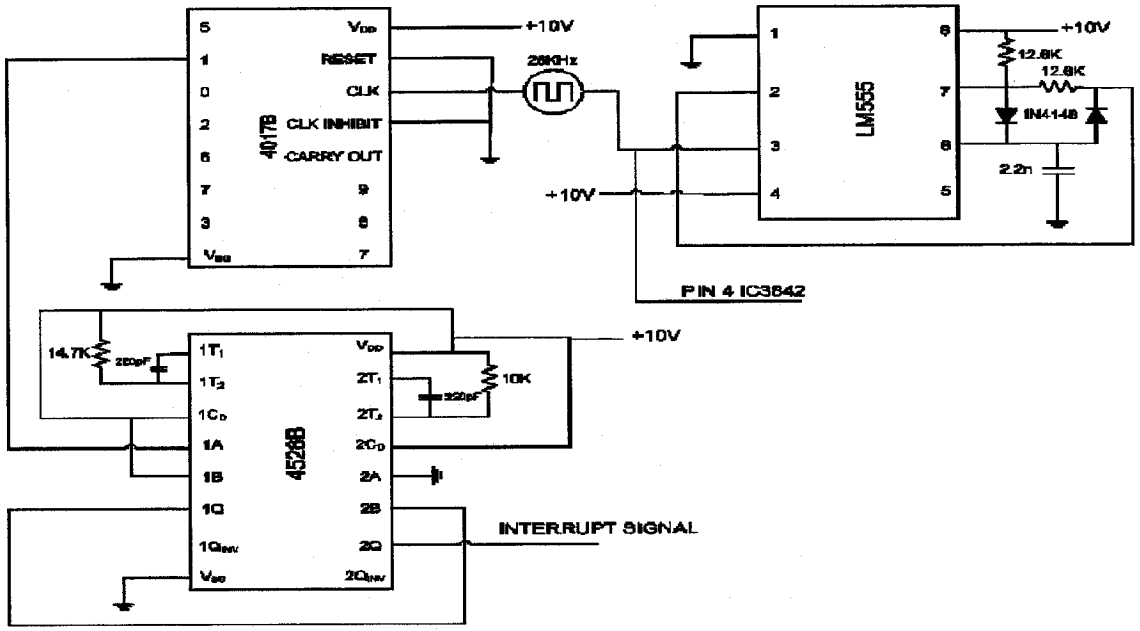

Fig.5.5 Clock and interrupt generator circuit for standard scheme

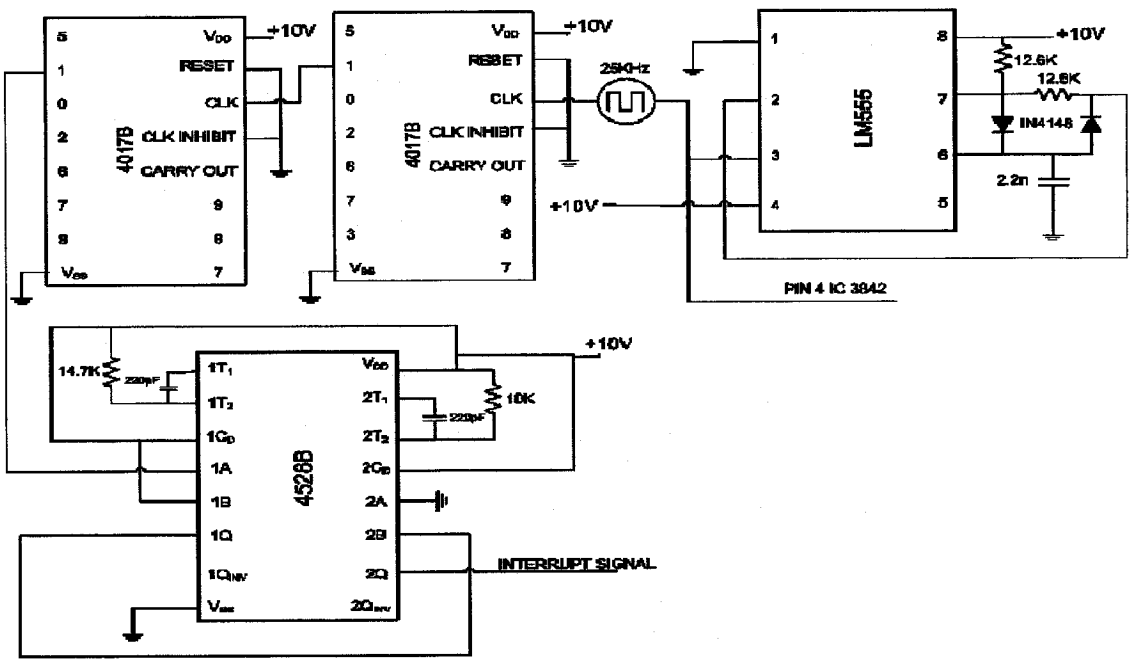

Fig.5.6 Clock and interrupt generator circuit for Fuzzy logic based scheme

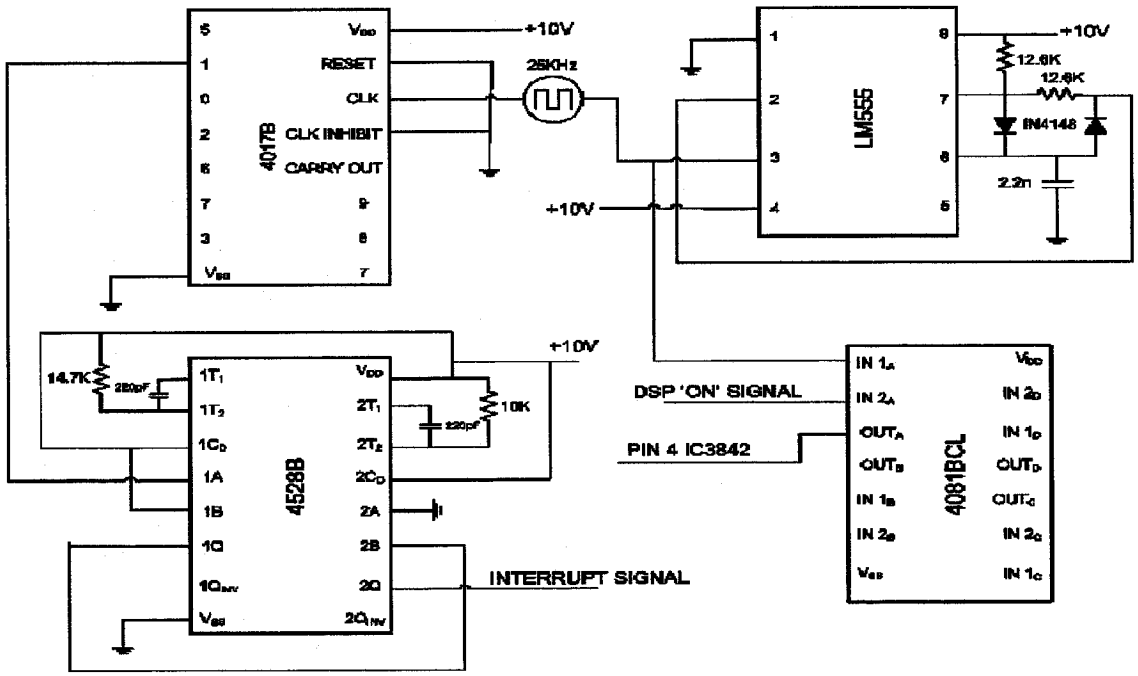

Fig.5.7 Clock and interrupt generator circuit for both non-switching zones based schemes

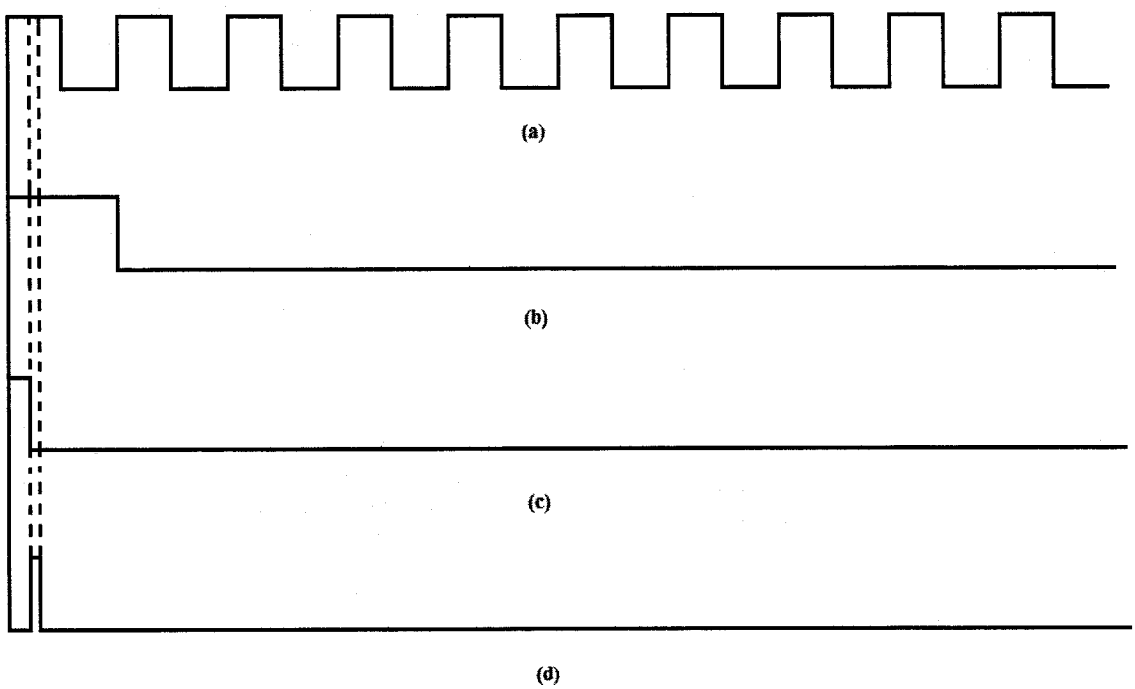

Fig.5.8 (a) Clock signal at the output of the 555 Timer, (b) Output of the 4017 Decade Counter, (c) Output of the first Multivibrator (d) Output of the second Multivibrator

The clock and interrupt generator circuit for the non-switching based MPPT schemes is shown in Fig.5.7. In this an extra AND gate is added with two inputs: a 25 kHz clock signal from the 555 timer and a signal from the MPPT DSP DS1104 microcontroller to disable the clock signal during operation in the Non-switching zone and keep the switch 'ON' for duty ratio = 1. It must be noted here that only a single non-MPP zone corresponding to lower values of I_{PV} is considered for the experimental case. The sampling frequency here is again 2.5 kHz, hence only a single decade counter is used.

5.2.5 Sample and Hold DSP

A DS1103 dSPACE microcontroller interface board is used to sample values of PV voltage and current. An external interrupt signal is provided by the clock and interrupt generator circuit to the external interrupt input of the DSP board corresponding to the desired sampling instant. The Simulink schematic corresponding to this operation is shown in Fig.5.9.

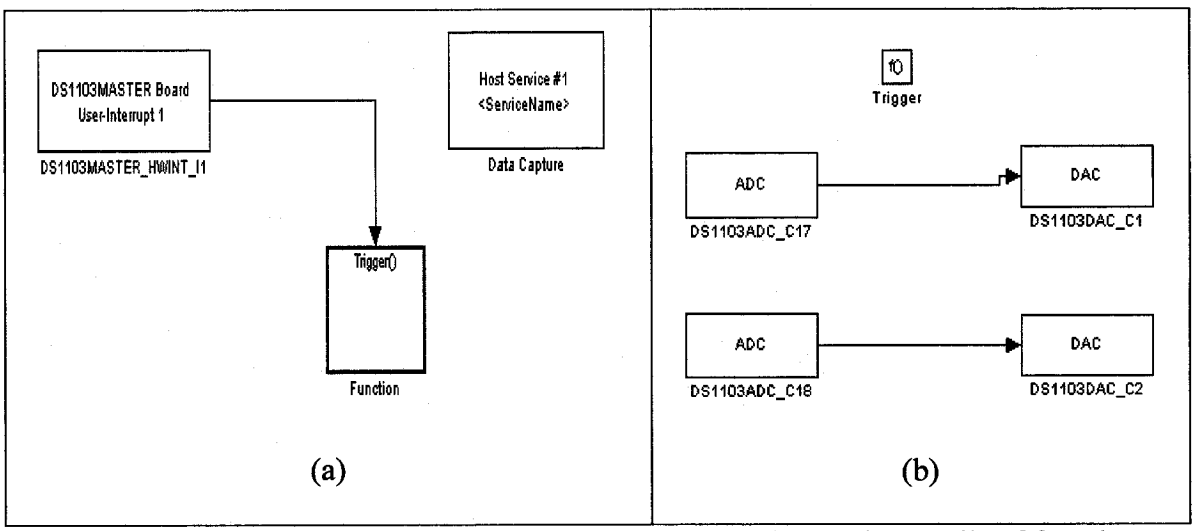

Fig.5.9 (a) Simulink schematic for the Sample and Hold DSP (b) Details of function block

5.2.6 Analog Peak Current Control Circuit

The peak current control logic is implemented in an analog fashion with the use of the PWM 3842 IC as shown in Fig.5.10 to overcome the limitations of the dSPACE Microcontroller. Fig.5.10 shows the 3842 PWM IC connected to the MPPT boost converter. The peak reference current (I_{REF}) is set by supplying a voltage V_{REF} to pin 2 of the 3842 IC through the feedback network comprising of two 10K resistors. The relation between I_{REF} and voltage V_{REF} was verified by experimental testing and the results are displayed in Fig.5.11. It can be seen from Fig.5.11 that very low values of I_{REF} cannot be imposed. In the operating region the linear equation that defines the relationship between I_{REF} and V_{REF} is given by:

$$V_{REF} = -0.61 I_{REF} + 3.732 \quad (5.1)$$

The actual current is measured as a voltage across a 0.2 Ω resistor connected between the drain of the MOSFET and ground which is supplied to pin 3 of the 3842 IC through RC filter network. A 25 kHz clock signal is supplied to pin 4 from IC 555 timer to set the frequency of operation of the boost converter, which is also supplied to the sampling circuit to synchronize the sampling instant with the switching of the MOSFET. The gating signal for the MOSFET is supplied directly from pin 6 of the 3842 IC to the gate of the MOSFET through a 10 ohm resistor.

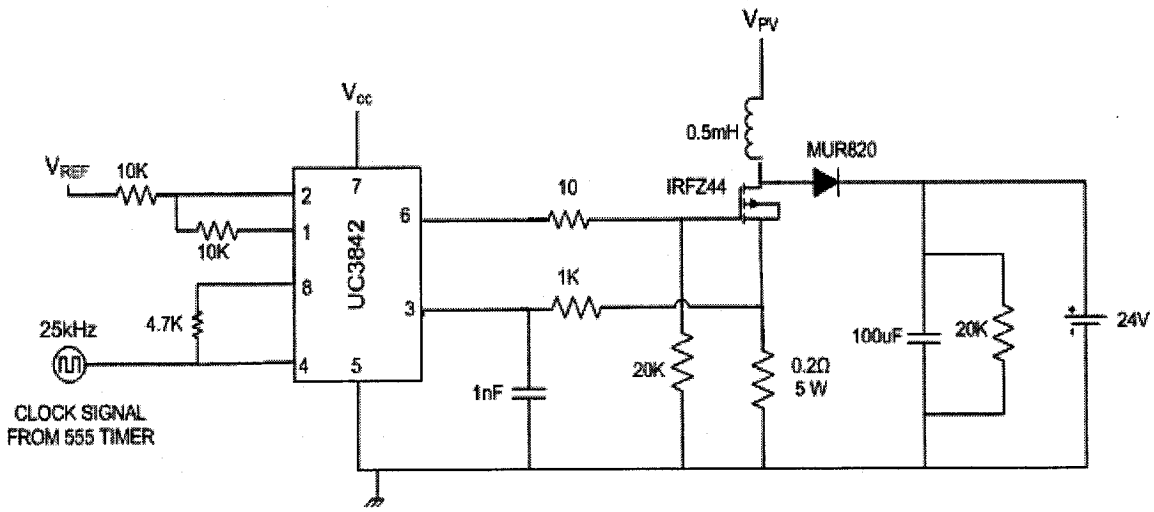

Fig.5.10 Detailed connections of PWM 3842 IC for Peak Current Control

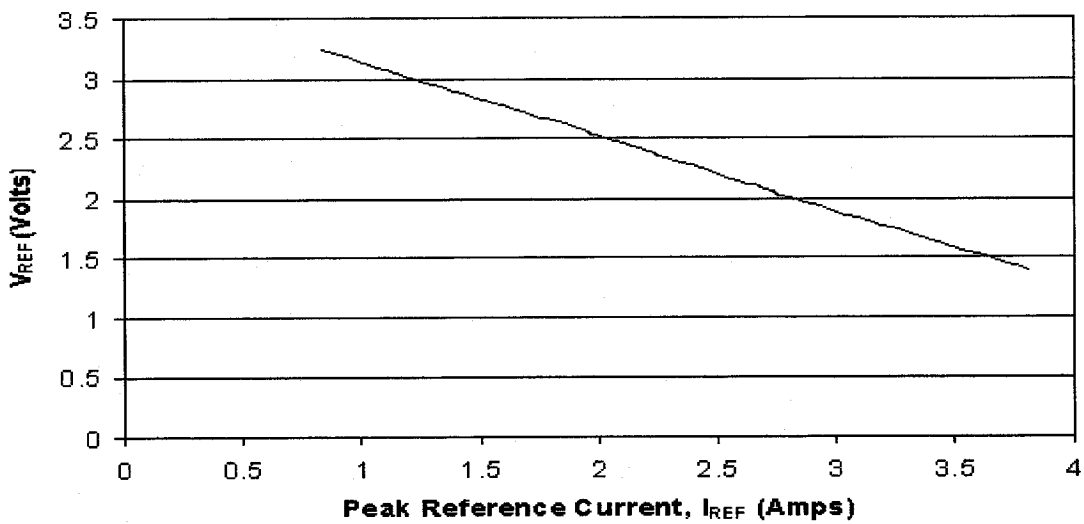

Fig.5.11 V_{REF} versus I_{REF} characteristics of the PWM 3842 IC

5.2.7 PV Current and Voltage measurement circuitry

A LA 55P Hall effect current sensor is used to sense the input PV current. The gain of the LA55P current sensor is 1000:1 i.e. a current of 1 A flowing through the wire results in a current of 1 mA flowing through the output resistor. An output resistor of 680 ohms is selected. Also, 4 turns of wire is inserted through the LA55P current sensor to boost the output of the current sensor, considering the limitation on the output resistor.

The output of the current sensor is fed to the Sample and Hold DSP. Suppose we have a current of 3.45A flowing through the wire. The output of the current sensor will be $\frac{3.45\times4\times680}{1000} = 9.384\text{V}$. Hence the gain of the current sensor is 2.72. Experiments were also carried out using Hall-effect probes and the gain was found to be 2.69 which almost match with the theoretical results.

The input to the A/D converter in the DSPACE system is limited to +10...-10. Hence a suitable voltage-divider network is needed to limit the sensed PV Voltage. Since the maximum open circuit voltage we worked with was 21.7 V. Hence, we used a voltage-divider network of 5.1 K in series with 6.3K. The input PV voltage is supplied to the series combination of 5.1K and 6.3K and the output of the 5.1K resistor is supplied to the A/D converter. Thus a voltage of 21.7 V would correspond to $\frac{21.7\times5.1K}{5.1K+6.3K} = 9.7$ V. Thus the voltage gain would be 0.447.

5.2.8 MPPT DS1104 DSP Microcontroller

The MPPT algorithm for the four peak current control based MPPT techniques are implemented in the DS1104 dSPACE system. The control schematics in Simulink for each individual algorithm will be discussed in section 5.3. After samples of PV current and voltage are processed by the MPPT DSP microcontroller, the peak reference current converted to a suitable voltage value is supplied to the 3842 IC for the PCC implementation.

The gains of the sampled PV voltage and current values in the Simulink schematics are selected as follows:

As we know the A/D converter converts a signal of +10....-10 to +1....-1 in the Simulink schematic and the gain of the current sensor is 2.69 as was calculated before. Hence, to work with actual values of PV current in the Simulink schematic a suitable gain is required, which is calculated as 10/2.69 = 3.72.

Also, the gain of the voltage resistor network is 0.447 as was calculated before. Hence, to work with actual values of PV voltage in the Simulink schematic the gain required is calculated as 10/0.447 = 22.37.

5.3 RTI SIMULINK SCHEMATICS

5.3.1 Control Schematic of the Standard scheme with Fixed ΔI_{REF} [2]

The control schematic for the standard scheme with fixed ΔI_{REF} is shown in Fig.5.12. It can be seen that the dSPACE system picks up sampled values of I_{PV} and V_{PV} and then provides a suitable dc voltage to the 3842 IC to impose the desired reference current.

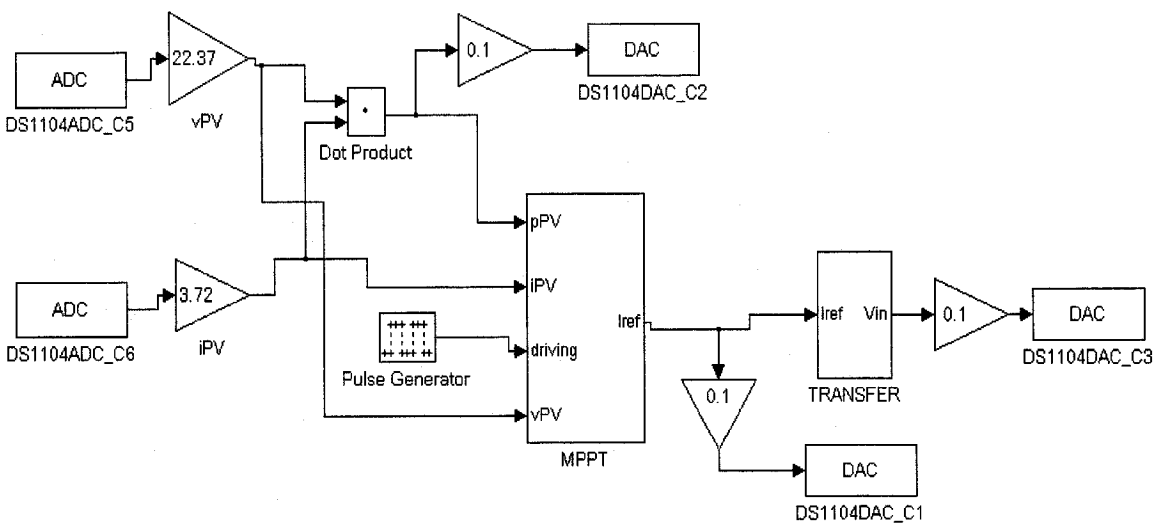

Fig.5.12 Control schematic for standard scheme with fixed ΔI_{REF}

Details of the MPPT block are shown in Fig. 5.13. This is similar to the block used in the simulation schematic with the exception of the ANTI-STICK block and the DEAD-ZONE unit that were not used. The ANTI-STICK block [2] is used to prevent the operating point from sticking in one place if the differences in consecutive samples of I_{PV} or P_{PV} i.e. ΔI_{PV} or ΔP_{PV} are too small to be distinguished by the A/D converters, so that the perturbation direction which is the product of ΔI_{PV} or ΔP_{PV} is zero and so I_{REF} will not be perturbed again. The ANTI-STICK maintains the same perturbation direction of the previous cycle if ΔI_{PV} or ΔP_{PV} is zero. When the values of ΔI_{PV} or ΔP_{PV} are small, they cannot be computed correctly due to noise. Hence when ΔI_{PV} or ΔP_{PV} fall into certain ranges the DEADZONE unit [2] outputs zero.

Two delay blocks are used in this case as opposed to three in [2] because in the present case the Clocking and interrupt generator circuit ensures that the Sample and Hold DSP samples noise free values of I_{PV} and P_{PV}. The first DELAY unit allows enough time to process the sampled values of I_{PV} and P_{PV} and obtain the original perturbation direction. Then the ANTI-STICK block is triggered to output the final perturbation direction in terms of the original perturbation direction. The second DELAY unit shifts the present samples of P_{PV} and I_{PV} to the $P_{PV}(k-1)$ and the $I_{PV}(k-1)$ blocks in preparation for the next cycle. The ACCUMULATOR block is also triggered to update I_{REF}.

The TRANSFER block, details of which are shown in Fig.5.14 is used to convert the desired value of I_{REF} to a suitable DC voltage which is input to pin 2 of the 3842 PWM IC so that it imposes the desired reference current.

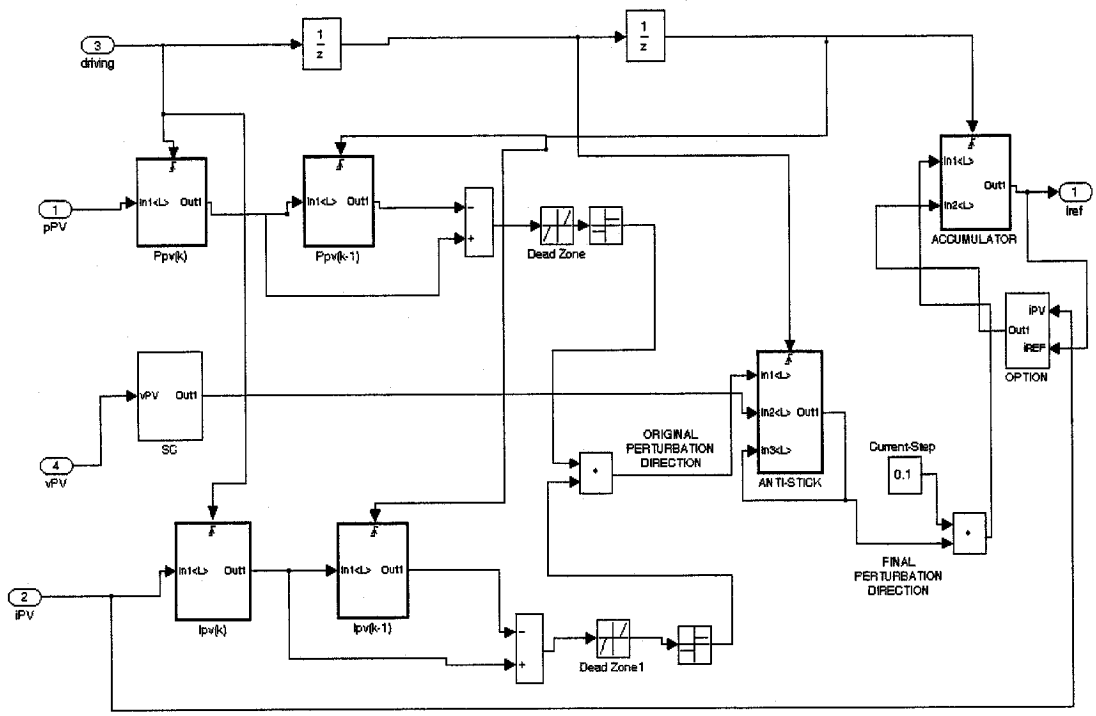

Fig.5.13 Details of the MPPT block for standard scheme

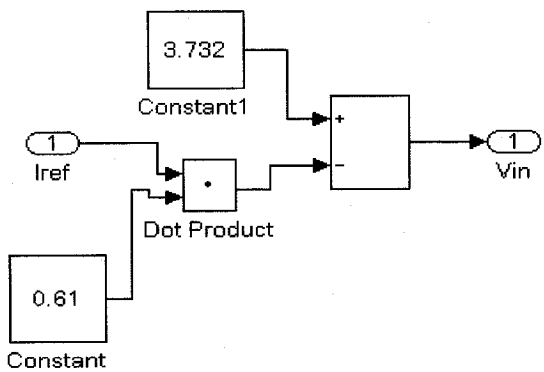

Fig.5.14 Details of TRANSFER block

5.3.2 Control Schematic of Fuzzy Logic based scheme with Variable ΔI_{REF}

The control schematic for the Fuzzy logic based scheme with variable ΔI_{REF} is shown in the Fig.5.15. In this case a special block called 'START' is required as in this case the ramp is not generated by the OPTION block because at start-up the variation of PV current and voltage and hence of PV power is almost zero, thus the fuzzy controller block outputs a zero incremental reference current. The details of the start-up block are shown in Fig.5.16.

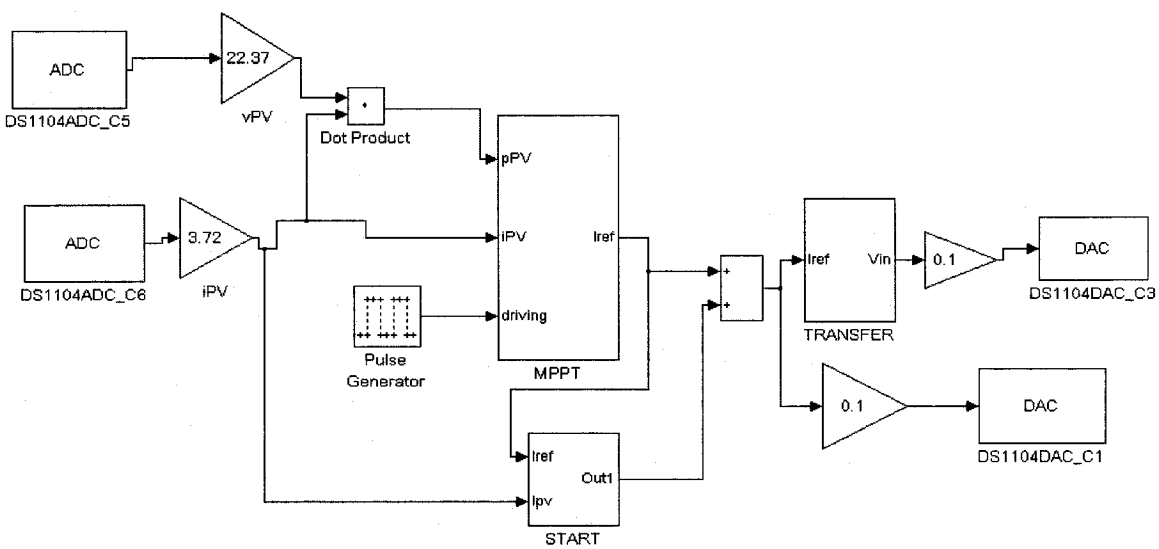

Fig.5.15 Control schematic for Fuzzy logic based scheme with variable ΔI_{REF}

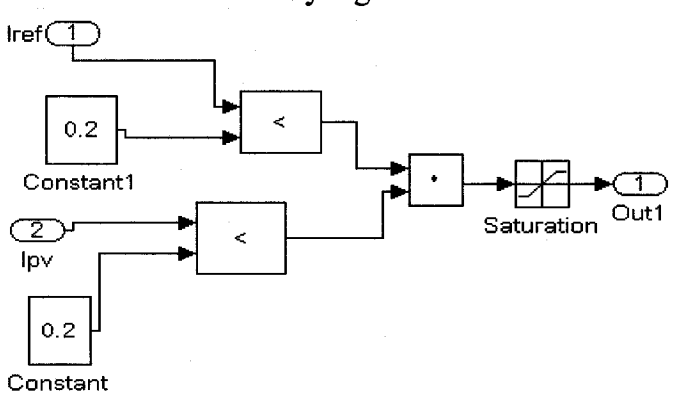

Fig.5.16 Details of the START block

Here the PV current and the reference current at the output of the accumulator block are input to the START block and compared with preset constants. If these values are below

their respective preset constants, the output of the START block is 0.5 which is added with the output of the accumulator block, so that the net reference current, I_{REF} at start-up is 0.5 A.

Once the system starts up the PV current and reference current at the output of the accumulator block will be higher than the preset constants and the output of the START block will be 0. Thus the net reference current I_{REF} will only be due to the output of the accumulator block.

The MPPT block shown in Fig.5.17 is similar to that used in the case of the simulations, but the DEADZONE blocks were used in this case too for reasons described before. As before the name of the .fis file corresponding to the fuzzy controller is entered in the Fuzzy controller block.

The TRANSFER block is the same as the case of the standard scheme with fixed ΔI_{REF}.

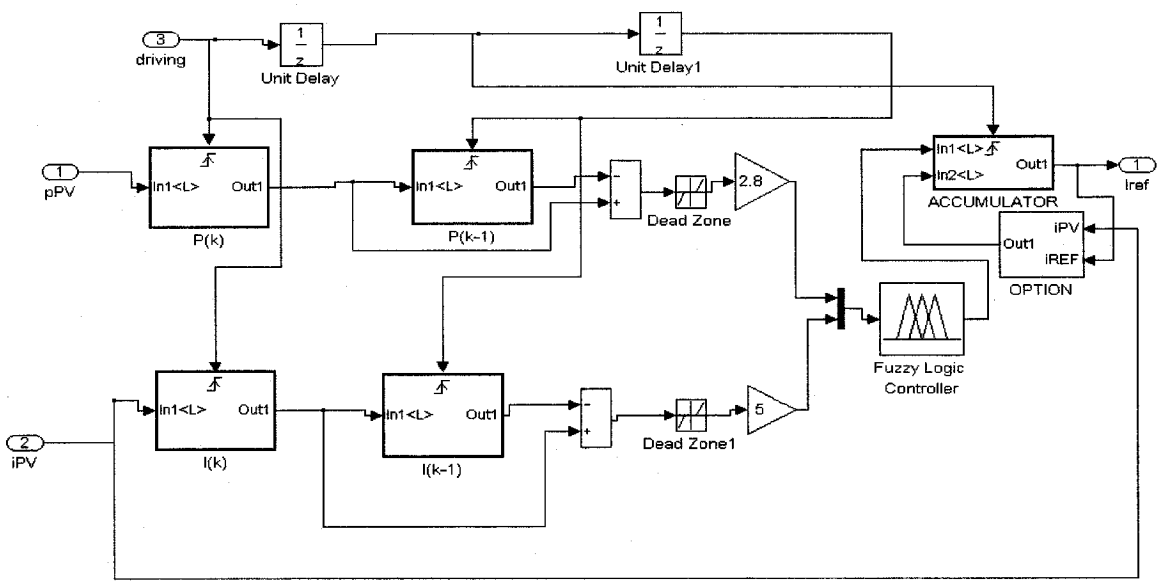

Fig.5.17 Details of the MPPT block for Fuzzy logic based scheme

5.3.3 Control Schematic for Non-Switching Zones and Fixed ΔI_{REF}

The control schematic in Simulink for non-switching zones and fixed ΔI_{REF} is displayed in Fig.5.18.

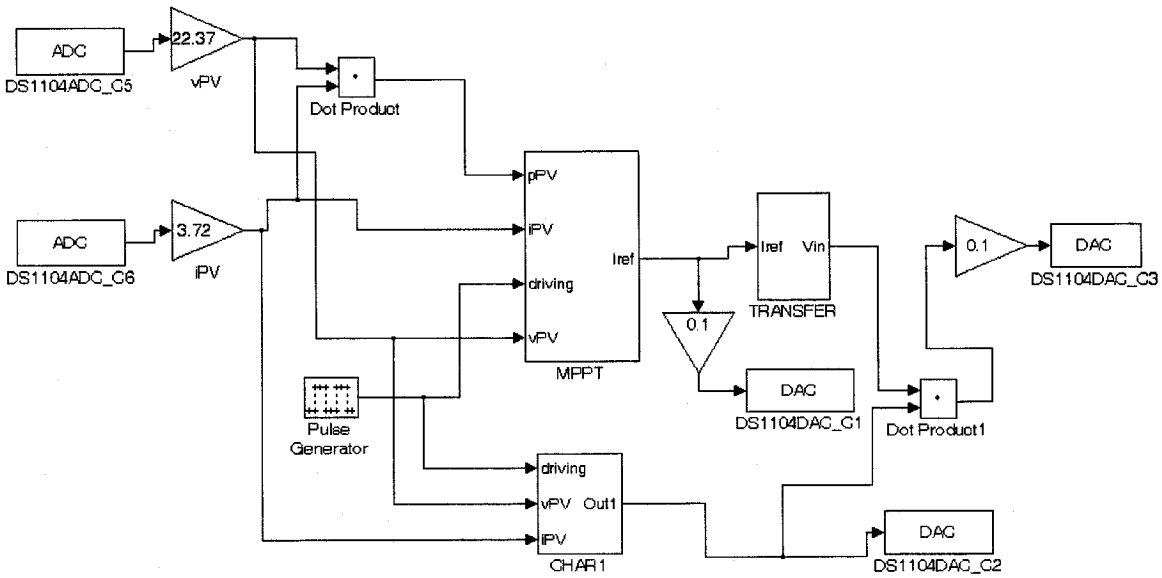

Fig.5.18 Control schematic for non-switching zones based schemes

Here the block CHAR1 shown in Fig.5.19 is used as in the case of the simulation to model the curve that separates the switching zones from the non-switching zone corresponding to lower values of I_{PV}. The equation for CHAR1 used in this case is:

CHAR1: $V_{TO} = 0.255I_{PV} + 18.615$

Thus when V_{PV} is greater than the voltage on the characteristic obtained from the measured value of I_{PV} the CHAR1 block outputs a 'LOW' signal which is given to the clock and interrupt generator circuit through the D/A converter to inhibit the clock signal to the 3842 IC through the use of the 4081 AND gate, which outputs a 'LOW' signal continuously. The continuous 'LOW' signal input to clock input (pin 4) of the 3842 IC ensures the switch operates with 100% duty cycle. If V_{PV} is less than the voltage on the characteristic, this corresponds to operation in the MPP region. Hence the CHAR1 block

outputs a 'HIGH' signal, which when supplied to the AND gate ensures the clock signal is sent to clock pin (pin 4) of the 3842 IC for operation in the PCC mode.

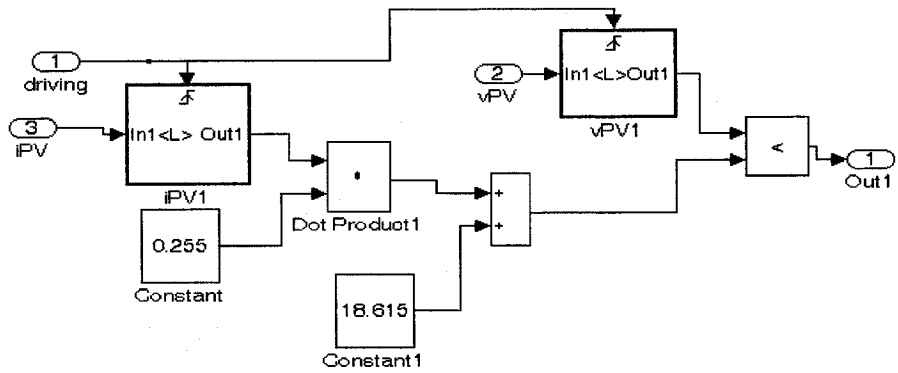

Fig.5.19 Details of the CHAR1 block

The MPPT block and the TRANSFER block are the same as those used in the standard scheme with fixed ΔI_{REF}. However in the case of the MPPT block the step size used was 0.05 A instead of 0.1A for the standard scheme with fixed ΔI_{REF}.

5.3.4 Control Schematic for Non-Switching Zones and Reduced Fuzzy Controller

The control schematic for non-switching zones and the reduced fuzzy controller are shown in Fig.5.18. The MPPT and the TRANSFER block is the same as that used in the case of the Fuzzy logic based scheme with variable ΔI_{REF}. However in the case of the MPPT block the name of the .fis file to be entered in the Fuzzy controller box would correspond to the reduced Fuzzy logic controller. The CHAR1 block is the same as that used with Non-switching zones and fixed ΔI_{REF}. However, to obtain the desired response the equation for CHAR1 used in this case is:

CHAR1: $V_{TO} = 0.28I_{PV} + 18.615$

5.4 EXPERIMENTAL RESULTS AND ANALYSIS

5.4.1 Standard scheme with Fixed ΔI_{REF}

Figure.5.20 shows the start-up process results for the standard scheme with fixed ΔI_{REF}. In the beginning the SAS is disconnected from the MPPT converter, however the MPPT system is already working. It is seen that I_{REF} increases because initially ΔP_{PV} and ΔI_{PV} are both zero, hence the output of the ANTI-STICK block is 1 so the same perturbation direction is retained. When the difference between I_{REF} and I_{PV} (which is zero initially as the SAS simulator is disconnected from the boost converter), exceeds the limit set by the OPTION block, the OPTION block outputs I_{PV} to the ACCUMULATOR block. Hence the I_{REF} is forced to I_{PV} (0 A), before the SAS is connected to the MPPT converter and then I_{REF} increases again forming a saw-tooth waveform.

Once the SAS simulator is connected to the MPPT converter the PV current rises, as also the PV power till the MPP is reached and the operating point oscillates about the MPP. The rise time in this case is seen to be 15 ms. In the simulations the refresh rate for the reference current was same as the switching frequency which was chosen to be 100kHz, while in the experimental case the refresh rate for the reference current is approximately 2.5 kHz due to the constraints of the DSP microcontroller, which requires a larger time-step to process the MPPT algorithm in real time. The rise time in the case of the simulations was 0.32 ms. Thus the expected rise time in the experimental case should be $0.32ms \times \frac{100kHz}{2.5KHz}$ = 13 ms, which is close to what we have experimentally. However one has to also account for the fact that the maximum duty ratio used for the PCC in the

case of the simulations was 70% as opposed to 50% used in the experimental case, which could mean that the rise time obtained experimentally is slower than expected.

The detailed steady state can be seen in Fig.5.21. In the steady state one can see that the operating point oscillates about the MPP. It is also seen that I_{PV} follows the variations in I_{REF}. Moreover from the detailed view of Fig.5.22 one can see that the reference current remains constant for 10 switching cycles, which is expected as the refresh rate for I_{REF} was set at one-tenth of the switching frequency.

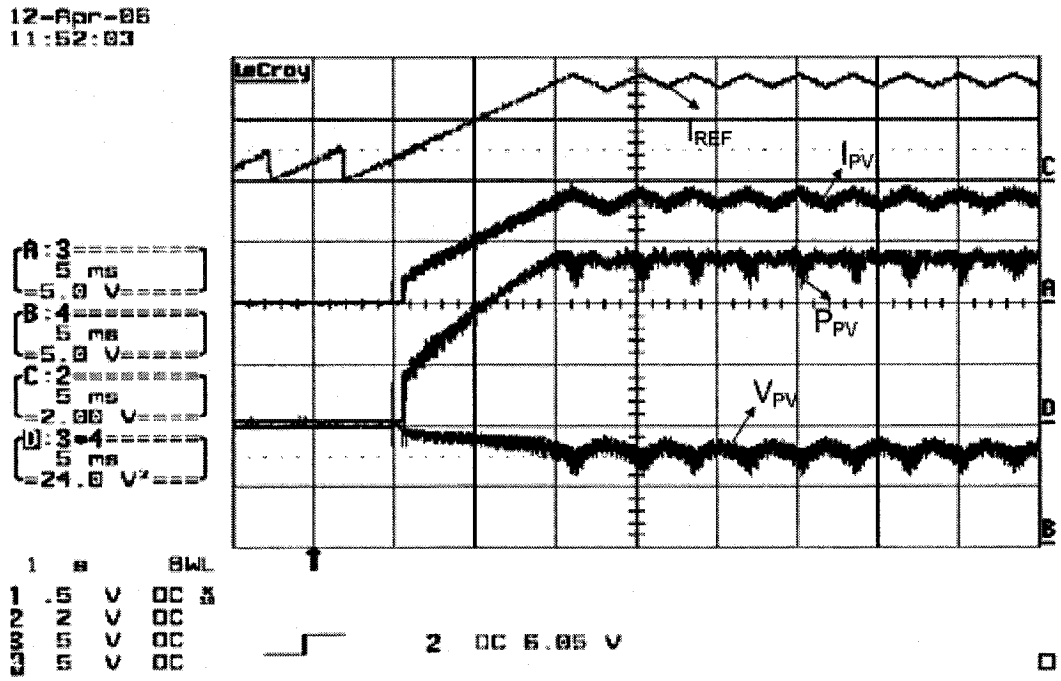

Channel A: I_{PV}:1.84A/div,B:V_{PV}:11.2V/div,C:I_{REF}:2A/div,D:P_{PV}:20.6W/div

Fig.5.20: Start-up of the standard scheme with fixed ΔI_{REF}

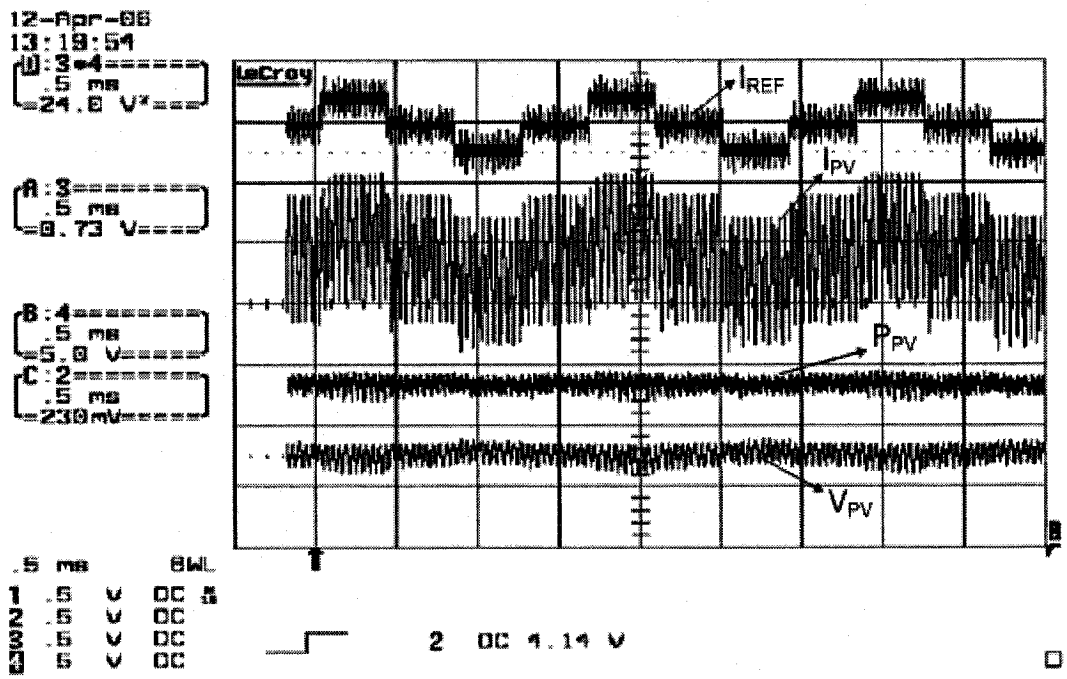

Channel A: I_{PV}:0.27A/div,B:V_{PV}:11.2V/div,C:I_{REF}:0.23A/div,D:P_{PV}:20.6W/div

Fig.5.21 Steady-state view of standard scheme with fixed ΔI_{REF}

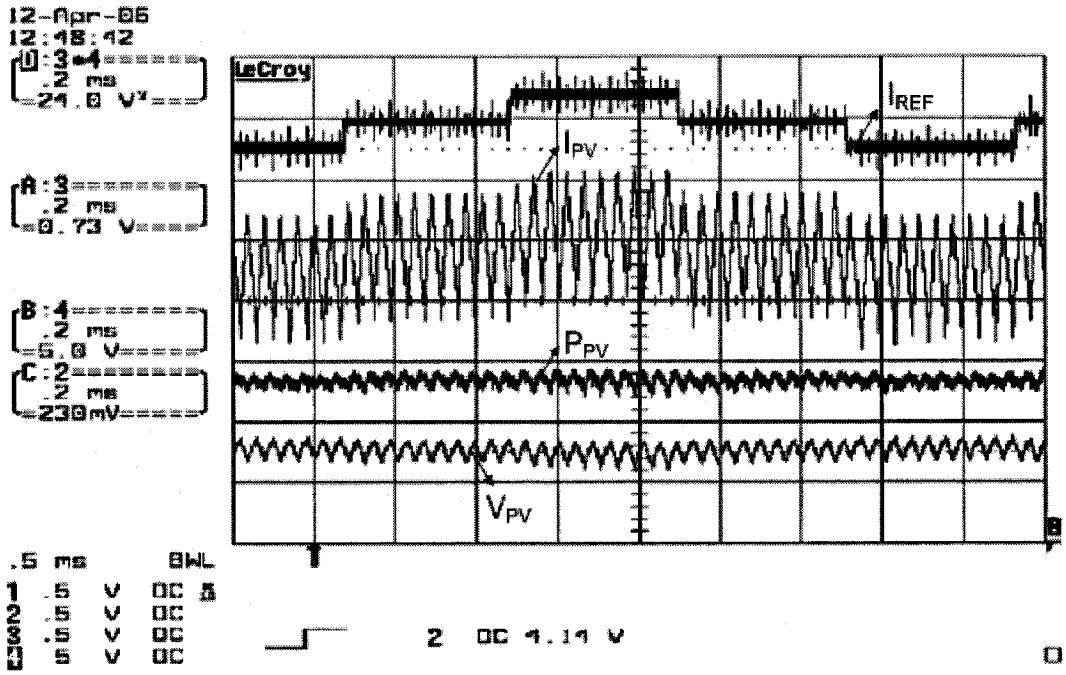

Channel A: I_{PV}:0.27A/div,B:V_{PV}:11.2V/div,C:I_{REF}:0.23A/div,D:P_{PV}:20.6W/div

Fig.5.22 : Detailed view of steady-state for standard scheme with fixed ΔI_{REF}

5.4.2 Fuzzy Logic based scheme with Variable ΔI_{REF}

Figure 5.23 shows the start-up of the Fuzzy logic based scheme with variable ΔI_{REF}. Before the system starts up I_{REF} is set at 0.5 A, which is the output of the START block as initially I_{PV} = 0A and the output of the ACCUMULATOR block is also equal to zero. The rise time in this case can be seen to be 120 ms. Again, in the simulations the refresh rate for the reference current was same as the switching frequency which was chosen to be 100 kHz, while in the experimental case the refresh rate for the reference current is approximately 250 Hz. The rise time in the case of the simulations was 0.27 ms. Thus the expected rise time in the experimental case should be $0.27ms \times \frac{100kHz}{250Hz}$ = 108 ms, which is close to what we have experimentally. Again, one has to also account for the fact that the maximum duty ratio used for the PCC in the case of the simulations was 70% as opposed to 50% used in the experimental case.

The detailed steady state can be seen in Fig.5.24 and Fig.5.25. Fig.5.24 shows the steady state over an extended time-scale to demonstrate that the reference current remains constant over a few sampling periods and the power drops are minimal. Fig.5.25 provides a detailed snapshot of the steady state. It can be seen that, as in the case of the simulations the current ripple is only due to the intrinsic switching of the converter and does not include the variations of I_{REF} that appear for the standard scheme with fixed ΔI_{REF}.

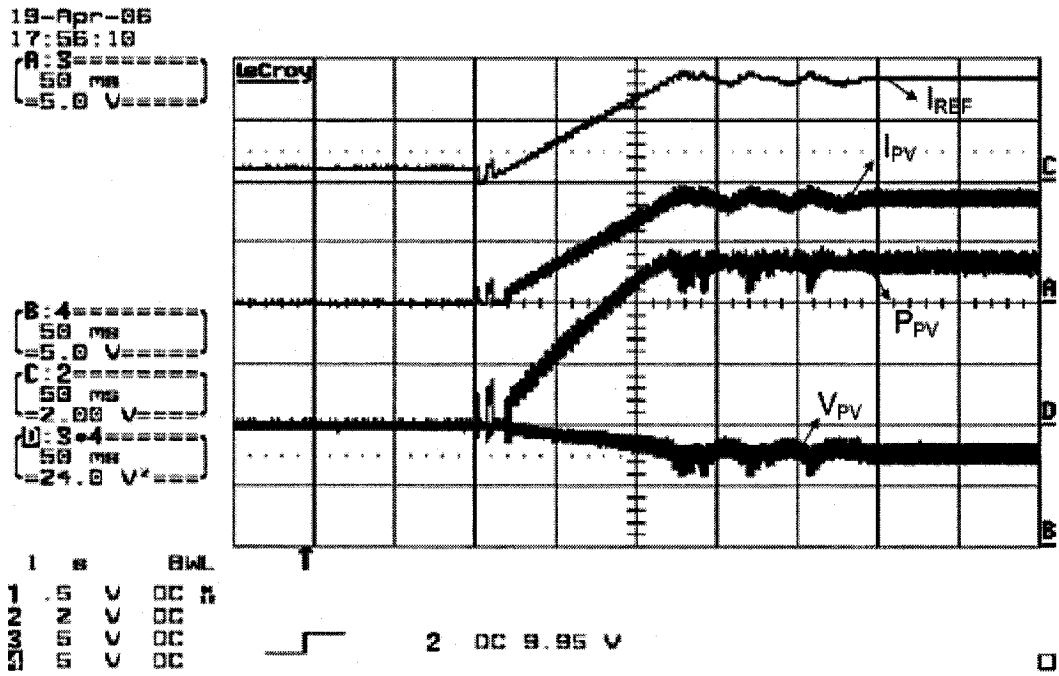

Channel A: I_{PV}:1.84A/div,B:V_{PV}:11.2V/div,C:I_{REF}:2A/div,D:P_{PV}:20.6W/div

Fig.5.23 Start-up of the Fuzzy logic based scheme with variable ΔI_{REF}

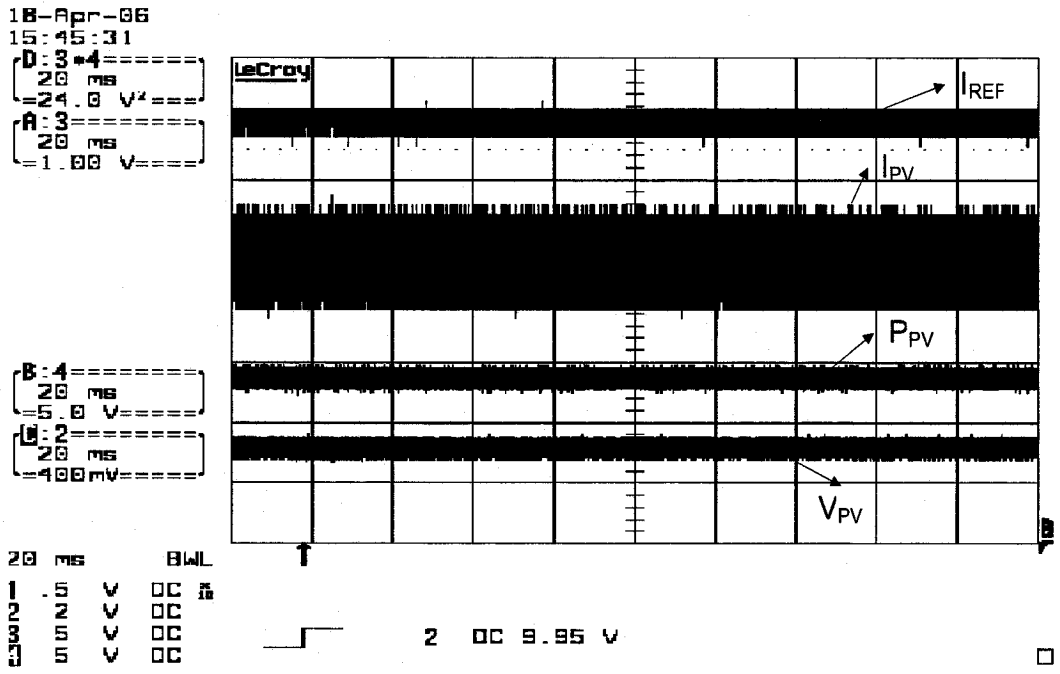

Channel A: I_{PV}:0.37A/div,B:V_{PV}:11.2V/div,C:I_{REF}:0.4A/div,D:P_{PV}:20.6W/div

Fig.5.24 Steady state of the Fuzzy logic based scheme with variable ΔI_{REF}

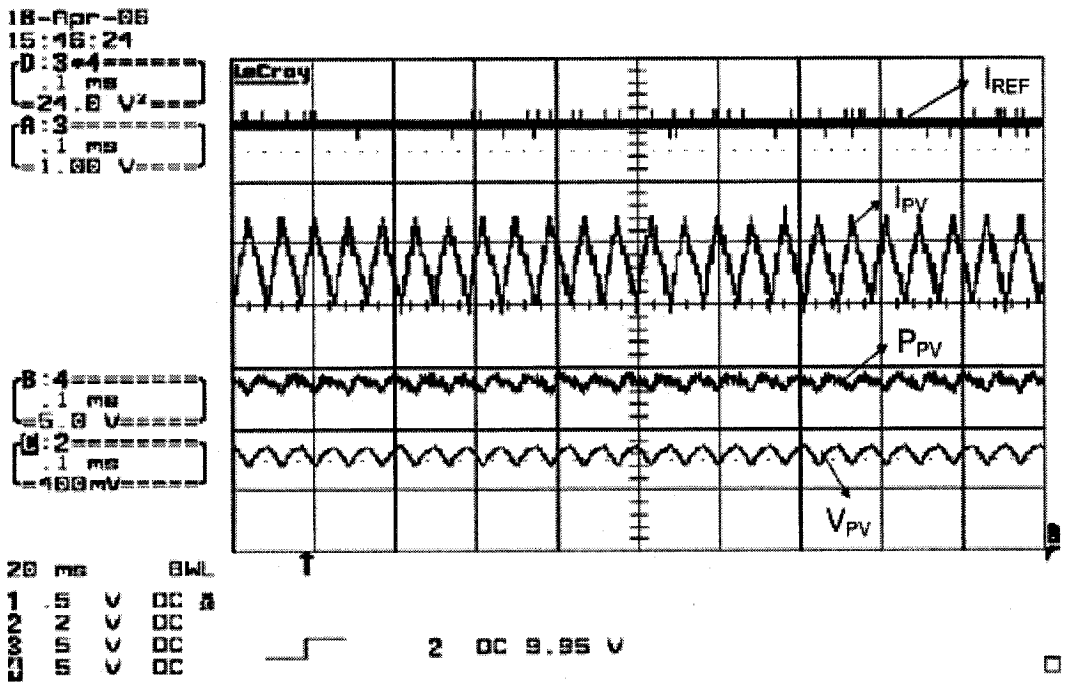

Channel A: I_{PV}:0.37A/div,B:V_{PV}:11.2V/div,C:I_{REF}:0.4A/div,D:P_{PV}:20.6W/div

Fig.5.25 Detailed view of the steady-state for Fuzzy logic based scheme with variable ΔI_{REF}

5.4.3 Non-Switching Zones and Fixed ΔI_{REF}

The start-up of the scheme with non-switching zones and fixed ΔI_{REF} is seen in Fig.5.26. It is seen that before the start-up I_{REF} still appears as a ramp due to reasons similar to the case with the standard scheme using ΔI_{REF}. However, the frequency of the ramp is lower than the case with the standard scheme using fixed ΔI_{REF} because of the lower value of ΔI_{REF} (0.05 A) used in this case as compared to 0.1 A used in the case of the standard scheme with the fixed ΔI_{REF}. Initially when SAS is connected to the converter the current ramps up because initially the switch is in the ON position with duty ratio equal to 1. Once the operating point of the system crosses in to the MPP containing region the standard PCC based MPPT algorithm operates and the reference current can be seen approaching the value corresponding to operation at the MPP in fixed steps. Initial drops

in power can be seen during start-up as due to the relatively large sampling interval used, it is quite possible that the PV current rises and crosses into the short-circuit region resulting in the abnormal behavior observed at start-up. It is believed that a shorter sampling interval should result in the anticipated operation at start-up as was seen in the case of the simulation results. It is also possibly due to this reason that the rise time is 6ms, which is longer than that seen in the case of the simulations. It is not possible to compare the simulation and the experimental waveforms at start-up for this particular case because the obtained waveforms look different.

The detailed steady-state waveform can be seen in Fig.5.27 and Fig.5.28. In the steady-state the operation is similar to the standard scheme with fixed ΔI_{REF}. However, the power drops and ripple in I_{PV} are lower because of the lower value of ΔI_{REF} used in this case as compared to the standard scheme.

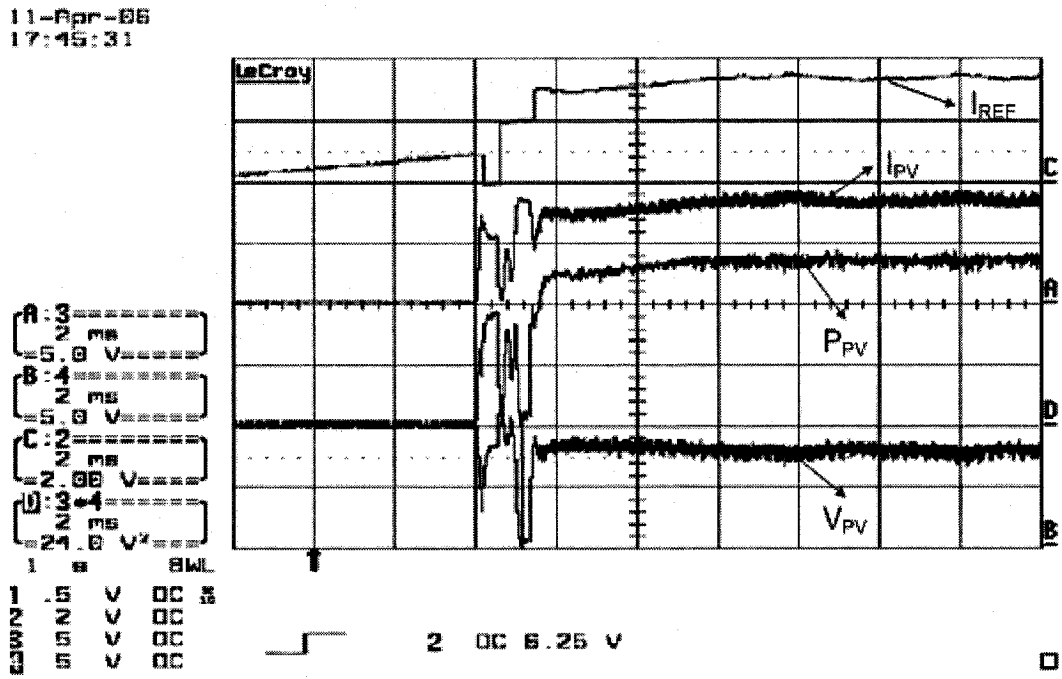

Channel A: I_{PV}:1.84A/div,B:V_{PV}:11.2V/div,C:I_{REF}:2A/div,D:P_{PV}:20.6W/div

Fig.5.26: Start-up of scheme with non-switching zones and fixed ΔI_{REF}

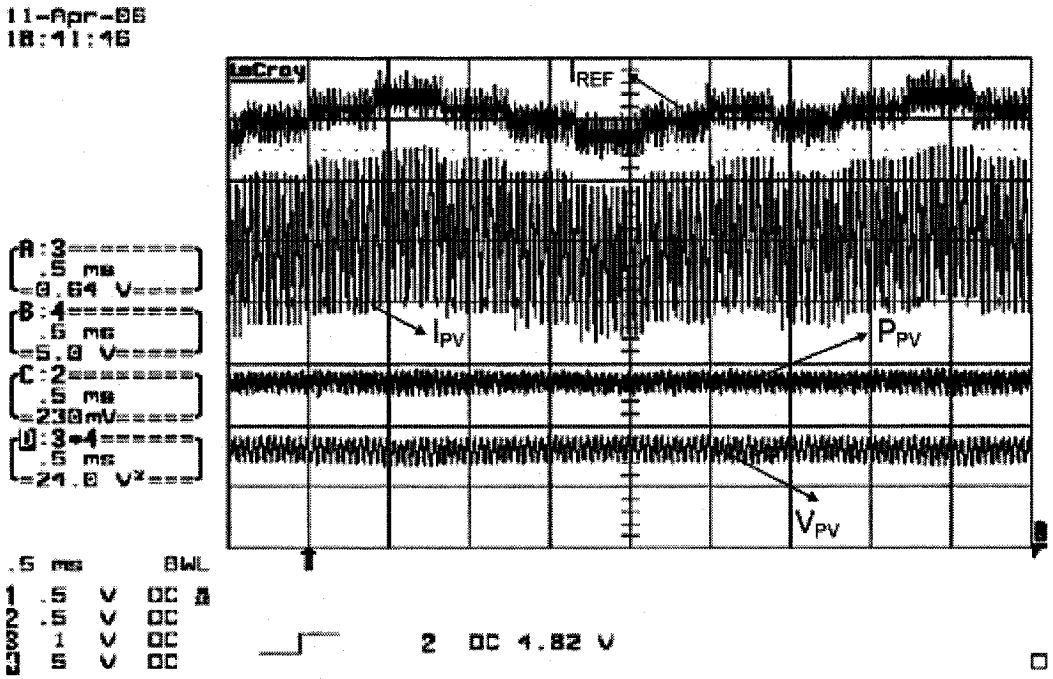

Channel A: I_{PV}:0.24A/div,B:V_{PV}:11.2V/div,C:I_{REF}:0.23A/div,D:P_{PV}:20.6W/div

Fig.5.27: Steady state of scheme with non-switching zones and fixed ΔI_{REF}

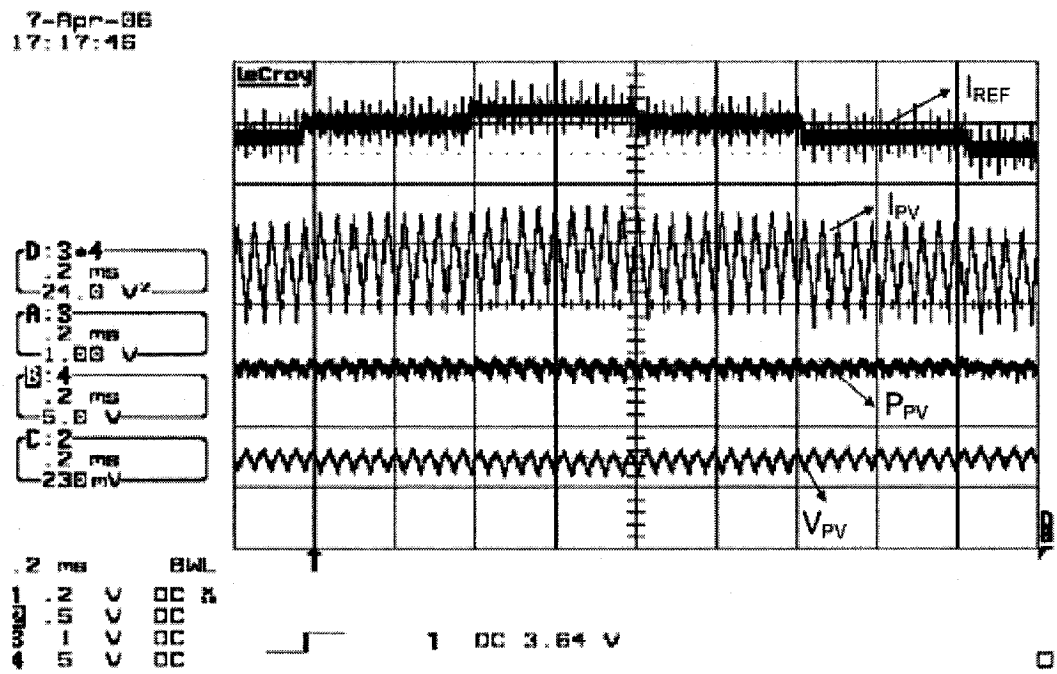

Channel A: I_{PV}:0.37A/div,B:V_{PV}:11.2V/div,C:I_{REF}:2A/div,D:P_{PV}:20.6W/div

Fig.5.28: Detailed view of steady-state for scheme with non-switching zones and fixed ΔI_{REF}

5.4.4 Non-Switching Zones and Reduced Fuzzy Controller

Figure 5.29 shows the start-up for the scheme employing Non-switching zones and the reduced Fuzzy controller. The difference between the simulation and experimental waveforms at the start-up associated with the scheme involving non-switching zones and fixed ΔI_{REF} could be seen in this case as well and for the same reasons. However, once the operating point transfers to the MPP containing region, the reference current increases in increments corresponding to the Fuzzy set PS of the ΔI_{REF} variable of the reduced Fuzzy controller and the increments gradually get to zero, once the operating point reaches the MPP. In this case the rise time is seen to be 10 ms. The rise time could be reduced by increasing slope of the characteristic that divides the MPP and the non-MPP containing regions. This could also be reduced by redefining the reduced Fuzzy controller so that it could output a higher maximum ΔI_{REF} as compared to the 0.025A used in the present case.

The detailed steady state can be seen in Fig.5.30. As expected the reference current remains almost constant. Peak-to-peak ripple in I_{PV} and the power drops are minimum similar to the case of the Fuzzy logic scheme with variable ΔI_{REF}

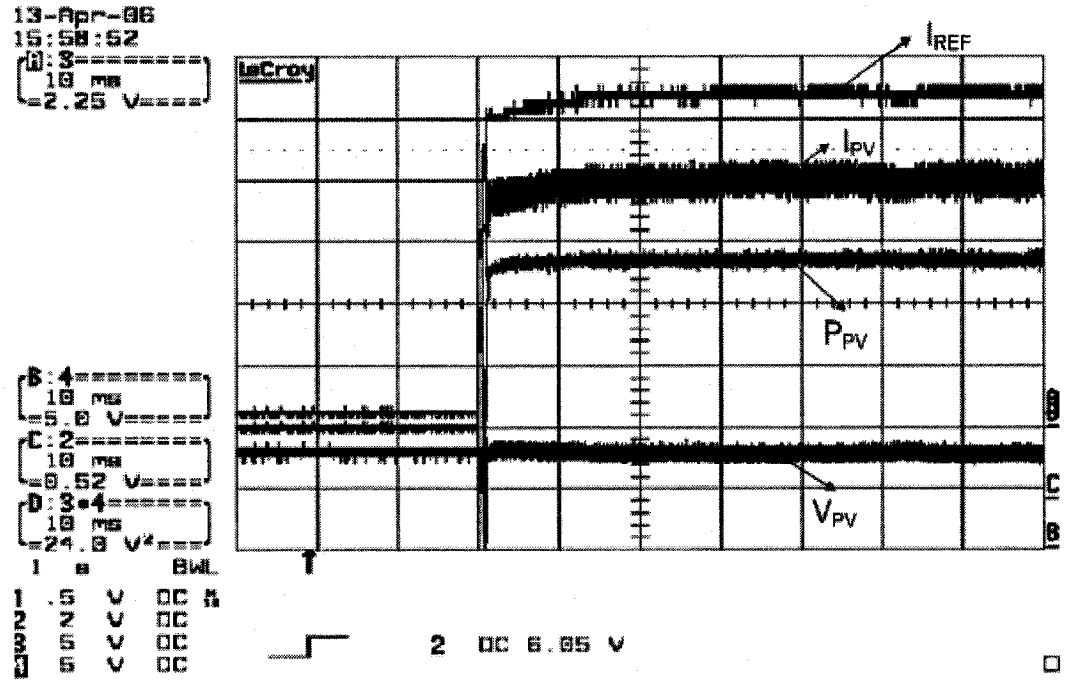

Channel A: I_{PV}:0.83A/div,B:V_{PV}:11.2V/div,C:I_{REF}:0.52A/div,D:P_{PV}:20.6W/div

Fig.5.29 Start-up of scheme with non-switching zones and reduced fuzzy controller

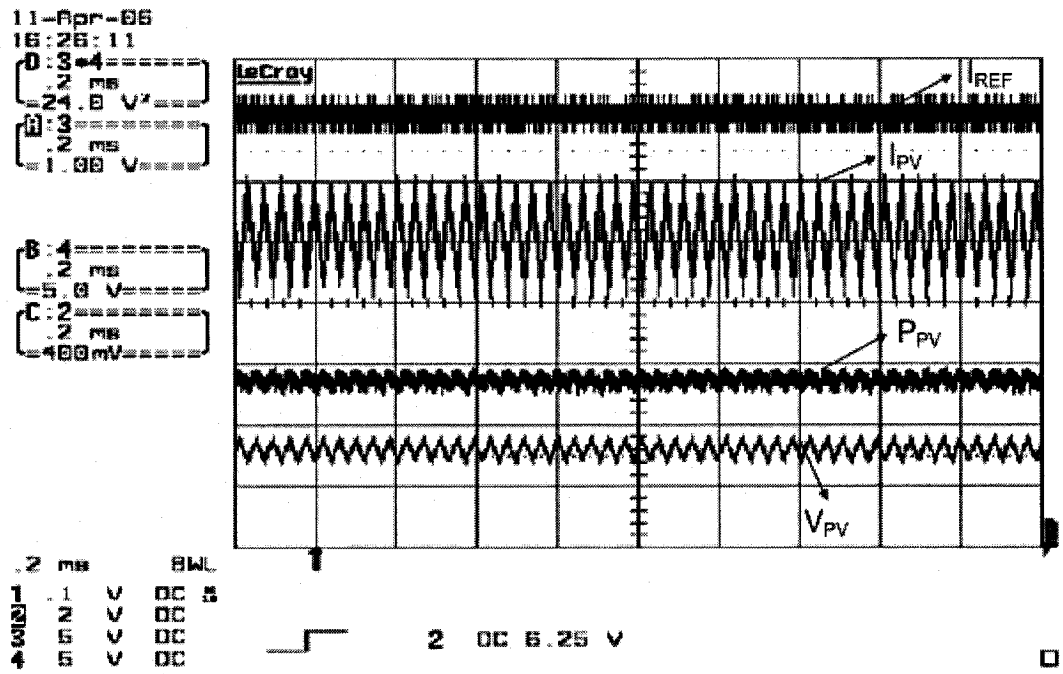

Channel A: I_{PV}:0.37A/div,B:V_{PV}:11.2V/div,C:I_{REF}:0.4A/div,D:P_{PV}:20.6W/div

Fig.5.30 Steady-state of scheme with non-switching zones and reduced fuzzy controller

5.4.5 Comparison Table

	Standard scheme with Fixed ΔI_{REF} (0.1 A)	Fuzzy Logic based Scheme with Variable ΔI_{REF}	Non-switching zones and Fixed ΔI_{REF} (0.05 A)	Non-switching zones and Reduced Fuzzy
Rise time	15 ms	120 ms	6 ms	10 ms
Power Drops	High	Low	Low	Low
Peak-peak current ripple	High	Lowest	Lower than standard scheme	lowest

Table 5.1 Comparison of the four peak current control based MPPT schemes based on experimental results

5.5 CONCLUSIONS

In this chapter experimental verification of the previously discussed PCC based MPPT algorithms, is carried out. An analog implementation of the peak current control strategy is suggested to achieve a switching frequency higher and independent of the sampling frequency, that is limited by the processing speed of the DSP and the complexity of the MPPT logic.

The control schematics in MATLAB/Simulink for the Real Time Implementation with a dSPACE microcontroller of the four peak current control based MPPT techniques are provided and discussed. From the experimental results it can be seen that the non-switching zones based schemes possessed the best rise times. The fuzzy logic based scheme using variable ΔI_{REF} had the slowest rise time because of the very low update rate for ΔI_{REF} on account of the large processing time required for the complex fuzzy controller. In the experimental case the standard scheme with a fixed ΔI_{REF} has a faster

rise time than the fuzzy logic based scheme with variable ΔI_{REF} on account of a higher update rate for I_{REF} in the standard scheme.

In the steady-state the fuzzy logic based schemes with variable ΔI_{REF} and the non-switching zones based schemes presented low power drops and low peak-to-peak current ripple. The standard scheme with a fixed ΔI_{REF} presented higher power drops and higher peak-to-peak current ripple.

CHAPTER 6

CONCLUSIONS

6.1 SUMMARY

P&O MPPT algorithms that use one-cycle control schemes such as peak current control and instantaneous sampling of PV panel voltage and current values have been shown to possess fast transient responses and low power drops in the steady-state. They have also been shown to possess accurate tracking of the MPP under rapidly varying atmospheric conditions. However, the use of a fixed incremental reference current step-size yields a compromise between transient and steady state performance. Chapter 2 proposes the use of a fuzzy logic controller in the conventional peak current control based algorithm to output a variable incremental reference current step-size depending on the location of the operating point of the system on PV panel $V_{PV} \times I_{PV}$ characteristic, so that a larger incremental step-size was used during the transient operation, which was almost reduced to zero in the steady-state. However, the use of a complex fuzzy controller leads to the requirement of a higher computation burden while implementing the system in real-time. To overcome this difficulty and for a faster transient response Chapter 3 proposes the use of hybrid schemes based on the division of PV panel $V_{PV} \times I_{PV}$ characteristic into three regions: two non-MPP containing regions or non-switching zones and one MPP containing region or switching zone. While operating in the non-MPP zones, the switch is operated with a duty cycle of 0 or 1 to accelerate the operating point

towards the MPP region, where the standard peak current control scheme operates with a lower incremental reference current resulting in better steady-state performance without compromising on the transient performance. It is also possible to use a reduced Fuzzy controller in the MPP zones with lesser membership functions and rules thus easing the computation burden, while providing the ideal response. In Chapter 4 simulation schematics for the four peak current control based MPPT schemes in MATLAB/Simulink are provided and the simulation results are presented. Simulations results show that the hybrid schemes using non-switching zones presented the fastest transient responses. The schemes using Fuzzy logic presented the lowest power drops. Chapter 5 presents the experimental evaluation of the four peak current control based MPPT schemes. An analog implementation of the peak current control logic is proposed to achieve a sampling frequency lower and independent of switching frequency. Hence, operation at higher switching frequencies is possible in spite of the computational constraints of the DSP microcontroller. Experimental results showed that schemes proposed in Chapters 2 & 3 of this thesis presented lower power drops in the steady state as well as lower peak-to-peak current ripple as compared to standard scheme with fixed incremental reference current step-size. The hybrid schemes using non-switching zones presented the fastest transient responses. From Chapters 4 & 5 one can see that there are differences between the simulation and experimental results mainly due to the constraints imposed by the experimental implementation of the prototype. For instance in the case of the simulations, the Fuzzy logic based scheme using a variable incremental reference current possessed a faster transient response than the standard scheme using a fixed incremental reference current, but had a slower transient response in the case of the experimental

implementation. This was because of the lower sampling frequency that had to be used in the case of the Fuzzy logic based system due to the large processing time required by the complex Fuzzy controller for Real-time implementation.

6.2 CONTRIBUTIONS

The major contributions of this thesis are:

[1] Proposed a Fuzzy logic controller based peak current control MPPT algorithm which uses a variable incremental reference current to achieve a simultaneously better transient and steady-state performance as compared to the standard scheme with a fixed incremental reference current.

[2] Proposed two hybrid MPPT schemes based on the division of PV panel $V_{PV} \times I_{PV}$ characteristic into two non-MPP containing or non-switching zones and one MPP containing or switching zones for best transient performance.

[3] Proposed an analog implementation of the peak current control logic using a 3842 PWM IC in order to overcome the constraints of the DSP microcontroller and achieve operation at a higher switching frequency, while still synchronizing the sampling of current and voltage values to the switching of the power converter to achieve sampling at commutation noise free instants.

[4] A laboratory prototype was built and the performance of the four peak current control based MPPT techniques was evaluated.

6.3 Suggestions For Future Work

[1] Implementation of the four peak current control based MPPT systems in an FPGA or a faster microcontroller to be able to operate the power converter at a higher frequency and achieve the goal of sampling frequency being equal to switching frequency as well as ensure digital implementation of the peak current control logic.

[2] Implement the peak current control based MPPT techniques with an actual PV panel to overcome limitations that may exist with the SAS simulator.

[3] Design of a suitable soft-switching MPPT converter to increase the overall efficiency of the system.

[4] Implement the peak current control based MPPT techniques with an interleaved boost converter configuration to reduce the ripple in the PV current while operating at lower switching frequencies or alternatively reduce the size of the passive components if switching frequency is to be kept constant.

REFERENCES

[1] UNESCO (2000), *Solar Electricity,*(Second edition), John Wiley and Sons, England.

[2] Liu, Xuejun (2004), *An Improved Perturbation and Observation Maximum Power Point Tracking Algorithm for PV Panels*, M.A.Sc Thesis in the Department of Electrical and Computer Engineering, Concordia University, Montreal, Canada.

[3] Northern Arizona Wind and Sun (1997-2006). *All about MPPT charge controllers,* retrieved on 23 May 2006 from http://www.solar-electric.com/charge_controls/mppt.htm.

[4] Windy Dankoff (2006) *Increase Solar Charging with a Power Tracking Charge Controller,* retrieved on 23 May 2006 from http://www.affordable-solar.com/charge.controllers.htm.

[5] Y. M. Chen, Y. C. Liu, F. Y. Wu, and Y. E. Wu, "Multi-Input Converter with Power Factor Correction and Maximum Power Point Tracking Features", *APEC'02, 17th Annual IEEE*, Vol. 1, 10-14 Mar. 2002, pp.490-496.

[6] C. Hua, J. Lin, and C. Shen, "Implementation of a DSP-Controlled Photovoltaic System with Peak Power Tracking", *IEEE Transactions on Industrial Electronics*, Vol. 45, Feb. 1998, pp. 99-107.

[7] Chihchiang Hua and Chihming Shen, "Control of DC/DC Converters for Solar Energy System with Maximum Power Tracking", *Industrial Electronics, Control and Instrumentation, 1997, IECON 97*, Vol. 2, Nov. 1997, pp. 827-832.

[8] E. Koutroulis, K. Kalaitzakis and N. C. Voulgaris, "Development of a Microcontroller-Based, Photovoltaic Maximum Power Point Tracking Control

System", *IEEE Transactions on Power Electronics*, Vol. 16, No.1, Jan. 2001, pp.46-54.

[9] P. Huynh and B. H. Cho, "Design and Analysis of a Microprocessor- Controlled Peak-Power-Tracking System", *IEEE Transactions on Aerospace and Electronic Systems*, Vol. 32, No.1, Jan. 1996, pp. 182-189.

[10] M.G. Simões and N.N. Franceschetti, "Fuzzy optimization based control of a solar array system," *Electric Power Applications, IEE Proceedings*, Vol. 146, No. 5, Sept. 1999 pp. 552-558

[11] N. Patcharaprakiti and S. Premrudeepreechacharn, "Maximum Power Point Tracking using Adaptive Fuzzy Logic Control for Grid-Connected Photovoltaic system,", *IEEE Power Engineering Society Winter Meeting*, 2002. Vol. 1, 27-31 Jan. 2002, pp. 372–377.

[12] T. Senjyu and K. Uezato, "Maximum Power Point Tracker Using Fuzzy Control for Photovoltaic arrays," *Proceedings of the IEEE International Conference on Industrial Technology*, 1994, 5-9 Dec. 1994, pp. 143–147.

[13] K. H. Hussein, I. Muta, T. Hoshino, and M. Osakada, "Maximum photovoltaic power tracking: An algorithm for rapidly changing atmospheric conditions", *Proc. IEE-Generation, Transmission, Distribution,* vol. 142, No. 1, Jan. 1995, pp. 59-64.

[14] Y. C. Kuo, T. J. Liang and J. F. Chen, "Novel Maximum-Power-Point-Tracking Controller for Photovoltaic Energy Conversion System", *IEEE Transactions on Industrial Electronics*, Vol. 48, No. 3, June 2001, pp.594-601.

[15] A. Brambilla, M. Gambarara, A. Garutti, and F. Ronchi, "New Approach To Photovoltaic Arrays Maximum Power Point Tracking", *PESC 99, 30th Annual IEEE*, Vol. 2, 27 June-01 July 1999, pp. 632-637.

[16] P. Midya, P. T. Krein, R. J. Turnbull, R. Reppa, J. Kimball, "Dynamic Maximum Power Point Tracker for Photovoltaic Applications", *Proc. PESC*, Baveno, Italy, 24-27 June 1996, pp.1710-1716.

[17] M. Andersen and B. Alvsten, "200W Low Cost Module Integrated Utility Interface for Modular Photovoltaic Energy Systems", *Proc. 95, IEEE IECON, 21st Conf.* Vol. 1, Nov. 1995, pp. 572-577.

[18] J. H. R. Enslin, M. S. Wolf, D. B. Snyman, and W. Sweigers, "Integrated Photovoltaic Maximum Power Point Tracking Converter", *IEEE Transactions on Industrial Electronics*, Vol. 44, no. 6, Dec. 1997, pp.769-773.

[19] T. Noguchi, S. Togashi and R. Nakamoto, "Short-Current Pulse-Based Maximum-Power-Point Tracking Method for Multiple Photovoltaic-and-Converter Module System", *IEEE Transactions on Industrial Electronics*, Vol. 49, No.1, Feb. 2002, pp.217-223.

[20] T. Hiyama and K. Kitabayashi, "Neural Network based estimation of Maximum Power Generation from PV Module using environmental information", *IEEE Transactions on Energy Conversion*, Vol.12, No. 3, Sept. 1997, pp. 241-247.

[21] L. Zhang, B. Yunfei and A. Al-Amoudi, "GA-RBF neural network based maximum power point tracking for grid-connected photovoltaic systems *International Conference on Power Electronics, Machines and Drives*, 2002, 4-7 Jun. 2002 pp. 18 – 23.

[22] R.M. Hilloowala and A.M. Sharaf, "A Rule-based Fuzzy Logic Controller for a PWM Inverter in Photovoltaic Energy Conversion Scheme", *IEEE Transactions on Industry Applications*, Vol. 32, No. 1, Jan.-Feb. 1996, pp. 57 – 65.

[23] X.J Liu and L.A.C. Lopes, "An Improved Perturbation and Observation Maximum Power Point Tracking Algorithm for PV Arrays," *Proceedings of the 35th IEEE Power Electronics Specialists Conference* (PESC-04), Aachen Germany, 20-25 Jun. 2004, pp. 2005-2010.

[24] Neil S. D'Souza, Luiz A. C. Lopes and XueJun Liu, "An Intelligent Maximum Power Point Tracker using Peak Current Control," *Proceedings of the 36th IEEE Power Electronics Specialists Conference* (PESC-05), Recife, Brazil, 12-16 Jun. 2005, pp. 172 -177.

[25] Neil S. D'Souza, Luiz A. C. Lopes and XueJun Liu, "Peak current control based Maximum Power Point Trackers for faster transient responses," *Canadian Conference on Electrical and Computer Engineering* (CCECE 2006), Ottawa, Canada, 7-10 May 2006, pp. 1310 -1314.

[26] Tsang E.C.C., Yeung D.S. and Wang X.-Z., "Learning weights of fuzzy production rules by a max-min neural network," *IEEE International Conference on Systems, Man and Cybernetics 2001*, Vol.3, 7-10 Oct. 2001 pp.1485-1490

[27] Passino, K. M. and Yurkovich, S. (1998) "*Fuzzy Control*", Addison Wesley Longman Inc, California - USA.

[28] Hirotaka Koizumi and Kosuke Kurokawa, "A novel maximum power point tracking method for PV module integrated convereter" , *Proceedings of the 36th IEEE Power*

Electronics Specialists Conference (PESC-05), Recife Brazil, 12-16 Jun. 2005, pp. 2081-2086.

[29] Sachin Jain and Vivek Agarwal, "A new algorithm for rapid tracking of approximate maximum power point in photovoltaic systems", *IEEE Power Electronics Letters*, Volume 2, Issue 1, March 2004 Page(s):16 – 19.

APPENDIX

A1. The programs to set SAS Simulating the Solar Panels behavior [2]

All programs to access the Agilent Solar Array Simulator (SAS) are written in Visual Basic.

1. The program to turn on the SAS in Simulator mode with I_{SC} = 3.45A, V_{OC} = 21.7V, I_{MPP} = 3.15A, and V_{MPP} = 17.5V is shown as follows:

```
Option Explicit

Sub Main()
  Dim defrm As Long
  Dim vi As Long

  Call viOpenDefaultRM(defrm)
  Call viOpen(defrm, "GPIB0::5::INSTR", 0, 0, vi)

  Call viVPrintf(vi, "CURR:SAS:ISC 3.45;IMP 3.15;:VOLT:SAS:VMP 17.5;VOC
              21.7" + Chr$(10), 0)

  Call viVPrintf(vi, "CURR:MODE SAS" + Chr$(10), 0)

  Call viVPrintf(vi, "Output on" + Chr$(10), 0)

  Call viClose(vi)
  Call viClose(defrm)

End Sub
```

2. The program to turn off the SAS is shown as follows:

```
Option Explicit
Sub Main()
  Dim defrm As Long
  Dim vi As Long

  Call viOpenDefaultRM(defrm)
```

```
    Call viOpen(defrm, "GPIB0::5::INSTR", 0, 0, vi)
    Call viVPrintf(vi, "*RST" + Chr$(10), 0)
    Call viClose(vi)
    Call viClose(defrm)
End Sub
```